

UC Merced

UC Merced Electronic Theses and Dissertations

Title

Efficiency enhancement of luminescent solar concentrations for photovoltaic technologies

Permalink

<https://escholarship.org/uc/item/7b60c6g6>

Author

Wang, Chunhua

Publication Date

2011-07-12

Peer reviewed|Thesis/dissertation

UNIVERSITY OF CALIFORNIA, MERCED

**Efficiency Enhancement of Luminescent Solar Concentrations for
Photovoltaic Technologies**

A dissertation submitted in partial satisfaction of the
requirements for the degree
Doctor of Philosophy

in

Environmental Science

by

Chunhua Wang

Committee in charge:

Professor Gerardo Diaz, Chair
Professor Carlos Coimbra
Professor Linda Hirst
Professor Valerie Leppert
Professor Roland Winston

2011

Copyright
Chunhua Wang, 2011
All rights reserved.

The dissertation of Chunhua Wang is approved, and it is acceptable in quality and form for publication on microfilm and electronically:

Chair

University of California, Merced

2011

DEDICATION

To my parents, my husband Hsiang-Hsuan Hung and my son
Michael Yuxian Hung

TABLE OF CONTENTS

Signature Page		iii
Dedication		iv
Table of Contents		v
List of Figures		viii
List of Tables		xvii
Acknowledgements		xviii
Abstract of the Dissertation		xx
Chapter 1	Introduction	1
	1.1 Solar Energy	1
	1.2 Solar Concentrators	4
	1.3 Luminescent Solar Concentrators (LSCs)	5
	1.4 Thesis Outline	8
	1.5 Summary	11
Chapter 2	Background	12
	2.1 Introduction	12
	2.2 PV Technologies	12
	2.2.1 Band Gap	13
	2.2.2 Absorption Coefficient	14
	2.2.3 Quantum Efficiency	16
	2.2.4 Spectrum Response (SP)	17
	2.2.5 IV curve	19
	2.3 Solar Concentrators	21
	2.3.1 Image-forming Concentrators	21
	2.3.2 Non-imaging Concentrators	22
	2.3.3 Luminescent Solar Concentrators (LSCs)	24
	2.4 Luminescent Materials	25
	2.5 Liquid Crystals as Matrix Materials	27
	2.5.1 Liquid Crystal	28
	2.5.2 Polarized Optical Microscopy	29
	2.5.3 Differential Scanning Calorimetry	31
	2.6 Spectroscopy	33
	2.7 Summary	35

Chapter 3	Near Infrared Quantum Dot Luminescent Solar Concentrators	37
3.1	Introduction	37
3.2	Fabrication and Characterization Process	40
3.2.1	Luminescent Materials and the Fabrication Process	40
3.2.2	Solar Simulator Spectrum	42
3.2.3	Solar Cells as Detectors	43
3.3	Optical Characterization	43
3.3.1	Absorption Properties	45
3.3.2	Emission Properties	47
3.4	Concentration Optimization	50
3.4.1	Concentration Study for Rhodamine B Dye LSC PVs	52
3.4.2	Concentration Study for CdSe/ZnS QD LSC PVs	53
3.4.3	Concentration Study for PbS QD LSC PVs	54
3.5	Re-absorption Characterization	55
3.6	Electrical Characterization	59
3.6.1	Current Ratio Measurements	59
3.6.2	Optical Efficiency Analysis	61
3.7	Output Power Stability Characterization	61
3.8	Optical Enhancement for Quantum Dots Thin Film LSCs	63
3.8.1	Optimization Methods	64
3.8.2	Optimization for Liquid Dye LSCs	64
3.8.3	Optimization for QDs Thin Film LSCs	67
3.9	Summary	69
3.10	Acknowledgements	71
Chapter 4	Organic Luminescent Solar Concentrators	72
4.1	Introduction	72
4.2	Experiments	76
4.3	Optical Characterization of Organic LSCs	81
4.4	Efficiency Enhancement and Optimal Design for Single Layer LSCs	86
4.4.1	Optical Enhancement for Small Samples	86
4.4.2	Optical Enhancement for Larger Samples	87
4.4.3	Size Dependent Optical Enhancement	88
4.4.4	Size Dependent Re-absorption Loss	91
4.4.5	Size Dependent Energy Loss from LSCs	92
4.5	Efficiency Enhancement for Multilayer Organic LSCs	95
4.6	Wavelength Selective Films for LSCs	101
4.6.1	Optimization principle	101
4.6.2	Spectral properties of 3M films	101
4.6.3	Transmitted current ratio	102

	4.6.4 Performance of LSCs with the wavelength selective film	103
	4.7 Stability Properties of Organic LSCs	107
	4.8 Concentration Performance for Diffuse Light	111
	4.9 Summary	113
	4.10 Acknowledgements	116
Chapter 5	Liquid Crystal Dye Alignment for New Generation Luminescent Solar Concentrators	118
	5.1 Introduction	118
	5.2 Theoretical Analysis	122
	5.3 Properties of Liquid Crystals as Matrix Materials	125
	5.4 Properties of Organic Dyes for Alignment	127
	5.5 Experiments	130
	5.6 Results and Discussion	132
	5.6.1 Spectrum properties of dyes in different matrix materials	132
	5.6.2 Phase transition properties of liquid crystal materials	142
	5.6.3 Alignment and Birefringence Properties Tested by Polarized Optical Microscopy	144
	5.7 Future Work	145
	5.7.1 Alignment of Dyes for Stacked Structures	145
	5.7.2 Order Parameter Characterization	146
	5.7.3 Stability Testing	146
	5.7.4 Further Design Optimization	146
	5.8 Summary	147
	5.9 Acknowledgements	149
Chapter 6	Conclusions	150
	6.1 New Luminescent Materials	150
	6.2 LSC Optimal Structure Design	152
	6.3 New Generation LSCs	154
Bibliography	157

LIST OF FIGURES

Figure 1.1: Solar powered light house at Montague Island, a National Parks and Wildlife sanctuary on the East coast of Australia.	3
Figure 1.2: Schematic of a LSC, the embedded luminescent material can be dispersed isotropically or anisotropically.	5
Figure 2.1: The absorption coefficient, α , in a variety of semiconductor materials at 300K as a function of the vacuum wavelength of light.	15
Figure 2.2: The quantum efficiency of a silicon solar cell. The square shape is for an ideal solar cell	17
Figure 2.3: The spectral response (SP) of a silicon solar cell under glass. . .	18
Figure 2.4: IV curve of a solar cell.	20
Figure 2.5: Limiting solar cell efficiency as a function of the material band gap for one-sun illumination. The calculations assume that the only recombination is radiative. In actual devices the efficiencies are lower due to other recombination mechanisms and losses in parasitic resistances.	22
Figure 2.6: Structure of a 2D compound parabola concentrator (CPC) for planar absorber.	23
Figure 2.7: Quantum dots absorb light at shorter wavelengths, and then emit light at longer wavelengths. The difference of the absorbed and emitted wavelengths depends on the band gap of the dots which can be tuned by the size distribution of the dots.	27
Figure 2.8: Schematic of mesogen alignment in a liquid crystal nematic phase.	29
Figure 2.9: Light passing through crossed polarizers appears dark.	30
Figure 2.10: Configuration of polarized optical microscope. Light from source becomes polarized after passing through the first polarizer, and is delayed and refracted by the tested birefringent specimen for different wavelengths. The generated extra ordinary and ordinary rays pass through the analyzer and recombine after interference.	30
Figure 2.11: DSC we used in Professor Linda Hirst’s lab at UC Merced. . . .	32
Figure 2.12: A typical result of DSC calibration for liquid crystals.	33
Figure 2.13: A typical absorption (Abs.) and emission (Em.) spectra of organic Lumogen Red F 305 dye material in toluene solvent. . .	35
Figure 2.14: The transmittance of Lumogen Red F 305 dye PMMA thin film LSCs.	35
Figure 2.15: The normalized emission spectra of Lumogen Red F 305 dye PMMA thin film LSCs.	36

Figure 3.1:	A schematic representation of a LSC PV system. Solar radiation is absorbed by luminescent materials integrated in a thin, flat-plate transparent waveguide materials (Glass, PMMA). Photons re-emitted by luminescent materials are guided to solar cells attached to the edge of the LSC. Quantum dot LSCs are LSCs with quantum dots as luminescent materials.	38
Figure 3.2:	The near infrared PbS QDs (Right) and the visible CdSe/ZnS QDs (Left) for prototyping of LSCs provided by the Evidot vendor. They are dispersed in toluene.	41
Figure 3.3:	Rhodamine B, as a high quantum yield laser dye, dissolved in ethylene glycol for comparison study at different concentrations.	41
Figure 3.4:	A LSC electrical characterization setup in the lab. The near infrared PbS QDs in toluene are filled in the glass box. Light shines the sample from the front surface. The PV cell is attached at the bottom short edge of the fabricated QD LSCs. Fluke multi-meter is used for reading the output open circuit voltage and the short circuit current.	42
Figure 3.5:	Normalized intensity distribution of the solar simulator we used in the lab.	43
Figure 3.6:	The solar cell as a detector for the electrical characterization of LSC concentration factors. It is produced by SunPower Company. The left and right sides are two electrodes.	44
Figure 3.7:	The efficiency of the solar cell used as a detector is characterized by one-sun solar simulator.	44
Figure 3.8:	The current voltage $I - V$ curve is recorded for the PV cell as a detector. The test results show that the fill factor of this PV cell is 0.72, and the calculated solar cell efficiency is 18%.	45
Figure 3.9:	The absorption properties of near infrared PbS QDs in toluene at different concentrations: at $10\mu M$, $30\mu M$, $50\mu M$, $70\mu M$ respectively. The peak absorption wavelength centers at 750nm. The inset shows that the higher the concentration, the stronger the absorption.	46
Figure 3.10:	Absorbance of PbS Quantum Dots in toluene at the peak emission wavelength as function of the concentration. The tested concentration values are $10\mu M$, $30\mu M$, $50\mu M$ and $70\mu M$ (Square). The solid line is the fitted result, which clearly shows the linear relationship.	47
Figure 3.11:	The absorption properties of visible CdSe/ZnS QDs in toluene at different concentrations: $2.5\mu M$, $3\mu M$, $3.5\mu M$, $4.5\mu M$, $6\mu M$ and $10\mu M$ respectively. The peak first excited emission centers at 620nm. The absorption wavelength range is less wide than the PbS QDs.	48

Figure 3.12: The comparison of the absorbance for the near infrared PbS QDs and CdSe/ZnS QDs at their peak emission wavelength. . .	49
Figure 3.13: Emission spectrum for the 50 μ M near infrared PbS QDs LSCs excited by wavelength at 500nm, 600nm, 700nm respectively. . .	49
Figure 3.14: Emission spectra of the 50 μ M near infrared PbS QDs LSCs. The peak absorption and emission wavelengths center at 750nm and 880nm respectively with Stokes Shift 130nm. Excitation wavelength: 500nm.	50
Figure 3.15: Comparison of absorption and emission properties of three luminescent materials: PbS quantum dots, CdSe/ZnS quantum dots, Rhodamine B dye. Excitation wavelength: 500nm.	51
Figure 3.16: For Rhodamine B dye LSC PVs, the tested output current ratio as a function of sample concentration.	52
Figure 3.17: For CdSe/ZnS QD LSC PV systems at different concentrations, the tested output current ratio as a function of time. The output current is very stable. (The samples were diluted from the 17.4 μ M CdSe/ZnS QDs.)	53
Figure 3.18: For CdSe/ZnS QD LSC PV systems, the tested output current ratio as a function of concentration. Due to re-absorption, samples with higher concentration produce less power. The optimum concentration for this design is around 3 μ M.	54
Figure 3.19: For the PbS systems at different concentrations, the tested output current ratio as a function of time. The output current is not very stable. (Samples at lower concentration are prepared by diluting from the 193 μ M PbS QDs from the vender.)	55
Figure 3.20: The tested output current ratio as a function of PbS QDs concentrations. The higher the PbS concentration, the higher the absorption. The output current drops much slowly after 10 minutes.	56
Figure 3.21: The emission spectra from the 10 μ M PbS QDs LSCs as the function of the excitation distance changing from 4mm to 28mm with steps 2mm. The excited wavelength is 408nm from a blue laser.	57
Figure 3.22: The intensity at peak emission from the 10 μ M PbS QD LSCs as the function of the excitation distance changing from 4mm to 26mm with each step increasing 2mm. The excited wavelength is 408nm from a blue laser.	58
Figure 3.23: The normalized emission spectrum from the 193 μ M PbS QDs LSC as the function of the excitation distance changing from 0mm to 22mm with each step increasing 2mm. The excited wavelength is 408nm from a blue laser. The emissions centers on 930nm.	59

Figure 3.24: Output current ratio from the PV cell attached at the edge surface of LSCs fabricated with near infrared QD PbS, visible QD CdSe/ZnS, and organic laser dye Rhodamine B respectively.	60
Figure 3.25: For the PbS QDs LSC at 50 μ M, the tested output current as a function of time up to 120 minutes. After 20 minutes of testing, the sample was put into the dark, then retested at 100 minutes, and continued testing until 120 minutes.	62
Figure 3.26: The outdoor testing of the current ratio as a function of PbS QD concentration. The higher the PbS concentration, the higher the absorption. The output current drops much slower after 10 minutes.	63
Figure 3.27: Optimum results for polished quartz cells filled with 400 μ M Rhodamine B, testing under sunlight.	65
Figure 3.28: Testing configuration by using PV cell from the long edge of the fabricated LSC. The PV cell with dimensions 12mm by 0.3mm is attached and moved along the long edge with each step increasing 0.5mm.	66
Figure 3.29: The current distribution along the long edge of the glass box without optimization (normalized), and optimized by white diffusers and silver reflective tapes.	67
Figure 3.30: Optimization by using a whiter diffuser for PbS QD thin film LSCs at different concentrations changing from 20 μ M to 60 μ M.	68
Figure 3.31: Optimization by using a whiter diffuser for CdSe/ZnS QD thin film LSCs at different concentrations changing from 1 μ M to 4 μ M.	69
Figure 4.1: Schematic of an organic luminescent solar concentrator (LSC).	73
Figure 4.2: Organic LSC samples fabricated by embedding dyes into plastic materials.	73
Figure 4.3: Schematic of experimental setup for optical enhancement of LSCs by attaching a white diffuser at the bottom of the LSC and adding refractive index matched optical gel between LSC edges and the attached PV cells.	77
Figure 4.4: The two layered stacked LSC plates for photovoltaics with the green LSC on top of the red LSC. Glass strips are used between surfaces of PV cells and the LSC edges.	78
Figure 4.5: Without applying glass strips shown in Fig. 4.4 between PV cells and LSCs, PV cells attached at the edge of the LSCs break due to different thermal expansion properties.	79
Figure 4.6: The prototyped “smart” window of stacked LSCs with PV cells attached at all edges in series. It is put on a solar tracker.	80
Figure 4.7: Steady state absorption (Abs.) and emission (Em.) spectra properties of the normally used high quantum yield Rh. B dye for LSCs.	82

Figure 4.8: Absorption and emission spectra of the tested (a) green and (b) red color emission organic dyes in plastic.	82
Figure 4.9: Transmittance of Lumogen red, yellow and green emission organic dyes in plastic materials.	84
Figure 4.10: Emission spectra of Lumogen red, yellow and green emission organic dyes in plastic materials.	84
Figure 4.11: Transmitted current ratio of outdoor- and indoor- use LSC samples.	85
Figure 4.12: Transmitted current ratio of outdoor- and indoor- use samples by stacking in different ways.	85
Figure 4.13: Current ratios by using different optimization methods for the small LSC sample with dimensions 4.5cm by 1.2cm by 0.32cm (Tested under sunlight).	87
Figure 4.14: Current ratio of the largest tested LSC with 60cm by 120cm by 0.32cm. Optimization methods: 1. No optimization; 2. Only optimized with a white diffuser attached at the bottom of the LSC; 3. Only optimized with refractive index matched optical gel added between the edge of the LSC and the PV cell; 4. Optimized with a white diffuser and optical gel (Tested under sunlight).	88
Figure 4.15: Size dependent optical enhancement by using a white diffuser for LSCs. The tested LSC has dimensions 6cm by 121cm by 0.32cm. In the test, it is partially covered to change the size of LSCs. (a) Output current ratio with (Diamond) and without (Square) attaching a white diffuser at the bottom surface as white and black backgrounds respectively; (b) The enhancement ratio by using a white diffuser with the change of the length of the exposed LSC (The change of the exposed size). The refractive index matched optical gel is not used in showing the size-dependent effect of the white diffuser on the current ratio.	90
Figure 4.16: Experimental setup for testing the output power contributed by different parts of the LSC. The black paper with a hole is covered from the top surface of the tested red emission LSC. The output open circuit voltage and short circuit current from the attached the PV cell are recorded when the position of the hole changes.	91
Figure 4.17: The output short circuit current from a PV cell attached at the red emission LSC strip by exposing it to sunlight. The LSC is with 121cm by 6 cm by 0.32cm. (Experimental setup is shown in Fig. 4.16).	92
Figure 4.18: The concentration factor, or the current ratio, as a function of the length of a LSC.	93

Figure 4.19: The energy loss from the system as a function of the length of the tested LSC.	94
Figure 4.20: A schematic of the experimental setup for efficiency enhancement of LSCs by attaching a white diffuser at the bottom of the tested LSCs (Stacked two layers of LSCs in this figure), and by adding refractive index matched optical gel between LSC edges and the attached PV cells. In the test, a larger piece of PV cell with 1.2cm by 1.2cm is masked with black tape to match the thickness of the tested LSC edges.	95
Figure 4.21: Output photocurrent for (1) Single green emission, (2) Single red emission and (3) Stacked green and red emission LSCs by using white diffusers and optical gel.	96
Figure 4.22: The monthly averaged total output power of the fabricated LSC system with vertical position at Merced and Denver (0°) and horizontal position (90°) at Merced.	99
Figure 4.23: Photo luminescent current from blue, green and red emission fluorescent plates stacked LSCs.	99
Figure 4.24: Experimental setup for characterizing the distribution of the output current along the stacked LSC edges by using PV cells. .	100
Figure 4.25: The output edge distribution of three layer stacked LSCs. There are blue, green and red emission fluorescent plates stacking from top to bottom in sequence. All of them are in square shape with length in 15.24cm (6in), 30.48cm(12in) and 60.96 cm (24in). . .	100
Figure 4.26: Transmittance of the 3M wavelength selective film. The film can reflect wavelength very effectively from 600nm to 750nm. .	102
Figure 4.27: The current ratio from each surface of a LSC with dimensions 35cm by 35cm by 0.32cm, and geometrical gain 28. The detector is a silicon PV cell with 1.2cm in length and 0.32cm in width. It is fabricated with the outdoor use red emission dyes.	104
Figure 4.28: The energy distribution from each surface of the LSC with dimensions 35cm by 35cm by 0.32cm, and geometrical gain 28. The detector is a silicon PV cell with 1.2cm by 0.32cm.	105
Figure 4.29: The current ratio from each surface of a LSC PV system with dimension 60cm by 120cm by 0.32cm and geometrical gain 62.5.	106
Figure 4.30: The energy distribution from each surface of the LSC with dimension 60cm by 120cm by 0.32cm and geometrical gain 64. The detector is a silicon PV cell with 1.2cm by 0.32cm.	107

Figure 4.31:	Picture of one group of LSCs for the stability testing. For each group, there are a LSC fabricated with green emission dyes and a LSC fabricated with red emission dyes. There are three such groups: the first group is kept in the dark; the second group is exposed to sunlight with black board attached at the bottom as black background, and the third group is exposed to sunlight with white board attached at the bottom as white background.	108
Figure 4.32:	The stability testing results for the three groups of LSCs fabricated with red and green emission dyes.	109
Figure 4.33:	(a) Transmittance and (b) emission spectra of green emission LSC for stability testing. The samples have been exposed to sunlight or kept in dark for two months.	110
Figure 4.34:	(a) Transmittance and (b) emission of red LSCs for stability testing. The samples have been exposed to sunlight or kept in dark for two months.	111
Figure 4.35:	Experimental set up for the performance of LSCs in collecting global and diffuse light. Prototypes of LSCs are fabricated by stacking green and red LSCs together.	112
Figure 4.36:	The concentration factors of LSCs from 4 edges for (a) global light and (b) diffuse light as function of the time in hours on 09/07/2010 without any optimization. (The background of the tested LSC is black and no optical gel has been applied.)	113
Figure 4.37:	Concentration factor of stacked LSC PV systems for concentrating both global and diffuse light during a typical sunny day at Merced, California from 8:00AM to later 2:00PM, Sep. 7, 2010.	114
Figure 5.1:	Schematic of a LSC, the embedded luminescent materials can be dispersed isotropically or anisotropically.	122
Figure 5.2:	Escape cone of a waveguide, where α_c is the critical angle. This angle is related to the refractive index of the waveguide material. Emitted light in this angle will escape from the LSC.	123
Figure 5.3:	Emission profiles of (a) an isotropic distribution of dyes in an LSC and (b) an anisotropic dye distribution in an LSC.	124
Figure 5.4:	Transmittance of the UCL018 sample by casting a very thin layer on a glass substrate. It is up to 90% for wavelengths from 350nm to 900nm.	126
Figure 5.5:	Polarized Optical Microscopy picture for UCL018 liquid crystal. Refractive index varies in different direction. We observed the dark area expanding when UCL018 is well aligned vertically to the glass surface.	127

Figure 5.6:	Phase transition sequence characterization for UCL018. The phase transition sequence is from crystal to nematic liquid crystal and nematic liquid crystal to isotropic transitions with the temperature peaks at 48C and 66C respectively	128
Figure 5.7:	Coumarin 6 dye powder.	128
Figure 5.8:	The normalized absorption and emission of Coumarin 6 dye in toluene solution.	129
Figure 5.9:	The absorption and emission of Coumarin 6 dye in toluene solution for the Lumogen Red F 305 organic dye.	130
Figure 5.10:	Coumarin 6 UCL018 liquid crystal spin coated samples at higher concentration (left) and lower concentration (right). The size is 2.54cm by 7.62cm (1in by 3in).	131
Figure 5.11:	Red F 305 UCL018 liquid crystal spin coated samples at higher concentration (upper) and lower concentration (lower). The size is 2.54cm by 7.62cm.	133
Figure 5.12:	Normalized (a) absorption and (b) emission of Coumarin 6 dye in a spin casted liquid crystal film compared with absorption and emission of the same dye in PMMA powder contained liquid mixture and in LC contained liquid mixture.	134
Figure 5.13:	Normalized (a) absorption and (b) emission spectra of the Coumarin 6 dye in pure toluene solution and in a plastic sheet. Comparing the absorption of the dye in diffused PMMA plastic films and in Toluene solution.	136
Figure 5.14:	Normalized absorption and emission properties of Coumarin 6 dye in diffused plastic films.	137
Figure 5.15:	Normalized absorption properties of Coumarin 6 in anisotropic cross linked and uncross linked liquid crystal films by spin coated on glass substrates, in isotropic PMMA films spin coated on glass substrates, and in anisotropic liquid crystal films filled in glass cells.	138
Figure 5.16:	Normalized emission properties of Coumarin 6 in anisotropic cross linked liquid crystal films spin coated on glass substrates, in isotropic PMMA films spin coated on glass substrates.	139
Figure 5.17:	Normalized absorption properties of Lumogen Red F 305 in anisotropic cross linked and uncross linked liquid crystal films spin coated on glass substrates, in isotropic PMMA films spin coated on glass substrates, and in anisotropic liquid crystal films diffused in glass cells. The top and bottom surfaces of the glass cells are coated with specific alignment coatings.	139
Figure 5.18:	Normalized emission properties of Lumogen Red F 305 in anisotropic cross linked and uncross linked liquid crystal films spin coated on glass substrates, in isotropic PMMA films spin coated on glass substrates.	140

Figure 5.19: Normalized emission properties of Lumogen Red F 305 in anisotropic cross linked liquid crystal films spin coated on glass substrates, and in cross linked anisotropic liquid crystal films diffused in glass cells. The top and bottom surfaces of the glass cells are coated with specific alignment coatings.	140
Figure 5.20: Normalized absorption and emission spectra of Lumogen Red F 305 anisotropic LSC films fabricated in glass cells.	141
Figure 5.21: Phase transition for cross-linked liquid crystal UCL018 contained Coumarin 6 dye. There are no peaks observed.	143
Figure 5.22: From the edge of the aligned (a) Lumogen Red F 305 and (b) Coumarin 6 samples (Glass Cells).	144
Figure 5.23: Transmittance of designed stacked LSCs with dyes aligned by liquid crystals. Fabricating anisotropic LSCs with these dyes, and then stacking these anisotropic LSCs into three layered structure, the absorption range of the stacked sample can absorb sunlight from 400nm to 600nm.	145

LIST OF TABLES

Table 3.1:	For the 400 μM Rhodamine B LSC PV system, the tested output current, calculated current ratio and the improvement by applying different optimization methods. A. Only Cells; B. Optical Gel (at the edges); C. Gel (at the edgess)+ White Paper(at the bottom); D. Gel (at the edges) + Reflective Silver Tape (at other edges); E. Gel (at the edges)+ Reflective Silver Tape (at other edges) + White Paper (at the bottom).	65
Table 4.1:	Tested output current I_{output} for the LSC with geometrical gain 28 at white background.	103
Table 4.2:	Tested output current I_{output} for the LSC with geometrical gain 62.5 at a black background.	105
Table 4.3:	Tested output current I_{output} for the LSC with geometrical gain 62.5 at a white background.	106

ACKNOWLEDGEMENTS

First, I would like to thank Professor Winston for his acceptance of my study in his group at UC Merced. In the past years, Professor Winston has been invaluable to me in his special way. He is always there to answer and advise me on the day-to-day basis with his positive attitude and encouragement on the project. His knowledge in physics and engineering, and his great explanation ability in teaching is a tremendous help to me, as is his patience.

Secondly, thanks to Professor Sayantani Ghosh and Professor Linda Hirst at UC Merced and Professor Sue Carter and Glenn Alers at UC Santa Cruz for their guidance and encouragement, to postdocs and students in their groups for their help and sharing of happiness of doing research. It's invaluable to be in touch with others working in the field.

Special thanks to Dave Pelka from Pelka and Associate Inc. and project managers from Abengoa Company for their consultancy in research and supporting in finance. Also, thanks to my committee members, and to Professor Raymond Chiao, Professor David Kelley and his postdoc Zhongjie for their valuable discussions.

Many group colleagues have helped me along the way including Bruce C. Johnston, Ron Durbin, Weiya Zhang, Yong Sin Kim, Lun Jiang, Heather Poiry, Kevin Balkoski, Kevin Rico, Uday Bali, Tara Backman, Bennett K Widyolar, Brian Sarracino-Aguilera, Javier Oxford, Robyn Lukens et al., and the staff at UC Merced, UC MERI and UC Solar.

An extra thanks to companies for providing us Photovoltaic cells, luminescent materials and Liquid Crystals.

Thanks to my friends who encouraged me along the way and made weekends lots of fun.

Finally, to my lovely family, mom, dad, my sisters Chunyan, Chunlian, Chunping and my brother Longlong, my physicist husband Hsiang-Hsuan, my

lovely little son Michael, and my parents-in law.

Thank you for all your encouragement, love, support and laughs.

ABSTRACT OF THE DISSERTATION

**Efficiency Enhancement of Luminescent Solar Concentrations for
Photovoltaic Technologies**

by

Chunhua Wang

Doctor of Philosophy in Environmental Science

University of California, Merced, 2011

Professor Gerardo Diaz, Chair

Solar energy is a prominent renewable source of electricity if cheap methods are designed for its concentration and conversion. With the purpose of improving power conversion efficiency and lowering the cost, luminescent solar concentrations (LSCs) are developed for collecting and concentrating both direct and diffuse light for Photovoltaic systems without tracking.

Nano-structured near infrared PbS quantum dots (QDs) as new luminescent materials are identified. This material is optically characterized by using steady state spectroscopic technologies and electrically characterized by outdoor testing. These properties are also compared with visible CdSe/ZnS QDs for LSC

PV systems and organic dye LSC PV systems. The results show the promising future of near infrared QDs as luminescent material for LSCs if their stability can be properly controlled.

Techniques for fabrication and characterization of LSCs as “smart” windows are developed. A range of prototypes are fabricated, optically and electrically characterized. A variety of optimal designs for improving the output power conversion efficiency are investigated both for QDs LSCs and for organic dye LSCs. For LSCs with organic dyes, the size dependent optimization methods are developed for both one layer and stacked structures.

The largest fabricated prototype has 60cm by 120cm by 0.32cm. It yields electric gain 4.23, which is much larger than that of fixed concentrators based on geometrical optics. Prototypes fabricated with new outdoor use organic laser dyes show the same electric gain but with 5.88× smaller in size 2.67× larger in optical efficiency. This results show that LSCs fabricated with outdoor use organic dyes are very promising if applied into stacked structures.

New generation LSCs with liquid crystals as matrix materials are explored. Properties of liquid crystals and dyes for the new generation LSCs are analyzed with the predicted theoretical improvement for trapping efficiency up to 21.3%. Such anisotropic LSCs containing identified organic dyes are successfully fabricated and optically characterized. Performances of these LSCs are compared with isotropic samples.

Chapter 1

Introduction

1.1 Solar Energy

Due to both of the effects of global warming and the increasing price of fossil fuels, it is becoming increasingly urgent to develop alternative energy sources [Abb11]. Solar energy, radiant light and heat from the sun, has been harnessed by humans since ancient times using a range of ever-evolving technologies. Solar radiation, along with secondary solar-powered resources such as wind and wave power, hydroelectricity and biomass, account for most of the available renewable energy on earth. Solar energy, in one form or another is the source of nearly all energy on the earth [GKK00]. with cheaper solar energy concentration and conversion methods, solar energy will become a very prominent renewable source of electricity.

The sun can be approximated as a black body at 5760 K with an irradiance of $1370W/m^2$ at one astronomical unit distance [WMB⁺05]. The peak wavelength is usually 503 nm (2.45 eV), but varies with solar weather. Due to a variety of absorption and scattering processes the spectrum observed on the Earth's surface is significantly different. The total irradiance is attenuated and there are a number of absorption valleys. In order to standardize the performance of photovoltaic devices,

researchers have devised a standard solar spectrum known as the Air Mass 1.5 standard. The Air-Mass 1.5 standard is intended to mimic a mean characteristic spectrum at a power density of $1000W/m^2$ [GKK00].

Solar technologies are broadly characterized as either passive solar or active solar depending on the way they capture, convert and distribute solar energy. Active solar techniques include the use of photovoltaic (PV) device and solar thermal collectors to harness the energy. Passive solar techniques include orienting a building to the Sun, selecting materials with favorable thermal mass or light dispersing properties, and designing spaces that naturally circulate air [GKK00].

PV technologies are the technologies that convert solar energy directly into electricity. A PV cell is a solar-electric cell that collects sunlight and converts it to electric. A number of solar cells electrically connected to each other and mounted in a support structure or frame is called a PV module. Multiple modules can be wired together to form an array. PV cells can be connected in both series and parallel electrical arrangements to produce any required voltage and current combinations, like the PV panel shown in Fig. 1.1 [HBte].

In Fig. 1.1, the light house is at Montague Island, a National Parks and Wildlife sanctuary on the East coast of Australia. It is solar powered by the small panel on the left. The large panel on the right powers the cottages which can partially be seen in the background. The cottages contain facilities for the National Parks' caretaker and facilities for researchers on the island. PV technologies are simple and elegant methods of harnessing the Sun's energy.

PV technologies have developed very rapidly [GH05]. In the last decade, the PV industry grew at a rate exceeding 30% per year. The first generation of PV cells is mainly based on silicon materials including mono-crystalline silicon, multi-crystalline silicon and ribbon silicon. Currently, solar-cell modules based on single-crystal and large-grain polycrystalline silicon wafers comprise more than 80% of the market. Bulk Si PV, which benefit from the highly advanced growth and fabrication processes developed for microelectronics industry, is a mature tech-



Figure 1.1: Solar powered light house at Montague Island, a National Parks and Wildlife sanctuary on the East coast of Australia.

nology. The light-to-electric power conversion efficiency of the best modules offered on the market is over 20%. While there is still room for improvement, the device performance is approaching the thermodynamic limit of similar to 28% for single-junction Si solar cells. The major challenge that the bulk Si solar cells face is, however, the cost reduction [AIM11, LMB⁺05].

One way to reduce the cost of PV electricity is to use thin film solar cells. The thin film solar cells based on amorphous, microcrystalline, and polycrystalline Si as well as cadmium telluride CdTe and copper indium diselenide Cu(In,Ga) - (S,Se)₂ compound semiconductors, have already proved their commercial viability and their market share is increasing rapidly. Another avenue to reduce the cost of PV electricity is to increase the cell efficiency beyond the Shockley-Queisser limit [GH05]. The so-called third generation photovoltaics technologies involve stacking PV cells with different band gaps allowing conversion of different parts of the solar spectrum at maximum efficiency [AIM11, Noz10].

The production of electricity from PV devices is currently uneconomical compared to fossil fuel or nuclear sources except for applications located off the electrical grid. The high cost associated with electricity derived from PV is due to their low efficiency, high materials cost of ultra-pure zone refined silicon, and the thick substrate necessary for an indirect band-gap material necessary to absorb as much as the incident radiation as possible. We describe these technologies in detail in Chap. 2.

Although the bulk of photovoltaic devices are used for purely practical and economic reasons, a potential benefit of PV is that PV is one of the most environmentally benign of any electricity generating source. The environmental impact of electricity generation, particularly the greenhouse effect, adds an important reason for examining PV technologies [Abb11].

1.2 Solar Concentrators

The fundamental need for PV to become competitive as power producers compared to conventional energy supply methods is to reduce cost by reducing the materials cost, reducing infrastructure and time needed for manufacture, and improving efficiency. Applying solar concentrating systems is one promising approach to lower initial costs as it decreases the amount of PV materials required [LA07, SRWY90].

Almost everyone has had experience with a light concentrator. A hand lens focused on the ground on a sunny day demonstrates the ease with which sunlight can be collected and concentrated. A survey of the literature over the past 10 years yields many different kinds of devices called concentrators. All of these systems, however different, are related in that they increase the number of photons on a surface or the irradiance above the level present without the device [WMB⁺05].

There are mainly two kinds of solar concentrators, one is based on geometrical optics, called passive concentrators, and another group is based on quantum

optics, called active solar concentrators. The passive concentrators include compound parabolic concentrators [GKK00] and Fresnel lenses. The active concentrators include luminescent solar concentrators, which is the main research topic of this dissertation [vSBS⁺08]. Theoretical limit of light concentrators will be discussed in Chap. 2.

1.3 Luminescent Solar Concentrators (LSCs)

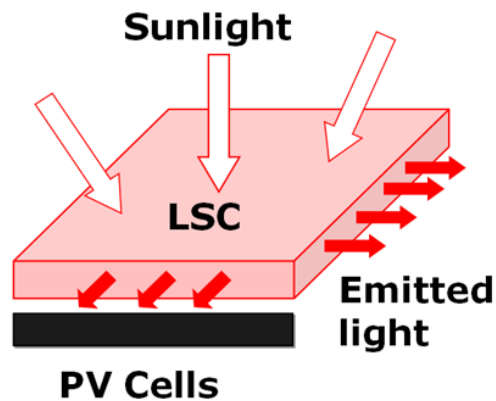


Figure 1.2: Schematic of a LSC, the embedded luminescent material can be dispersed isotropically or anisotropically.

A schematic of a LSC is shown in Fig. 1.2. Typically, it is a sheet of transparent waveguide materials with luminescent materials dispersed or cast inside. The transparent waveguide materials can be glass or plastic (matrix materials) etc, and the dispersed luminescent materials can be organic dyes [TCS05], organic semiconductor polymers [SOC07], nano-structured quantum dots [vSBS⁺08] or other luminescent materials [PP91, RSJ94]. The structure can also be a layer of planar waveguide with a thin-film coating on the face. Incident solar energy is absorbed by the dispersed organic luminescent material, and re-emitted into the

waveguide and transported to the edges of the LSC for collection by the solar cells.

This concentrator is a non-imaging solar concentrator since there are no images of the sun are formed at the edge surfaces of the LSC.

The LSC concept is suggested first in the 1970 [WL76, PKHG09, RB78], and is first used in scintillation counters for atomic physics. Although significant advances were made in early work [Bat81, THA87], after some years further progress was limited by the materials available at that time, in particular, luminescent materials. As the result, interest in this research was dormant for decades [Bat81]. Only recently new progress in materials [RWR08, WRR⁺10, WWW⁺10], especially the nanostructured semiconductor materials as well as theoretical advances rekindled interests. [DVN⁺11, Rei10, CMH⁺08, Noz10, WARR10a].

There are several advantages of LSCs comparing with concentrators based on mirrors and lens:

First, inexpensive abundant materials can be used to absorb the solar light and concentrate the light; a much smaller area of the expensive silicon PV is needed.

Second, unlike geometrical concentrators, the LSC concentrates both direct and diffuse light, making expensive tracking unnecessary. As a result, the cost per unit area is expected to be much less than for the currently available photovoltaic cells. The property of concentrating both direct and diffuse radiation without tracking, (work equally under diffuse light), makes them readily adaptable to most geographical locations and buildings [DCM⁺85].

Third, LSCs can separate the solar spectrum into two or more parts. These properties are like multi-junction solar cells [GH05].

Fourth, dyes can be chosen so that their absorption bands overlap with the peak emission of the Sun and their emission occurs at a wavelength range at which PV is efficient.

Finally, PV cells can accept “cool” photons and work efficiently, heat dissipation problems are reduced and the amount and cost of anti-reflection and filter

coatings currently used on windows can be reduced.

The LSC systems are highly versatile systems that could be incorporated into types of solar collectors to produce hybrid systems [ARW10, WARR10a, WARR10b, BOR84, ER95, MR97, YST09]. The geometrical concentration or geometrical gain of LSCs is defined as the area of the top surface over the area of the edges. The power conversion efficiency of the system is defined in the standard way as the electrical power from the solar cell divided by the power of the incident light on the top surface of the concentrator plate.

For the LSC PV systems, the power conversion efficiency is very low. In 1980s, 4% of power conversion efficiency of a stack two 40cm by 40cm LSCs was reported. The PV cells they used are GaAs cells. Recently, 5.5% four single plated LSCs was reported by using combined luminescent and phosphorescent materials [CMH⁺08]. The measured power conversion efficiencies ranges from 2.7% for a $5 \times 5\text{cm}^2$ LSC with one mc-Si cell at the side to 7.1% for a LSC with four GaAs cells attached to the sides with geometrical concentration of a factor 2.5 [SBB⁺08]. It is not possible to compare these efficiencies directly because the efficiency of the LSC strongly depends on the LSC dimensions, the number of attached solar cells and the use of mirrors at the sides or backside.

It was estimated that the maximum achievable conversion efficiency of LSCs that collect sunlight in the range of 300-900nm was $8 \sim 12\%$ [Rei10]. The development of LSCs is limited mainly by properties of luminescent materials and designed structures. These limits were not reached due to the following main reasons: (1) The incomplete absorption of the solar spectrum by any single material which serves as a colorant; (2) Self-absorption of the fluorescence by the emitting colorant; (3) Critical cone losses of the re-emitted centers, absorption and scattering of the host materials; (4) Lack of good contact between the LSC and the photovoltaic cell; (5) Reflection of light from the metallic surfaces of which the electrical contacts are made; (6) The decrease of performance efficiency of the collectors made of organic dyes with time is a result of photodecomposition of the colorant

and polymeric host material.

Recently, several methods are used including applying the use of photonic layers that act as band stop filters on the top surface of LSCs [DVV⁺10a, MRV⁺10], applying cylindrical structures [MYR07], applying mixtured dyes [BLH⁺07], semi-conducting polymers [SOC07], nanocomposite thin films [Noz10].

Also, the photo-luminescent (PL) efficiency of the emissive dye can be increased, solar cells can be optimized for monochromatic and bifacial excitation, and the absorption spectrum can be expanded into the near infrared. With these advances, the power efficiency of tandem LSCs may exceed 20% [ER95, GPHG09, JB09].

In this thesis, we identified and characterized new luminescent materials, designed LSCs at practical size to improve the LSC power conversion efficiency of LSCs, and develop new generation of LSCs with the application of liquid crystal materials.

1.4 Thesis Outline

In this chapter, we described the importance of improving LSC power conversion efficiency for photovoltaic solar energy collections, reviewed the state of the art on this research topic and show challenges from the development of LSCs. Then we described our research objective in improving the power conversion efficiency by identifying proper luminescent materials and design optimal LSC structures.

Chap. 2 presents some backgrounds on this research. The includes fundamental properties of solar cells since LSCs are applied mainly for PV technologies. Analyzing theoretical limitations for solar concentrators, especially for LSC based on the thermal dynamical theory can help us know how we can continue in this project. Chap. 2 also shows basic requirements for luminescent materials. Organic and inorganic materials possess unique characteristics, both satisfying some but not all of the requirements. In this chapter, properties of quantum dots (QDs)

as luminescent materials are described. Matrix materials play an important role in properties of LSCs. In this chapter, we also discuss properties of liquid crystals for fabrication new generation LSCs. This chapter also presents some of our experimental technologies.

In Chap. 3, near infrared QDs as new luminescent materials are identified for improving the power conversion efficiency of LSCs. We first describe the experimental fabrication and testing process, and then focus on characterization the fabricated samples. We characterized Optical properties of the near infrared QDs, visible QDs and organic dyes as possible luminescent materials. This optical comparison will show the potential efficiency improvement by near infrared QDs. Due to the re-absorption of luminescent materials, there is an optimum concentration for the seeded quantum dots. Manufacturing LSCs at this concentration, we will get the maximum output power. We will study the effects of the concentration on the output efficiency for each luminescent material. The re-absorption problem for each luminescent material is also characterized by the shifting of the peak emission wavelength. For the samples fabricated at their optimum concentrations, we will electrically characterize them and compared their electrical output properties. The output power stability problem of the near infrared quantum dots is analyzed and further characterized. The fabrication of thin film QD LSCs and the efficiency improvement by optical design are also described in this chapter.

In Chap. 4, we show a variety of designed optical structures for improving the power conversion efficiency of organic LSCs. In this chapter, properties of LSCs fabricated with outdoor use dye materials at a reasonable large size are compared with indoor use prototypes. We also characterize electrical properties of LSCs for PV technologies by applying optical optimization methods at different size and with different shapes. This chapter also shows the size and shape dependence of the optical efficiency enhancement for one layer and multi layer LSCs. Since we can further apply wavelength selective films on the top of the LSC surfaces to improve the output efficiency of the system, a wavelength selective film is fabricated and

applied to our fabricated LSCs. The energy balance analysis method for LSCs is given in this section and applied to one layer and multi layer stacked LSC systems.

The output power stability properties of LSCs are very important for collecting solar energy, which can be improved by selecting proper organic dyes [BMH99, KSB⁺07]. We tested the stability properties for a group of LSCs fabricated with indoor use dyes with the expecting that the specially designed LSCs with outdoor use dyes can perform better.

Since LSCs can be applied as “smart” windows by integrating into buildings to collect and convert solar energy into electrical power, we fabricate prototypes of LSC PV systems at practical sizes for such application. The concentration properties of these prototypes for both direct and diffuse lights are characterized and compared.

In Chap. 5, for the new generation LSCs, we describe principles of aligning dye molecules in efficiency improvement. As a proof of principle project, we focus on experimental characterization part. We describe properties of liquid crystals and organic dyes for producing LSCs. In this chapter we also show our experimental techniques in preparing liquid crystal dye molecules aligned anisotropic LSCs and PMMA isotropic LSCs. We then optically characterize spectrum properties of these fabricated prototypes, and compare anisotropic LSC samples with isotropic LSC samples. We also give phase transition properties of the liquid crystal after mixing with dye molecules, and characterize the alignment properties of anisotropic samples with differential scanning calorimetry (DSC) and polarized optical microscopy (POM) methods.

Finally, we conclude our work on this project and discuss the future work on further improvement in Chap. 6.

1.5 Summary

In this chapter, we briefly described main research topics of this thesis. A brief review on the development of LSCs is given. We showed that it is very important to improve power conversion efficiencies of LSC PV systems for solar energy to be competitive with conventionally energy supply methods by identifying proper luminescent materials and design optimum structures. Challenges from the development of LSCs in luminescent materials and structural designs are described. The organization and structure of the thesis are also presented in this chapter.

Chapter 2

Background

2.1 Introduction

In this chapter, a detailed description of PV technology is given in Sec. 2.2 as this thesis is concerned with the concentration of sunlight onto PV cells. Using solar concentrators, the cost of solar energy can be dramatically reduced. The theoretical concentration limitation for concentrators, especially for luminescent solar concentrators (LSCs) is discussed in Sec. 2.3 with the purpose to show that there is a great design space for LSCs in improving power conversion efficiency. In Sec. 2.4 and 2.5, properties of near infrared quantum dots as candidate luminescent materials, and liquid crystal polymers as a candidate of matrix materials for LSCs are described followed by a brief introduction of LSCs experimental characterization techniques.

2.2 PV Technologies

Photovoltaic effect was first discovered in 1839 by Alexandre-Edmund Becquerel, who noted that an electric current was produced when sunlight struck certain materials. A better understanding of the photovoltaic effect came with the development of quantum theory of solids in 1930 and in 1954 [PKHG09]. The first

usable solar cell was produced with 6% efficiency by Chaplin et al [GH05].

Materials presently used for photovoltaics include monocrystalline silicon, polycrystalline silicon, amorphous silicon. Silicon, which is a group IV in the periodic table, is also the most commonly used semiconductor material as it forms the basis for integrated circuit chips and is the most mature technology. Other PV materials include cadmium telluride and copper indium selenide/sulfide. Due to the growing demand for renewable energy sources, the manufacturing of solar cells and photovoltaic arrays has advanced considerably in recent years [AIM11].

To produce a solar cell, the semiconductor is contaminated or "doped". "Doping" is the intentional introduction of chemical elements, with which one can obtain a surplus of either positive charge carriers (p-conducting semiconductor layer) or negative charge carriers (n-conducting semiconductor layer) from the semiconductor material. If two differently contaminated semiconductor layers are combined, then a so-called p-n-junction results on the boundary of the layers [HBte].

In this thesis, we use silicon PV cells to attach to edges of LSCs to convert light into electricity. The reasons are because first over 95% of all the solar cells produced worldwide are composed of the semiconductor material Silicon; also as the second most abundant element in earth's crust, silicon has the advantage, of being available in sufficient quantities, and additionally processing the material does not burden the environment.

2.2.1 Band Gap

In semiconductors or insulators, electrons are confined to a number of energy bands, and forbidden from other regions. When an electron gains enough energy to participate in conduction, it is at a high energy state, or in conduction band. When the electron is bound, and thus cannot participate in conduction, the electron is at a low energy state, or in valence band. The band gap of a semicon-

ductor is the minimum energy required to excite an electron that is stuck in its bound state into a free state where it can participate in conduction. Band gap is the energy difference between the top of the valence band and the bottom of the conduction band[HBte].

When the band gap is met, the electron can break free of the valence bond, and excite into the conduction band and can therefore participate in conduction. A hole is created in the empty space where the electron used to be in the valence band. This hole also participates in conduction. Knowing the band gap is useful in PV applications as it allows us to understand how much energy is needed from the sun for conduction to occur, and for the ultimate generation of electricity in the devices. When the energy of a photon is equal to or greater than the band gap of the material, the photon is absorbed into the material and excites an electron into the conduction band.

In a semiconductor, even at room temperature, some electrons can be excited to the band gap, thus giving rise to electrical conductivity. Normal values of the energy of this band gap for semiconductors lie within the range of a few tenths of electron-volts to approximately 2eV, whereas for insulators these energies are significantly higher. Due to this energy gap, the most important characteristic of semiconductor is the so-called absorption edge. For wavelength λ , at which the photon energy $E = hc/\lambda$ is greater than the band gap, light is, depending upon the thickness of the materials, almost completely absorbed. However, For wavelength at which the photon energy is lower than the band gap, no absorption takes place [GH05].

2.2.2 Absorption Coefficient

While the band gap of the semiconductor material determines if a photon can be absorbed, the absorption coefficient determines how far into a material light of a particular wavelength can penetrate before it is absorbed, so it depends on

the material and also on the wavelength of light which is being absorbed. Semiconductor materials have a sharp edge in their absorption coefficient, since light which has energy below the band gap does not have sufficient energy to excite an electron into the conduction band from the valence band. Consequently this light is not absorbed [HBte].

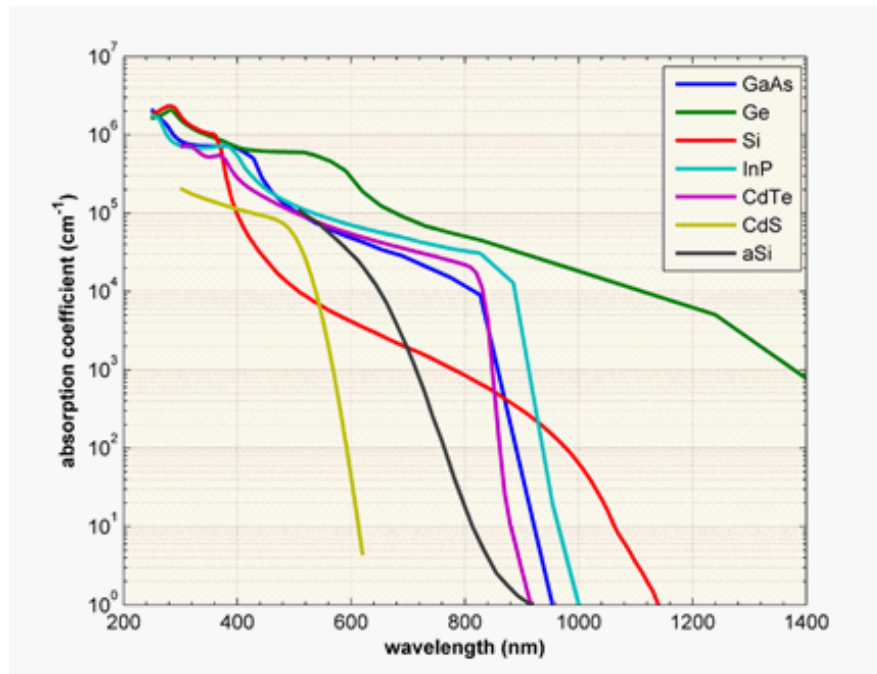


Figure 2.1: The absorption coefficient, α , in a variety of semiconductor materials at 300K as a function of the vacuum wavelength of light.

Fig. 2.1 [HBte] presents the absorption coefficient, α , in a variety of semiconductor materials at 300K as a function of the vacuum wavelength of light. Ge has the largest absorption coefficient for most of wavelengths since it is a direct band semiconductor. Silicon is an indirect semiconductor. In this case, the minimum of the conduction band and the maximum of the valence band lie at different crystal momentums.

Since absorption coefficients for different wavelengths are different, different wavelengths penetrate different distances into a semiconductor before most of the light is absorbed. The larger the absorption coefficients, the smaller the absorption

depth which gives the distance into the material at which the light drops to about 36% of its original intensity, or alternately has dropped by a factor of $1/e$. Since high energy light (short wavelength), such as blue light, has a large absorption coefficient, it is absorbed in a short distance (for silicon solar cells within a few microns) of the surface, while red light (lower energy, longer wavelength) is absorbed less strongly [HBte].

2.2.3 Quantum Efficiency

The “quantum efficiency” (Q.E.) is the ratio of the number of carriers (electrons or holes) collected by the PV cell to the number of photons of a given energy incident on the solar cell. The quantum efficiency may be given either as a function of wavelength or as energy. If all photons of a certain wavelength are absorbed and the resulting minority carriers are collected, then the quantum efficiency at that particular wavelength is unity. Because of the energy band gap, the quantum efficiency for photons with energy below the band gap is zero. A quantum efficiency curve for an ideal solar cell is shown in Fig. 2.2[HBte]. Quantum efficiency is usually not measured much below 350 nm as the power from the AM1.5 contained in such low wavelengths is low.

While quantum efficiency ideally has the square shape shown in Fig. 2.2, the quantum efficiency for most solar cells is reduced due to recombination effects.

The “external” quantum efficiency of a silicon solar cell includes the effect of optical losses such as transmission and reflection. Since it is often useful to look at the quantum efficiency of the light left after the reflected and transmitted light has been lost. “Internal” quantum efficiency is defined as the efficiency with which photons that are not reflected or transmitted out of the cell can generate collectable carriers. By measuring the reflection and transmission of a device, the external quantum efficiency curve can be corrected to obtain the internal quantum efficiency curve.

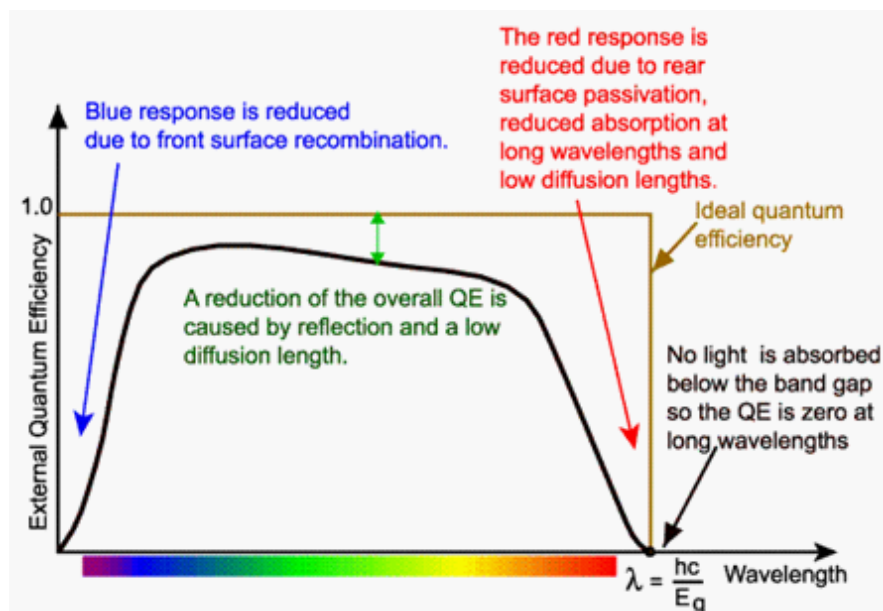


Figure 2.2: The quantum efficiency of a silicon solar cell. The square shape is for an ideal solar cell

2.2.4 Spectrum Response (SP)

The spectral response is conceptually similar to the quantum efficiency. The quantum efficiency gives the number of electrons output by the PV cell compared to the number of photons incident on the device, while the spectral response is the ratio of the current generated by the solar cell to the power incident on the solar cell. A spectral response curve is shown in Fig. 2.3 [HBte]. At short wavelengths below 400 nm the glass absorbs most of the light and the cell response is very low. At intermediate wavelengths the cell approaches the ideal. At long wavelengths the response falls back to zero.

Unlike the square shape of QE curves, the spectral response decreases at small photon wavelengths. At these wavelengths, each photon has a large energy, and hence the ratio of photons to power is reduced. Any energy above the band gap energy is not utilized by the solar cell and instead goes to heating the solar cell. The inability to fully utilize the incident energy at high energies and the inability to absorb low energies of light represents a significant power loss in solar

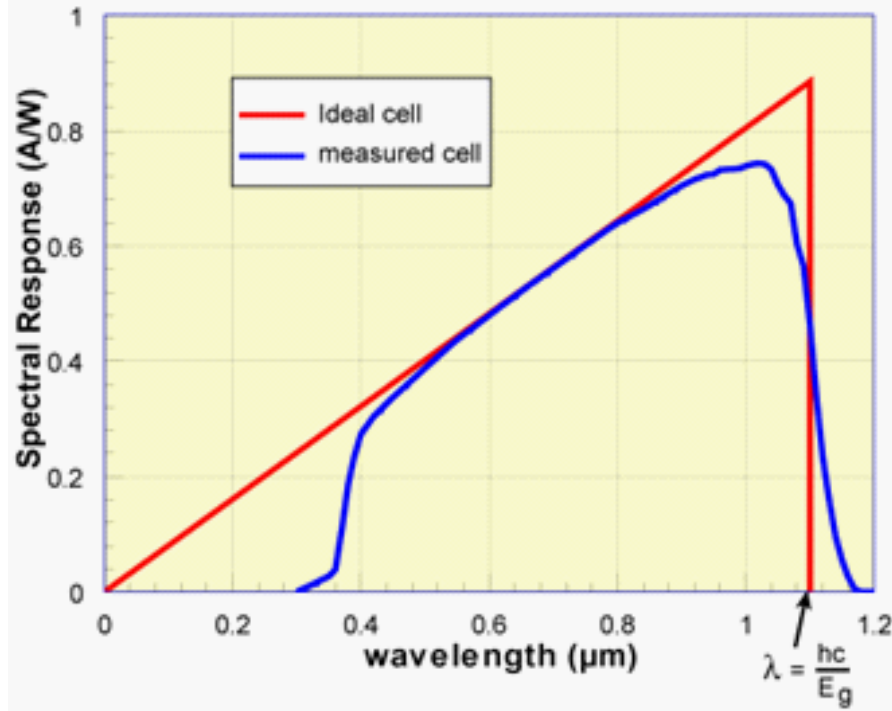


Figure 2.3: The spectral response (SP) of a silicon solar cell under glass.

cells consisting of a single P-N junction.

Spectral response is important since it is the spectral response that is measured from a solar cell, and from this the quantum efficiency is calculated. The quantum efficiency can be determined from the spectral response by replacing the power of the light at a particular wavelength with the photon flux for that wavelength. This gives

$$SR = \frac{q\lambda}{hc} \eta_{QE}. \quad (2.1)$$

From Fig. 2.3, we can see that the spectral response for silicon solar cells is higher for wavelengths in the range of 400nm to 1000nm. Luminescent dye materials can absorb light in short visible wavelengths of the solar spectrum, and emit light at long wavelengths through down conversion process [vS08]. This down-conversion process can generate more than one lower energy photons per incident high-energy photon [MR97], [MLU⁺00]. Based on this principle, it is shown that

the photocurrent density of LSC PV system is increased compared to a single solar cell of equal active area from about 8.5 up to $10mA/cm^2$.

In this thesis, we apply different luminescent dyes to down-shift the wavelengths where the spectral response of the solar cell is low to wavelengths where the spectral response is high to improve the power conversion efficiency of solar cells. It was reported that quantum dots with an emission at 603 nm increase the multi-crystalline solar cell short-circuit current by nearly 10 % [LMB⁺05, vSMS⁺05, Ric06].

2.2.5 IV curve

The IV curve of a solar cell is the superposition of the IV curve of the solar cell diode in the dark with the light generated current. For actual diodes, a diode equation is

$$I = I_0(e^{\frac{qV}{nkT}} - 1), \quad (2.2)$$

where n is ideality factor, which is a number between 1 and 2, and n typically increases as the current decreases. In real devices, the saturation current is strongly dependent on the device temperature [HBte].

A typical IV curve of a solar cell is presented in Fig. 2.4 [HBte]. When the voltage across the solar cell is zero, or the solar cell is short circuited, the current through the solar cell is short-circuit current. It is usually written as I_{sc} , the short-circuit current is shown on the IV curve. When the open circuit voltage V_{oc} is also shown in this figure.

The I_{sc} current is due to the generation and collection of light-generated carriers. For an ideal solar cell at most moderate resistive loss mechanisms, the short-circuit current and the light-generated current are identical. Therefore, the short-circuit current is the largest current which may be drawn from the solar cell. It occurs when the voltage across the device is zero. The open-circuit voltage is

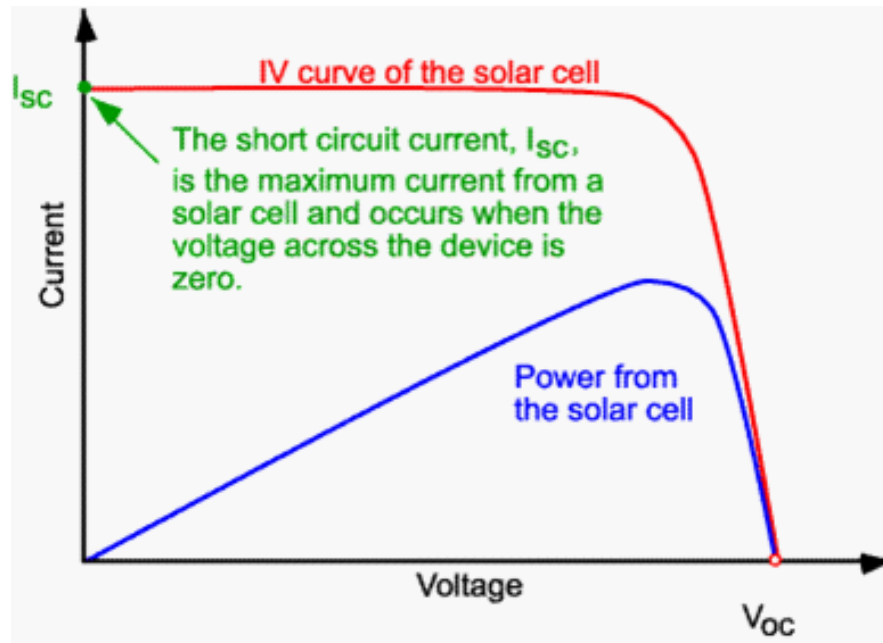


Figure 2.4: IV curve of a solar cell.

the maximum voltage we can obtain from a solar cell. The IV properties of solar cells are used to characterize properties of LSCs [KSB⁺07].

In our experiments, we tested the short-circuit current from PV cells [KSB⁺07] to characterize properties of LSCs. The value depends on a number of factors which are described below:

(1) The area of the solar cell. To remove the dependence of the solar cell area, it is more common to list the short-circuit current density (J_{sc} in mA/cm^2) rather than the short-circuit current.

(2) The number of photons (i.e., the power of the incident light source). I_{sc} from a solar cell is directly dependant on the light intensity.

(3) The spectrum of the incident light. For most solar cell measurement, the spectrum is the AM1.5 spectrum.

As shown in Fig. 2.4, the short-circuit current and the open-circuit voltage are the maximum current and voltage respectively from a solar cell. However, at both of these operating points, the power from the solar cell is zero. The “fill

factor”, more commonly known by its abbreviation “FF” or f , is a parameter which, in conjunction with V_{oc} and I_{sc} , determines the maximum power from a solar cell. The FF is defined as the ratio of the maximum power from the solar cell to the product of V_{oc} and I_{sc} . Graphically, the f is a measure of the “squaresness” of the solar cell and is also the area of the largest rectangle which will fit in the IV curve.

The efficiency of a solar cell η_{power} is defined as:

$$P_{max} = V_{oc}I_{sc}f, \quad (2.3)$$

$$\eta_{power} = \frac{P_{max}}{P_{in}} = \frac{V_{oc}I_{sc}f}{P_{in}}, \quad (2.4)$$

where V_{oc} is the open-circuit voltage; I_{sc} is the short-circuit current; η_{power} is the efficiency.

By detailed balance analysis, the maximum efficiency of photovoltaic devices can be calculated with the assumption that the mobility is infinite which allowing collection of carriers no matter where they are generated and complete absorption of all photons above the band gap. Fig. 2.5 shows the optimum PV cell efficiency as function of band gaps.

2.3 Solar Concentrators

By using solar concentrators to increase the power density of solar radiation, the cost of solar energy can be reduced [LA07]. This section presents image-forming concentrators and non-imaging concentrators [WMB⁺05]. LSC as one type of non-imaging concentrators, is described [SRWY90]. The theoretical limitations for both image-forming and non-imaging concentrators are analyzed to show the space for design of concentrators.

2.3.1 Image-forming Concentrators

The image-forming concentrators of conventional form include parabolic mirrors, lenses of short focal length [LBV11] and so forth. They take a large area

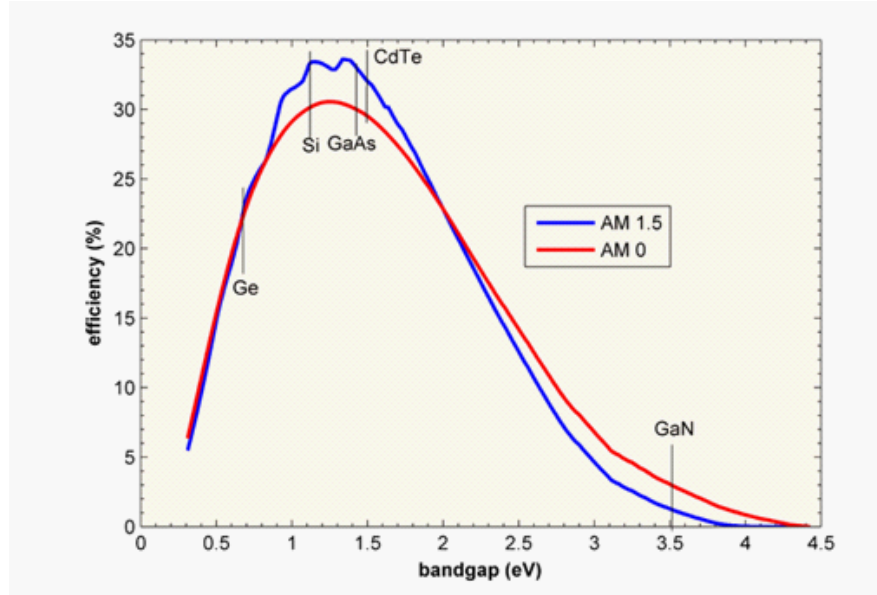


Figure 2.5: Limiting solar cell efficiency as a function of the material band gap for one-sun illumination. The calculations assume that the only recombination is radiative. In actual devices the efficiencies are lower due to other recombination mechanisms and losses in parasitic resistances.

of sunlight and direct it towards a specific spot by bending the rays of light and focusing them. From the sine law of concentration limit [WMB⁺05], whatever the theoretical possibilities, practical concentrators based on classical imaging-forming designs fall a long way short of the ideal.

The concentration limit of an image-forming concentrator such as a telescope disk absorber falls short of the fundamental limit by a factor of 4. The 2D or parabolic trough concentrators, which are straightforwardly generalized as a strip absorber rather than a disk absorber, fall significantly short of the sine law of concentration limit by a factor of 2 or π .

2.3.2 Non-imaging Concentrators

A Compound parabolic concentrator (CPC) is a prototype of a series of non-imaging concentrators that approach very close to being ideal and having the maximum theoretical concentration ratio. The structure of the compound parabola

concentrator (CPC) for planar absorber is shown in Fig. 2.6. The design is based on the edge rays [WMB⁺05], where a_1 and a_2 are the area of the absorber and the receiver, and the angle θ_i is the angle between the extreme ray of the beam and the axis of the concentrator.

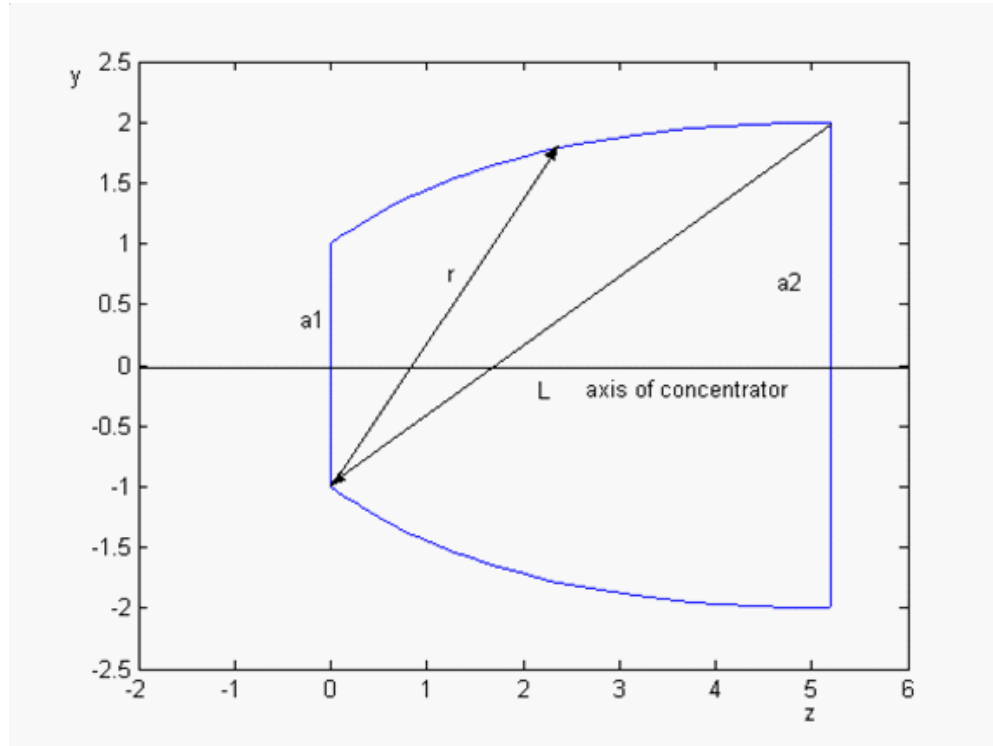


Figure 2.6: Structure of a 2D compound parabola concentrator (CPC) for planar absorber.

The concentration ratio for the 2D CPC for planar absorber shown in Fig. 2.6 is:

$$C = \frac{1}{\sin \theta_i}, \quad (2.5)$$

which is the maximum value of a solar concentrator. The absorber can be a cylindrical absorber, and is the absorber used in our solar cooling project in our group.

It can be seen that this CPC comes very close to being an ideal concentrator [WMB⁺05]. Also, it has the advantages of being a very practical design, easy to

make for all wavelengths, since it depends on reflection rather than refraction, and of not requiring any extreme materials properties. The only disadvantage is that it is very long compared to its diameter. This can be overcome if we incorporate refracting elements into the basic design. The CPC is the most efficient concentrator. For 3D, it that can approach the theoretical limit for concentrators:

$$C \leq \frac{n^2 \sin^2 \theta_2}{\sin^2 \theta_1}, \tag{2.6}$$

where C is the concentration factor, θ_1 and θ_2 are input and output angles at receivers respectively, n is the index of the materials. If diffuse light is to be concentrated, $\theta_1 = 90^\circ$, and therefore the maximum concentration is limited to n^2 which is about a factor of two for most available transparent materials [WMB⁺05].

2.3.3 Luminescent Solar Concentrators (LSCs)

For solar concentrators based on lens and mirrors with tracking systems, they can only concentrate direct light very effectively. As a result, the applications of these concentrations are limited in the morning and in the afternoon and in cloudy days. LSCs can concentrate both direct light and diffuse light, which make them especially useful in these situations. The configuration is shown in Fig. 1.2.

For LSCs, the maximum concentration of the fluorescent concentrator has been determined by Yablonovitch and Smestad et al [Yab80, SRWY90]. They pointed out that the concentration factor is determined by:

$$C \leq \left(\frac{\nu'}{\nu}\right)^2 e^{\frac{h(\nu-\nu')}{kT}}, \tag{2.7}$$

where ν and ν' are frequency of absorbed and emitted light respectively. The maximum concentration C of the system depends sensitively on the Stokes shift, which gives a potential of huge increase! The factor $(\nu'/\nu)^2$ arises as a correction factor because etendue is related to the four-dimensional Poincaire' invariant, not full six-dimensional phase space [WMB⁺05].

For the power conversion efficiency, as discussed in Chap. 1, it is much lower than the above theoretical predicted value [Rei10]. The energy loss that we need to consider is:

(1) The absorption efficiency of luminescent materials, η_{abs} , due to its absorption spectrum with respect to the solar spectrum. This is determined by the fraction of the solar spectrum absorbed by the dye. Practically all dyes absorb only part of the solar spectrum. It is possible to incorporate more than one dye into a collector, leading to a stack of absorption and reemission [TBBD10];

(2) Quantum efficiency (QE) of luminescent materials, η_{QE} ;

(3) Efficiency of light trapping by total internal reflection. It increases with increasing refractive index of the collector material. In practice they are only little difference of available materials [ESMEB⁺03, BMH99, KBD09, PP91].

New progresses in materials as well as theoretical advances are made recently.

2.4 Luminescent Materials

Sunlight that is incident on the front surface of a luminescent solar concentrator (LSC) is absorbed and subsequently re-emitted by luminescent materials. The resulting luminescence is transported to the edge of the LSC sheet and concentrated onto photovoltaic devices. Despite its potential for generating low-cost solar power, LSC development faces numerous challenges, the majority of which are related to the luminescent materials used in their design. Earlier LSC research focused on organic dyes, and while several of the shortcomings with these materials have been solved over time, some major challenges remain. Recently new progress in materials is focusing on new nano-structured luminescent materials such as quantum dots [Row07]. In this section, some basics on these materials are reviewed.

As we focus on the application of LSCs for silicon PV cells, the requirements for the luminescent materials to maximize LSC performance with Si solar cells are

(1) Absorption of all wavelengths with wavelength less than 950nm with high absorption coefficients and an emission peak 1000nm; (2) Minimum re-absorption losses due to overlap of absorption and emission spectra; (3) Near-unity fluorescence quantum yield (FQY); (4) Long-term outdoor stability. Nano-structured quantum dots materials are one of the available luminescent materials [RWR08].

Quantum dots as luminescent materials, are semiconductors whose electronic characteristics are closely related to the size and shape of the individual crystal [Noz10, SJL⁺10, GLS⁺11]. Typically, they are represented as small clusters of several hundred atoms with a diameter of 5 nm or less. The small physical dimensions of quantum dots act to restrict the wave function of electrons and holes. This is known as quantum confinement and it acts to increase the energy of electrons and holes located inside the quantum dot. Researchers have studied quantum dots [ZMGN98] in transistors, solar cells, LEDs, and diode lasers. They have also investigated quantum dots as agents for medical imaging and hope to use them as qubits.

Applying particle in a box model (also known as the infinite potential well), the energy levels are discrete and are determined by the size of the particle L :

$$E_n = \frac{n^2 h^2}{8mL^2} \quad (2.8)$$

where m is the mass of the particle, and h is the Plank's constant, and $n = 1, 2, \dots$ is the quantum number of the energy level.

Some quantum dots are small regions of one material buried in another with a larger band gap. These can be so-called core-shell structures, e.g., with CdSe in the core and ZnS in the shell [vSFVdH⁺01]. These QDs absorb and emit light in visible wavelengths, and have been studied as luminescent materials for the applications in LSCs [vSBS⁺08], and have shown the photo oxidation and photon bleaching effects [BCL⁺11, KSB⁺07, BCL⁺11]. Other nano-structured materials including nanorods are in development [JLK09, BKY⁺07].

Due to quantum confinement, different sized quantum dots have different

energy band gap [SLS⁺11]. As a result, the absorbed wavelengths by the quantum dots at different sizes will be different. Correspondingly, the wavelengths of emit light will be different. Tuning the size of the quantum dots, we can tune optical properties of quantum dots. As shown in Fig. 2.7, quantum dots absorb light at shorter wavelength, and then emit light at longer wavelength.

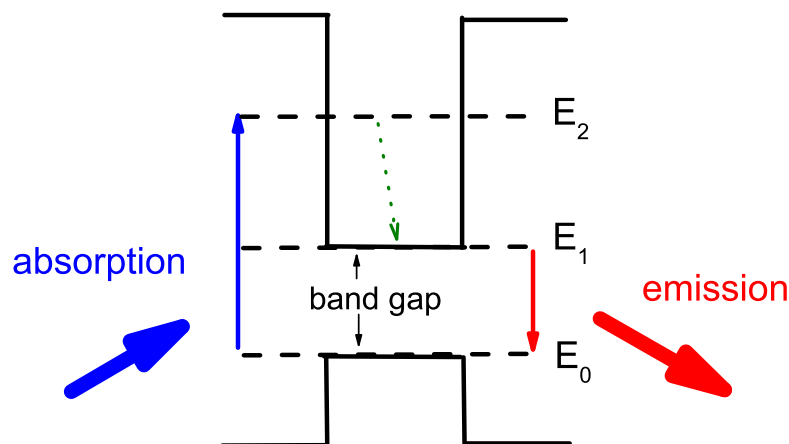


Figure 2.7: Quantum dots absorb light at shorter wavelengths, and then emit light at longer wavelengths. The difference of the absorbed and emitted wavelengths depends on the band gap of the dots which can be tuned by the size distribution of the dots.

A quantum yield [S JL⁺10] of 300 percent for 2.9nm diameter PbSe (lead selenide) quantum dots is reported when the energy of the photon absorbed is four times than that of the band gap [Noz05]. This multiple excitons generation start to form as soon as the photon energy reaches twice the band gap. Quantum dots made of lead sulfide (PbS) also showed the same phenomenon [TPS⁺11, EBJ⁺05]. Our research on characterizing quantum dots as luminescent materials for LSCs focus on near infrared PbS quantum dots and the visible CdSe/ZnS quantum dots.

2.5 Liquid Crystals as Matrix Materials

This section presents basic properties of liquid crystal materials and the technologies of characterizing their properties. Liquid crystal can be considered as

matrix materials for LSCs if they are transparent and with high refractive index. More details will be shown in Chap. 5.

2.5.1 Liquid Crystal

Liquid crystal or a liquid crystal phase is a state of matter that has properties between those of a conventional liquid and those of a solid crystal [CH97]. For example, an LC may flow like a liquid, but its molecules may orient in an ordered way. It is an ordered fluid phase with some degree of anisotropy. Liquid crystals are widely used in liquid crystal displays, but in fact the kind of liquid crystal used in such displays represents a small subgroup of the family of liquid crystal phases and materials. In this thesis, we show another application of liquid crystal materials for solar energy collections. They can be used as matrix materials in luminescent solar concentrators for improving LSC trapping efficiency [VKH⁺09, MRV⁺10].

Thermotropic phase is one of Liquid crystals. As temperature changes, the thermotropic liquid crystals exhibit a phase transition into the LC phase. In this phase, the order of the molecules can be forced to a certain direction by applying an electric field or with the help of a specific coating. The order of these molecules can be further fixed by shining with UV light.

Due to the orientational preference of the molecules in a liquid crystal, materials in a liquid crystal phase show birefringence. This birefringence originates from bulk anisotropy. As a result, the refractive index of materials has different values in different directions. A non-polarized monochromatic light ray passing into materials in the liquid crystal phase can be resolved into two components with orthogonal polarization directions. As each of these rays will experience a different refractive index, one will travel faster than the other, creating a phase difference between the two.

One of the most common liquid crystal phases is the nematic phase. In the nematic phase, rod-shaped molecules of the liquid crystal material do not

have position order, but they self-align to have short-range directional order with their long axes roughly parallel. Thus, the molecules flow freely and their mass positions are randomly distributed as in a liquid. However, the molecules maintain their long-range directional order. Most nematics are uniaxial. They have one axis that is longer and preferred, with the other two being equivalent. A schematic of molecular nematic phase is shown in Fig. 2.8 [Keb02].



Figure 2.8: Schematic of mesogen alignment in a liquid crystal nematic phase. .

2.5.2 Polarized Optical Microscopy

Polarized optical microscopy is one of the most powerful and simple techniques in characterizing materials in the liquid crystal phase [Wea03, VVSL⁺11].

As we know, if electric field vectors of light are restricted to a single plane by filtration, then the light is said to be polarized with respect to the direction of propagation and all waves vibrate in the same plane. If light is incident on crossed polarizers, it can not propagate shown by Fig. 2.9. However, if samples with birefringence are put between the two polarizers, we may see differently.

Utilizing the birefringence properties of materials in the liquid crystal phase, we can characterize the alignment of molecules with polarized optical microscope.

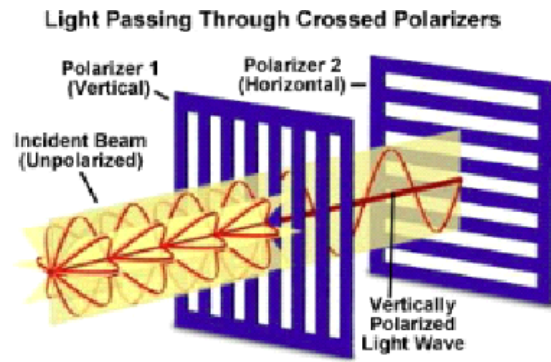


Figure 2.9: Light passing through crossed polarizers appears dark.

The configuration of a polarized optical microscope is shown in Fig. 2.10[RD11], .

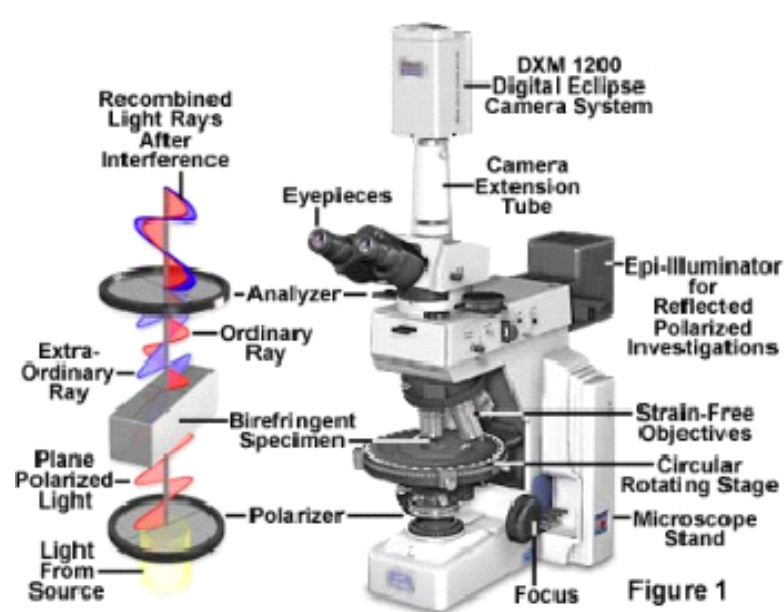


Figure 2.10: Configuration of polarized optical microscope. Light from source becomes polarized after passing through the first polarizer, and is delayed and refracted by the tested birefringent specimen for different wavelengths. The generated extra ordinary and ordinary rays pass through the analyzer and recombine after interference.

The working process of the polarized optical microscopy is as follows:

(1) Light from an incandescent source is passed through a polarizer, so that all of the light getting through must vibrate in a single plane. The beam is then

passed through a prism that separates it into components that are separated by a very small distance - equal to the resolution of the objective lens.

(2) The beams pass through the condenser, then the specimen. In any part of the specimen in which adjacent regions differ in refractive index the two beams are delayed or refracted differently.

(3) When they are recombined by a second prism in the objective lens, there are differences in brightness or responding to differences in refractive index or thickness in the specimen.

We may see different colors from polarized microscopy from a sample material in the liquid crystal phase because different wavelengths from the source are retarded by different amounts on passing through the sample. If we raise the temperature of the sample, the sample will change its phase from liquid crystal to the isotropic liquid phase and there is no birefringence of the bulk material; we will see dark from the microscopy.

Samples for characterization are often prepared between glass plates (or another substrate), liquid crystal molecules may orient themselves with a planar (homogeneous) alignment (the molecular long axis lies parallel to the substrate), or with a homeotropic (vertical) alignment (the molecular long axis lies perpendicular to the substrate). Specific coatings can be applied to the glass to achieve the desired alignment. From polarized optical microscopy, the nematic phase with a homeotropic alignment will result in an optically isotropic phase and will appear black. For a planar alignment, however, the anisotropy of the phase becomes apparent and we see the defect texture [Hir12].

2.5.3 Differential Scanning Calorimetry

Differential scanning Calorimetry (DSC) is a thermal characterization technique which is often used to identify and study phase transitions. Differential scanning calorimeters measure the difference in the amount of heat required to

increase the temperature of a sample and reference as a function of temperature. Through the testing, the sample materials and the reference materials are maintained at nearly the same temperature. This technique was developed by E. S. Watson and M. J. O'Neill in 1962 [O'N64]. This technique is particularly valuable in liquid crystal materials as it assists in the accurate measurement of transition temperatures for different phases [Hir12].

If the instrument is calibrated correctly, for a material that exhibits no thermal phase transitions, this heat-flow curve will be a flat line. Since there is a sudden change in heat flow into the sample to maintain the temperature, extra heat is either required for the phase transition to take place or heat is released by the transition. This change is measured as a deviation from the baseline heat flow curve, either a peak (for an endothermic process), a trough (for an exothermic process) or perhaps a more subtle change, such as a change in slope (typical for the polymer glass transition) [Hir12]. Fig. 2.11 shows the DSC instrument we used in Professor Linda Hirst's lab at UC Merced.



Figure 2.11: DSC we used in Professor Linda Hirst's lab at UC Merced.

Fig. ?? presents typical results of DSC calibration for liquid crystals. There are two peaks in the heating process and one peak in the cooling process, which

means that there are phase changes for the material if the temperature of the material rises from 5°C to 100°C . The specific phase sequence needs to be verified by optical microscopy.

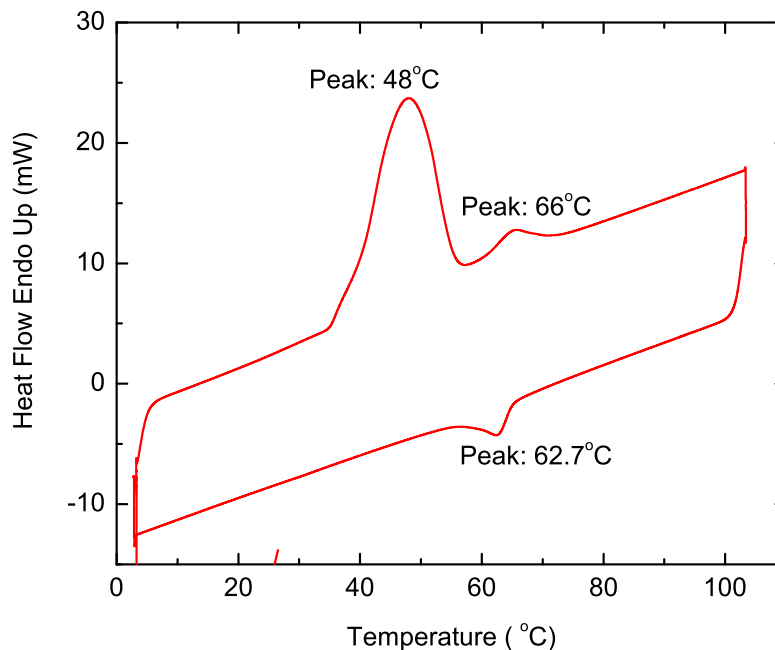


Figure 2.12: A typical result of DSC calibration for liquid crystals.

2.6 Spectroscopy

When light passes through a sample or is reflected from a sample surface, the intensity of the beam is attenuated. Spectroscopy is the measurement of this attenuation. We can do absorption measurements for one wavelength or over an extended spectral range. UV-Vis spectroscopy is usually applied to molecules in solution in a cuvette. This is very useful for characterizing materials such as pigments, coatings, windows, and filters [BMH99, CH97].

We use Perkin-Elmer Lambda 35 UV/VIS spectrophotometer for the absorption and transmission testing. This is a double-beam instrument, meaning that the monochromarized lamp output is split into two beams, one beam pass-

ing through the sample cell of the sample compartment and the other through the reference cell of the sample compartment. The instrument then calculates the ratio between the intensity of light after passing through the sample cell and the intensity after passing through the reference cell. The base ten logarithm of this ratio gives the absorbance of the sample.

We use Perkin Elmer LS 55 luminescence spectrometer or fluorimeter for the emission testing. It consists of a xenon lamp producing broadband UV- VIS excitation light, an excitation monochromator that selects a narrow frequency range of light produced by the lamp, a sample holder that contains the sample to be measured, optics to collect the light emitted by the sample, an emission monochromator that selects a narrow frequency range of the light emitted by the sample, and a photomultiplier that detects the intensity of the emitted light. During the emission testing, the wavelength of the light emitted by the sample is scanned. The transmission ability of the samples is also tested by using PV cells.

The difference between the fluorimeter and the spectrophotometer is that this apparatus' beam does not scan through different wavelengths. Instead, it uses a constant wavelength to excite the sample. The wavelength that is used to excite the sample will be equal to the peak absorption wavelength for that particular sample.

Fig. 2.13 presents a typical absorption (Abs.) and emission (Em.) spectra of organic Lumogen Red F 305 dye material in toluene solvent. The transmittance is also taken for the same dye materials but embedded in PMMA plastic materials as thin film LSCs shown in Fig. 2.14.

The corresponding emission spectrum of Lumogen Red F 305 dye in PMMA thin film shown in Fig. 2.15 shows that the wavelength of the peak emission is 618nm, which is about 20nm of red shifting from the emission spectrum in liquid toluene solvent.

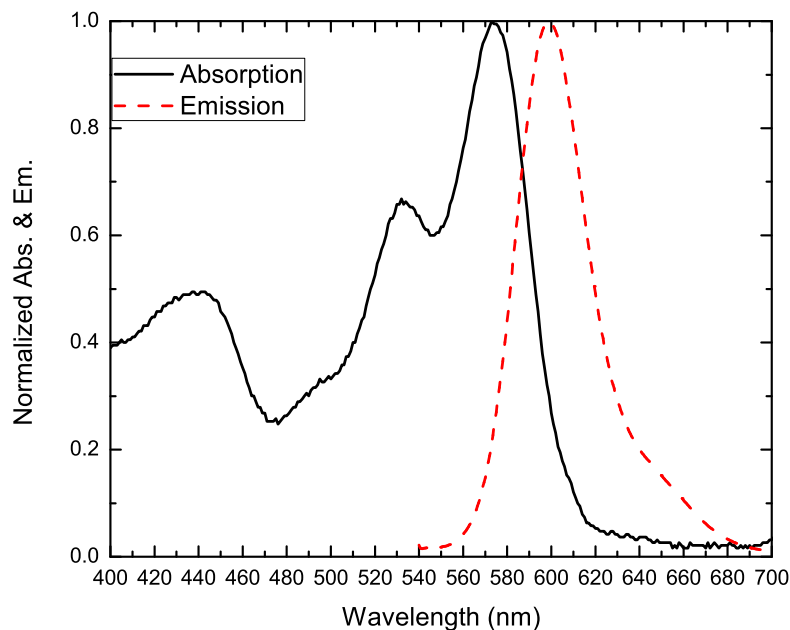


Figure 2.13: A typical absorption (Abs.) and emission (Em.) spectra of organic Lumogen Red F 305 dye material in toluene solvent.

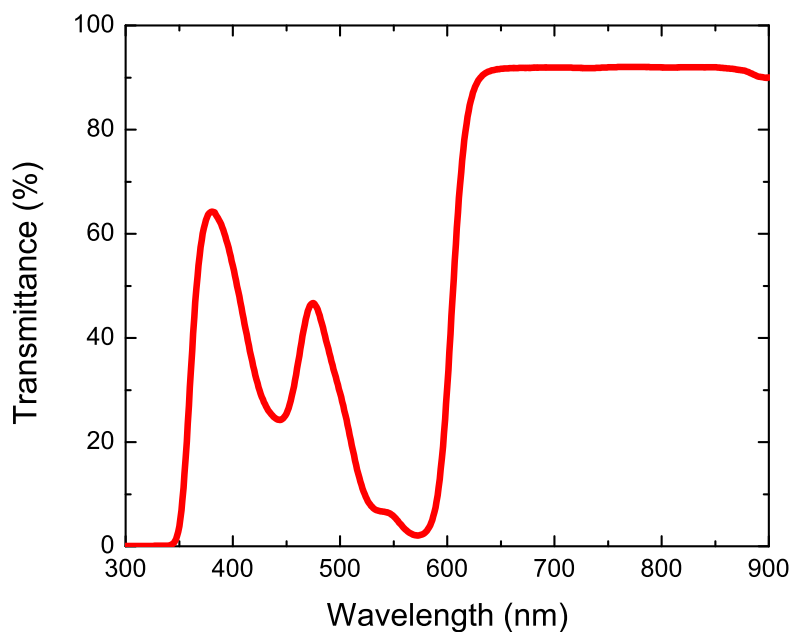


Figure 2.14: The transmittance of Lumogen Red F 305 dye PMMA thin film LSCs.

2.7 Summary

In this chapter, a detail description of PV technologies is given with the emphasis on power conversion properties of PV cells. We showed that by applying

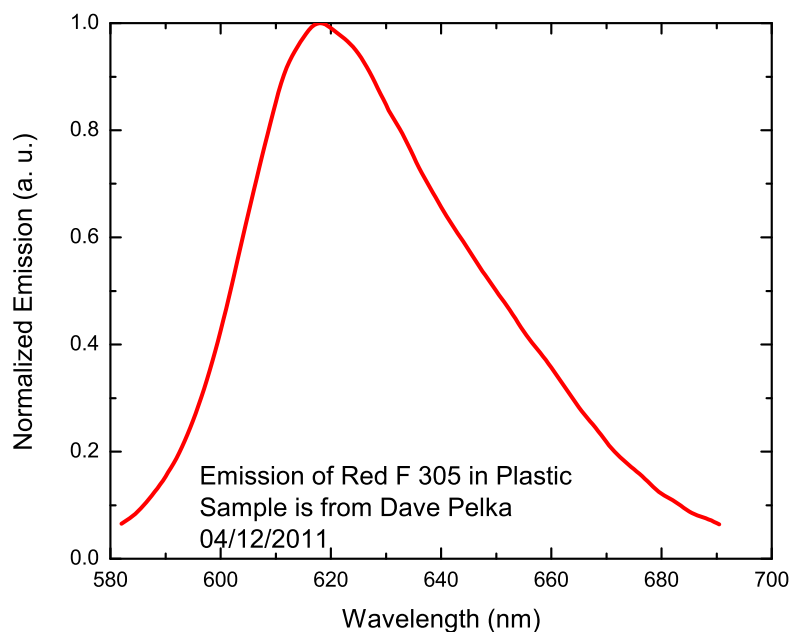


Figure 2.15: The normalized emission spectra of Lumogen Red F 305 dye PMMA thin film LSCs.

solar concentrators, efficiencies of PV cells can be dramatically improved, and the cost of the converted energy can be greatly decreased. After briefly describing properties of image-formed solar concentrators and nonimaging solar concentrators, theoretical concentration limitations for both of them, especially for LSCs are analyzed with the purpose of showing that there is a great design space for LSCs in improving their power conversion efficiencies. In this chapter, properties of quantum dots as a promising luminescent material for LSCs are described. Liquid crystal materials as matrix materials for new generation LSCs are illustrated. Finally, some experimental characterization techniques are described.

Chapter 3

Near Infrared Quantum Dot Luminescent Solar Concentrators

3.1 Introduction

A Luminescent Solar Concentrators (LSC), as one of the non-imaging solar concentrators [SRWY90], has the great potential in reducing the cost of solar energy by reducing the materials cost, reducing infrastructure and time needed for manufacturer, and improving the power conversion efficiency of PV cells. The LSC is the only known concentrator that can achieve high values of concentration factor without tracking the Sun. However, the development of LSC was limited by the stringent requirements on the dye materials. Due to self absorption and poor stability of luminescent materials [Rei10], as we know to date, the reported highest power conversion efficiency is 7.1 % [SBB⁺08].

In order to further improve the power conversion efficiency, it is very important to identify proper luminescent materials. Nanostructured materials including quantum dots (QDs) have the potential to further improve the efficiency and reduce the cost of PV [Noz10, CBB⁺04]. These nanoscale structured materials include QDs [Noz10, vSBS⁺08] and nanorods [JLK09, JK11]. If we seed QDS into

transparent plastic or liquid materials, we can make QD LSCs. These LSCs can utilize novel nano-scale quantum structured technology to render the concept of fluorescent dye solar concentrator a practical proposition.

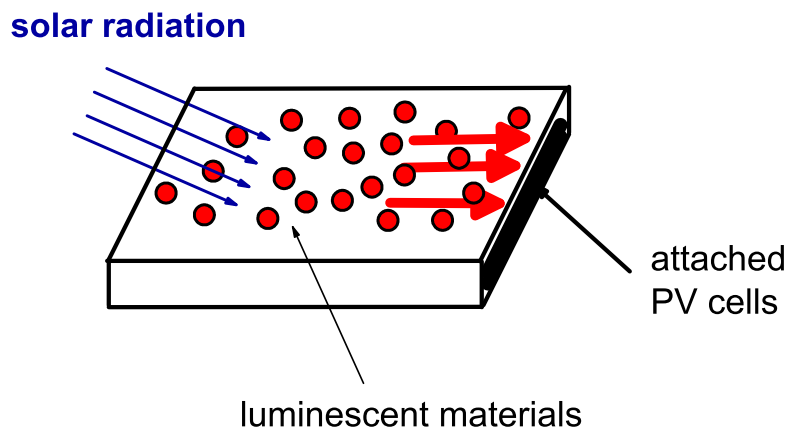


Figure 3.1: A schematic representation of a LSC PV system. Solar radiation is absorbed by luminescent materials integrated in a thin, flat-plate transparent waveguide materials (Glass, PMMA). Photons re-emitted by luminescent materials are guided to solar cells attached to the edge of the LSC. Quantum dot LSCs are LSCs with quantum dots as luminescent materials.

As shown in Fig. 3.1, the quantum dot LSC(QDLSC) comprises quantum dots (QDs) seeded in materials such as plastics and glasses that are suitable for incorporation into building facades. PV cells attached to the edges convert the concentrated light into electricity for use in buildings. Sunlight (isolation) incident on the surface of the concentrator is partly refracted into the luminescent materials, and after absorption by QDs, photons are re-emitted isotropically at a lower frequency. Since the refractive index of the doped layer is considerably higher than that of the external medium, for example air, a large proportion of the emitted photons can be trapped within the plate and transported by total internal reflection to the edges. Reflective mirrors can be further mounted on three of the edges and on the back surface, so light can only emerge along the fourth edge where it is absorbed by PV cells.

Applying QDs as luminescent materials for LSCs has the following advan-

tages: (1) High luminescence quantum yield can be achieved in QDs at room temperature; (2) Absorption threshold can be tuned simply by choice of dot diameter; (3) Red shift between absorption and luminescent is determined primarily by the spread of dot size [BMHO00], which in turn can be optimized by choice of growth conditions [GLS⁺11]; (4) Re-absorption therefore can be minimized and high efficiencies and high concentration ratios can be achieved; (5) Degrade less than organic dyes as they are crystalline semiconductors. QDs PV would theoretically be cheaper to manufacture, as they can be made “using simple chemical reactions”.

Quantum dots have recently become commercially available in sufficient purity and quantity and have not been previously studied for fully integrated LSC applications [Red08, SLS⁺11], especially the near infrared quantum dots [KMDN09].

In the future, near infrared (NIR) QDs might be the ideal luminescent materials for QD LSC devices as their broad spectral absorptions and the possibility of multi exciton generation (MEG) [Noz10]. Also, the QD LSC devices are compatible with existing screen-printing and mass manufacturing lines with sufficient lifetime and efficiency to enable rapid development by manufacturers.

In this chapter, we first describe the experimental fabrication and testing process in Sec. 3.2, and then focus on characterizations of the fabricated samples. The characterization for spectral properties of the near infrared QDs, visible QDs and organic dyes as possible luminescent materials is given in Sec. 3.3. This spectral comparison will show the potential efficiency improvement by the near infrared QDs. Due to the re-absorption of the luminescent materials, there should be an optimal concentration for the seeded quantum dots. Manufacturing LSCs at the optimal concentration, we will get the maximum power output. In Sec. 3.4, we study the effects of the dye concentration on the output efficiency, and give the optimal concentration for each luminescent material in fabrication. In Sec. 3.5, the re-absorption problem for each luminescent material is characterized by the peak emission wavelength red shift testing. For samples fabricated at their

optimal concentrations, we electrically characterize and compare their electrical output in Sec. 3.6. The stability of output power from the near infrared QDs are issued and further characterized in Sec. 3.7. The fabrication of thin film QD LSCs and the efficiency improvement by optical design are described in Sec. 3.8. We finally conclude our research on the near infrared QD LSC for PV systems in Sec. 4.9.

3.2 Fabrication and Characterization Process

In this section, we describe properties of QDs we used in our experiments, including near infrared quantum dots and visible quantum dots. The organic laser dyes will also be given for a comparison study. Furthermore, the fabrication and testing process will be explained in detail. Finally, properties of the light source and the solar cells as detectors will be given.

3.2.1 Luminescent Materials and the Fabrication Process

In experiments, we selected the near infrared PbS QDs and the visible CdSe/ZnS QDs for the prototype. They are dispersed in toluene, and are provided by the Evidot vendor, as show in Fig. 3.2. The core lead sulfide QDs have the size/diameter 2 to 6nm, emit at the wavelengths in near infrared. The core shell CdSe/ZnS QDs have the size/diameter 4 to 6nm, and emit at visible wavelength. The low concentration samples for concentration study are obtained by diluting the respective stock solutions. Rhodamine B, which has been known as a high quantum yield laser dye, is dissolved in ethylene glycol at different concentrations for comparison study as shown in Fig. 3.3. These luminescent materials in liquid solutions are encapsulated in glass (quartz) boxes to efficiently hinder oxygen diffusion.

The size of the glass box is approximately $45\text{mm} \times 12\text{mm} \times 4\text{mm}$. The geo-



Figure 3.2: The near infrared PbS QDs (Right) and the visible CdSe/ZnS QDs (Left) for prototyping of LSCs provided by the Evidot vendor. They are dispersed in toluene.



Figure 3.3: Rhodamine B, as a high quantum yield laser dye, dissolved in ethylene glycol for comparison study at different concentrations.

metric gain G is $G = A_{top}/A_{detector}$, where A_{top} is the area of the LSC illuminated by the light source, and $A_{detector}$ is the area of the collecting edges. For our samples, $G = 10$. It represents a good balance between high geometric gain and high optical efficiency [Bat81].

The Optical efficiency is measured by using a white light-emitting diode (LED) and solar simulator. High efficiency silicon PV cells from Sun Power are used. The set up is shown in Fig. 3.4.

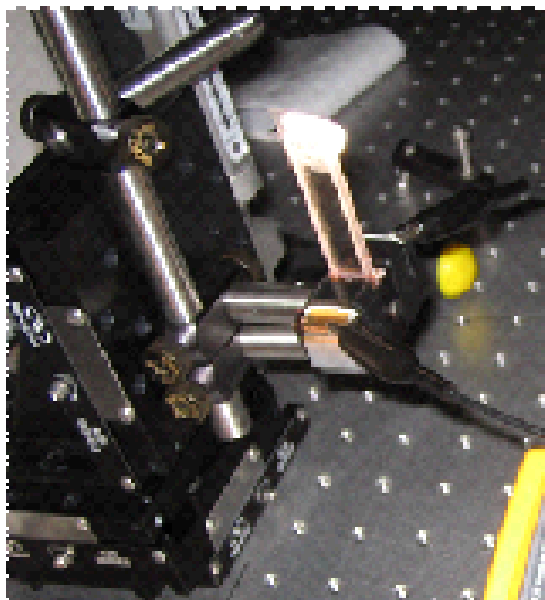


Figure 3.4: A LSC electrical characterization setup in the lab. The near infrared PbS QDs in toluene are filled in the glass box. Light shines the sample from the front surface. The PV cell is attached at the bottom short edge of the fabricated QD LSCs. Fluke multi-meter is used for reading the output open circuit voltage and the short circuit current.

The steady-state absorption and photoluminescence spectra are taken with UV-Vis spectrometers.

The re-absorption properties are characterized by recording the output spectrum distributions from the edge surface of the LSC sample when we move the position of the point that the laser shines on.

3.2.2 Solar Simulator Spectrum

A solar simulator is used for characterization. Fig. 3.5 shows the normalized spectrum distribution of the solar simulator we used on our lab.

The power output of the solar simulator is about a tenth of one sun. We tested the power output when we shine light on it from a piece of high efficiency silicon PV cell. Second, we tested the power output from the same PV cell under direct one sun. From these tested values, we calculated the power output ratio.

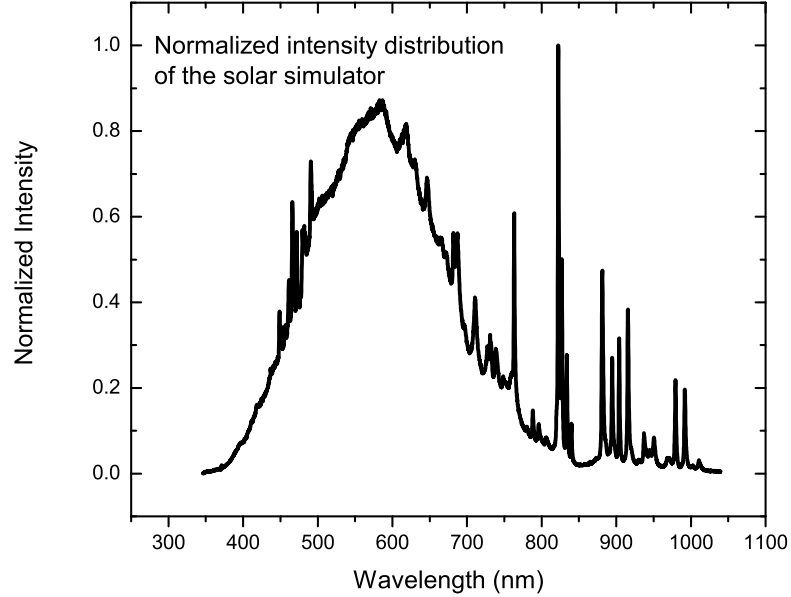


Figure 3.5: Normalized intensity distribution of the solar simulator we used in the lab.

During the test, we also verified that the output power of the PV cell can be considered as linearly relating to the input solar radiation, so for our tests, up to one sun input, the higher the input solar radiation, the higher the power output.

3.2.3 Solar Cells as Detectors

We used a solar cell as a detector for the electrical characterization of LSC concentration factors. The solar cell is provided by SunPower Company, as shown in Fig. 3.6. The efficiency of this PV cell is characterized by one-sun solar simulator as shown in Fig. 3.7, and the current voltage curve tracer is recorded with the fill factor $f = 0.72$ and efficiency $\eta_{PV} = 18\%$ from Fig. 3.8.

3.3 Optical Characterization

It is very important to spectrally characterize the absorption and emission wavelength ranges of the luminescent materials to know the response of the mate-



Figure 3.6: The solar cell as a detector for the electrical characterization of LSC concentration factors. It is produced by SunPower Company. The left and right sides are two electrodes.

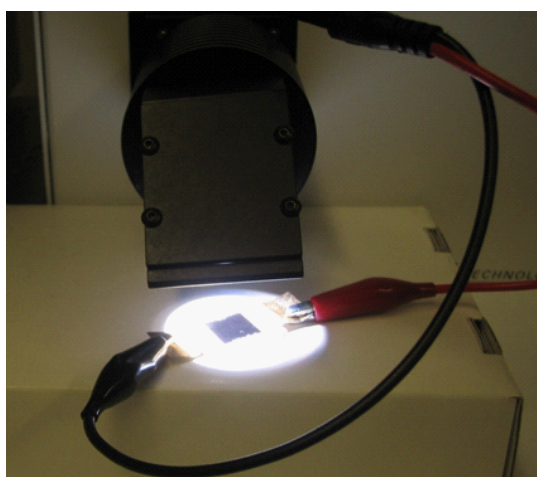


Figure 3.7: The efficiency of the solar cell used as a detector is characterized by one-sun solar simulator.

rials to solar spectrum and to study further the re-absorption properties of these materials. In this section, we characterize the absorption and emission properties of the near infrared PbS QDs at different concentrations, and then compare with the absorption properties of the visible CdSe/ZnS QDs and the organic dyes.

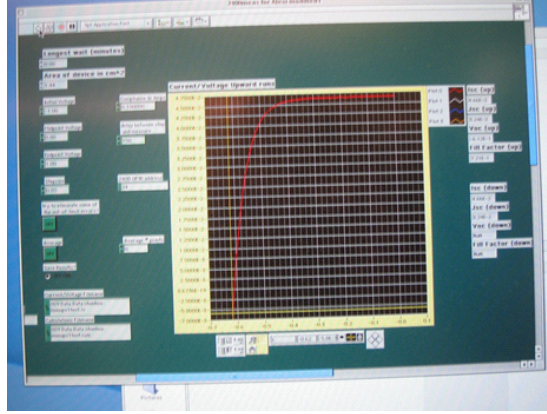


Figure 3.8: The current voltage $I - V$ curve is recorded for the PV cell as a detector. The test results show that the fill factor of this PV cell is 0.72, and the calculated solar cell efficiency is 18%.

3.3.1 Absorption Properties

Using a UV-Visible Perkin-Elma spectrometer, we measured the absorption spectra of the near infrared PbS QDs in toluene solution. UV/Vis spectrophotometer that measures the intensity of light passing through a sample (I), and compares it to the intensity of light before it passes through the sample (I_o). The ratio I/I_o is called the transmittance, and is usually expressed as a percentage ($\%T$). The absorbance, A , is based on the transmittance:

$$A = -\log \frac{\%T}{100\%}. \quad (3.1)$$

The testing result is shown in Fig. 3.9. It gives the absorption properties of near infrared PbS QDs in toluene at different concentrations. These concentrations are $10\mu M$, $30\mu M$, $50\mu M$, $70\mu M$. They are diluted from $193\mu M$ from the vender. From this figure, we can see that the absorption range of the PbS QDs is very wide over the solar spectrum. They absorb wavelength up to 900nm. From the inset, we can see that the higher the concentration of the solution, the stronger the absorption abilities of the solution. The peak emission centers at 750nm.

For each concentration, the absorbance at the peak emission wavelength is a function of the concentration. We show this relationship in Fig. 3.10. We know

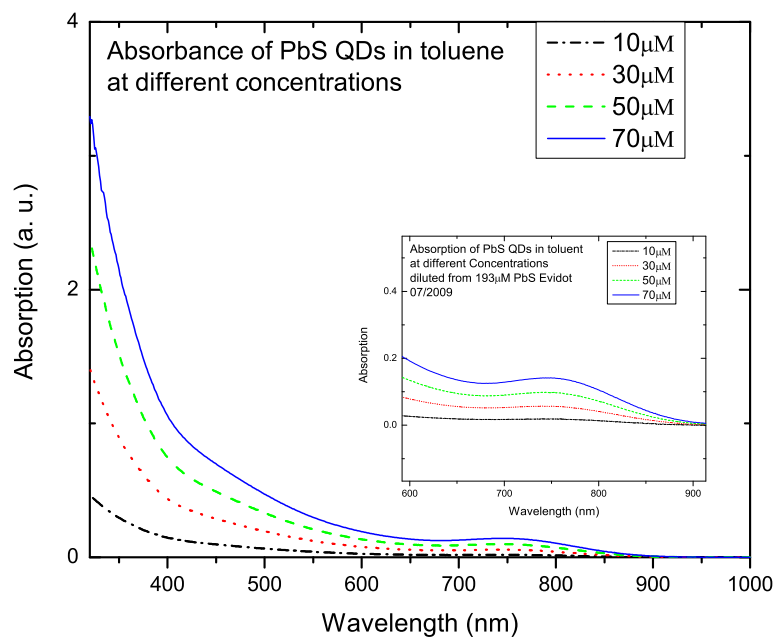


Figure 3.9: The absorption properties of near infrared PbS QDs in toluene at different concentrations: at $10\mu M$, $30\mu M$, $50\mu M$, $70\mu M$ respectively. The peak absorption wavelength centers at 750nm . The inset shows that the higher the concentration, the stronger the absorption.

that the absorbance is a function of the PbS molar absorptivity (L/mol/cm) ε , the path length of the sample b , and the concentration of the PbS QDs in solution (mol/L). In our experiments, for the same luminescent material, the thickness of the glass box in which the sample is contained (cm) is fixed. So the absorbance is linearly related to the concentration of the PbS solution. The linear relationship between concentration and absorbance is both simple and straightforward, which is why people often use absorbance as a measure of the absorption rather than $\%T$.

Using the same method, we tested the absorption performance of the visible CdSe/ZnS QDs at different concentrations. The results are shown in Fig.3.11.

The peak emission centers at 620nm . We can see that the higher the concen-

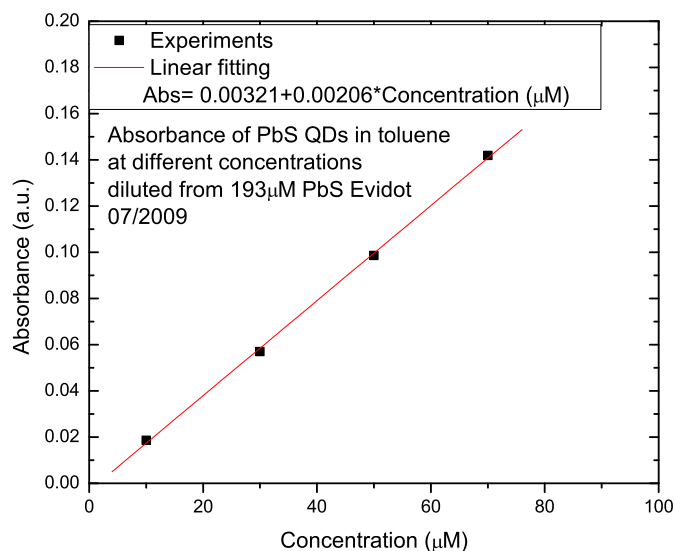


Figure 3.10: Absorbance of PbS Quantum Dots in toluene at the peak emission wavelength as function of the concentration. The tested concentration values are $10\mu\text{M}$, $30\mu\text{M}$, $50\mu\text{M}$ and $70\mu\text{M}$ (Square). The solid line is the fitted result, which clearly shows the linear relationship.

tration, the stronger the absorption. Also, the absorbance of the CdSe/ZnS QDs samples at the peak emission wavelength 620nm as a function of the concentration is given in Fig. 3.12, with the comparison to the PbS QDs.

Fig. 3.12 shows that for the same absorption, a much higher concentration of PbS QDs is required. Since the same glass box is used in the test, the path length b is the same, however, the extinction coefficient for CdSe/ZnS QDs is much higher than PbS QDs.

3.3.2 Emission Properties

To further characterize the emitting properties of the near infrared PbS QDs, we tested their luminescent emission spectral properties. The result is shown in Fig. 3.13 for $50\mu\text{M}$ PbS LSCs.

Exciting the sample with wavelengths at 500nm, 600nm, 700nm respec-

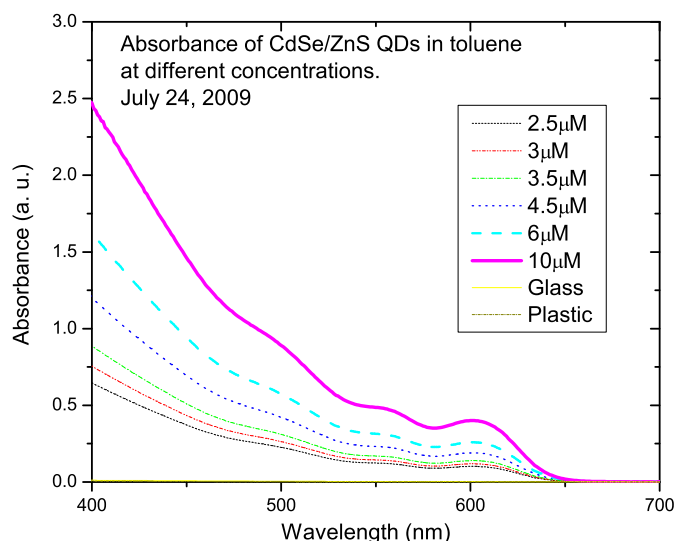


Figure 3.11: The absorption properties of visible CdSe/ZnS QDs in toluene at different concentrations: $2.5\mu\text{M}$, $3\mu\text{M}$, $3.5\mu\text{M}$, $4.5\mu\text{M}$, $6\mu\text{M}$ and $10\mu\text{M}$ respectively. The peak first excited emission centers at 620nm. The absorption wavelength range is less wide than the PbS QDs.

tively, the emission intensity decreases, but the wavelength at peak emission has not changed very obviously. The emission wavelength range from the PbS QDs is very sensitive to the silicon PV cells, which will show the higher efficiency output. The decreasing of the emission intensity is related to the absorption properties of the sample. PbS QDs absorb stronger at 500nm than at 700nm.

The normalized absorption and emission spectra for PbS QDs are shown in Fig. 3.14.

For comparison, the normalized absorption and emission spectra of PbS QDs, CdSe/ZnS QDs and Rhodamine B dye are shown in Fig. 3.15. From this figure, we can compare the spectral properties of these samples, especially the Stokes shift for each material.

By comparing the spectral properties of visible QDs LSCs and the Rhodamine B laser dye LSCs, we see that the absorption spectrum of the dye is very

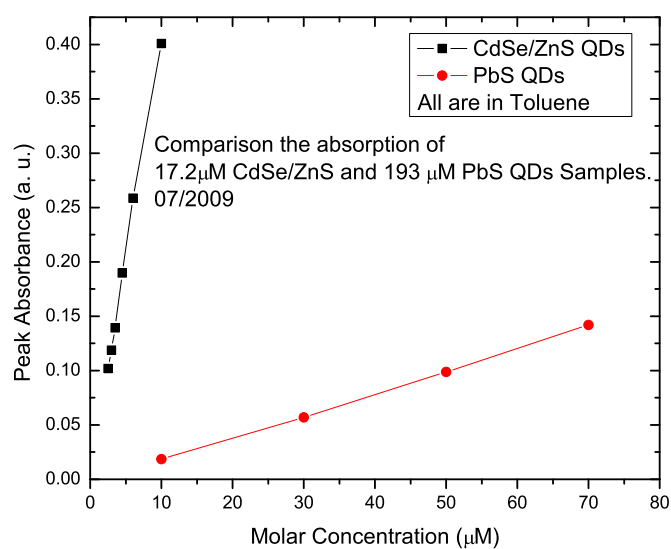


Figure 3.12: The comparison of the absorbance for the near infrared PbS QDs and CdSe/ZnS QDs at their peak emission wavelength.

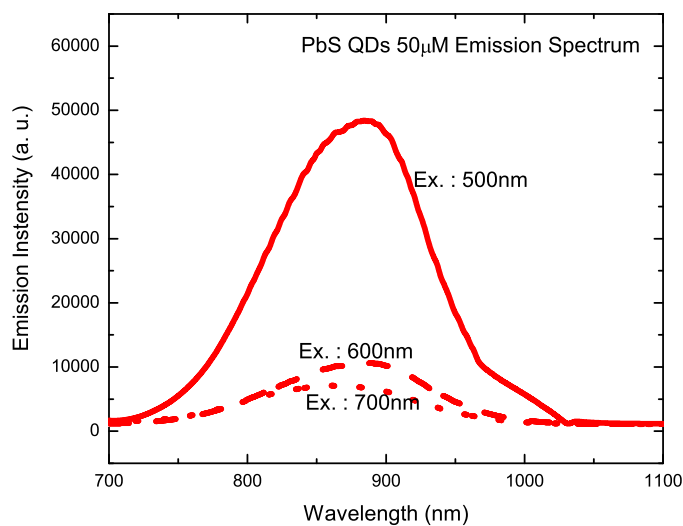


Figure 3.13: Emission spectrum for the $50\mu\text{M}$ near infrared PbS QDs LSCs excited by wavelength at 500nm, 600nm, 700nm respectively.

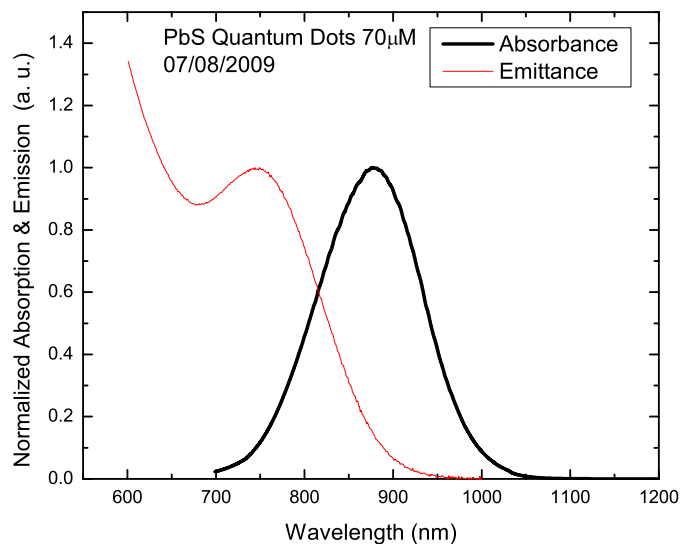


Figure 3.14: Emission spectra of the $50\mu\text{M}$ near infrared PbS QDs LSCs. The peak absorption and emission wavelengths center at 750nm and 880nm respectively with Stokes Shift 130nm . Excitation wavelength: 500nm .

narrow. It is from 500nm to 600nm over the solar spectrum, while QDs like CdSe/ZnS and PbS have much broader absorption spectra. Also, PbS QDs have the broadest absorption spectrum and less overlap area compared with CdSe/ZnS QDs. Very importantly, the Stokes shift of PbS LSCs is 130nm , which is much larger than others.

It is worthy to notice that we can get the required properties because the absorption threshold of QDs can be tuned by selecting the proper dot diameter, and the red shift of emission is related to the spread of QD sizes.

3.4 Concentration Optimization

As we know, higher concentration may result in higher re-absorption. For the luminescent materials, we need to characterize the optimum concentration for prototypes. In this section, we first study the concentration dependence of

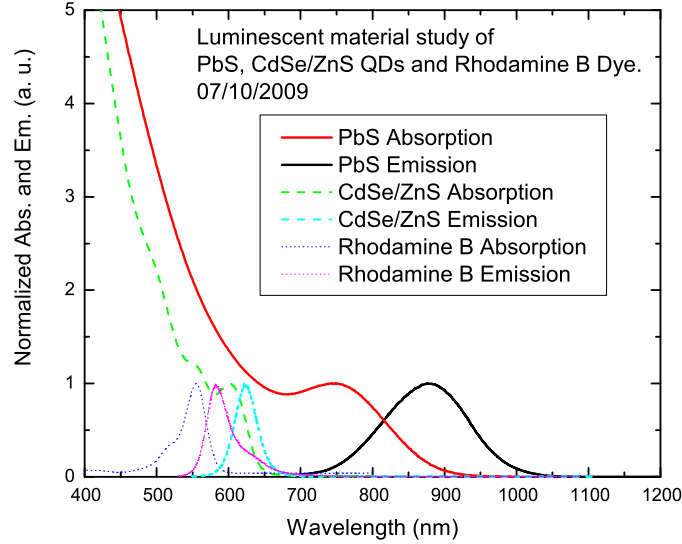


Figure 3.15: Comparison of absorption and emission properties of three luminescent materials: PbS quantum dots, CdSe/ZnS quantum dots, Rhodamine B dye. Excitation wavelength: 500nm.

laser dyes (Rhodamine B dye). We test the concentration dependence for visible CdSe/ZnS QDs. Finally we study the concentration dependent performance of near infrared PbS QDs by comparison with the other two luminescent materials. The results will show us how to optimize the concentration of luminescent materials in fabrication to get the maximum output efficiency.

The testing method or process is described as follows: First, we fabricate LSC PV systems for each luminescent material at different concentrations. A high efficiency PV cell is attached as a detector. Second, we tested the open circuit voltage V_{LSC} and the short circuit current I_{LSC} from these LSC PV systems. The results show that the open circuit voltage V_{LSC} did not change very obviously during the test. As a result, the output power is strongly related to the short circuit current, I_{LSC} , [DCM⁺85]. Third, using the same PV cell but towards the light source directly, we tested the open circuit voltage V_{PV} and the short circuit current of the PV cell, I_{PV} . Finally, we calculated the current ratio R_I

by I_{LSC}/I_{PV} . From the analysis, R_I can be considered as the electrical gain or concentration factor of the LSC system.

For each luminescent material, based on the values of current ratio R_I for each concentration, we can obtain the optimum luminescent material concentration.

3.4.1 Concentration Study for Rhodamine B Dye LSC PVs

We have fabricated Rhodamine B LSC PV systems with concentrations ranging from $50\mu\text{M}$ to $1000\mu\text{M}$. With the tested short circuit output current from these systems, we further calculated the current ratio values. The calculated output current ratio is plotted in Fig. 3.16 as a function of the concentration.

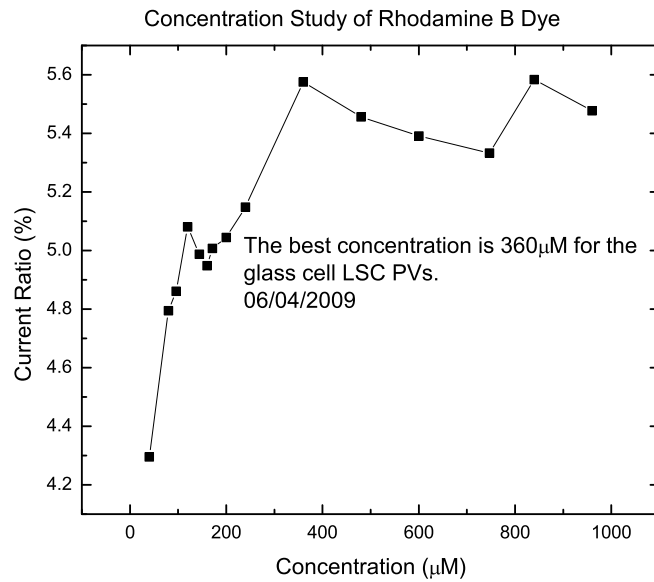


Figure 3.16: For Rhodamine B dye LSC PVs, the tested output current ratio as a function of sample concentration.

With the increasing of the concentration up to $1000\mu\text{M}$, the current ratio reaches the highest peak at $360\mu\text{M}$. Further considering the material cost, the results show that the optimum concentration for fabrication of LSC PV is around

360 μ M. We have tested the current ratio for systems with much higher concentration (up to 5000 μ M). The tested result shows that the output values from those samples are much lower than the current ratio for 360 μ M systems. This is due to the heavy reabsorption at high dye concentrations.

3.4.2 Concentration Study for CdSe/ZnS QD LSC PVs

For CdSe/ZnS QDs, the maximum concentration that we obtained from Evidot Company is 17.4 μ M. We have fabricated the CdSe/ZnS QD LSC PV systems at lower concentration by diluting higher concentration samples. The concentration of these samples changes from 2.5 μ M to 10 μ M. The tested short circuit output current from these systems is shown in Fig. 3.17.

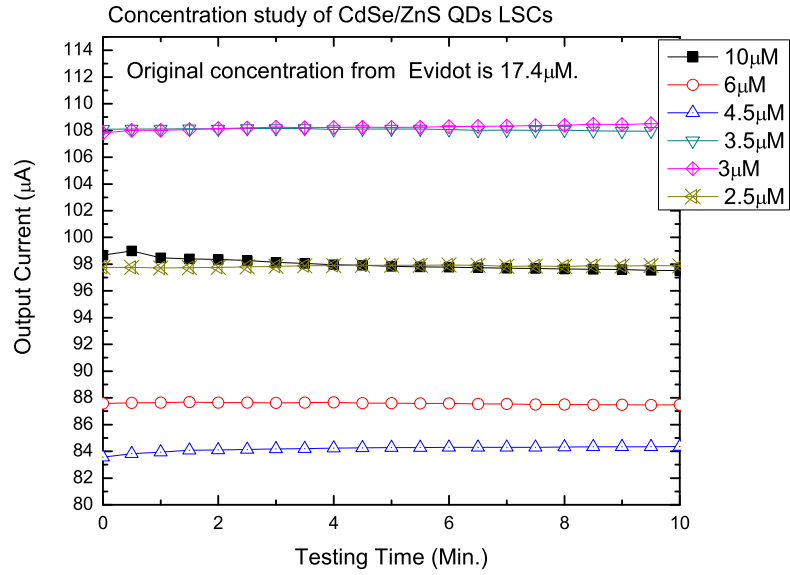


Figure 3.17: For CdSe/ZnS QD LSC PV systems at different concentrations, the tested output current ratio as a function of time. The output current is very stable. (The samples were diluted from the 17.4 μ M CdSe/ZnS QDs.)

The output signal is very stable. We further calculated the current ratio values. The calculated current ratios are plotted as a function of the sample concentration in Fig. 3.18. With the increasing of the concentration to 10 μ M, the current ratio reaches the highest peak at 3.0 μ M. Further considering the material

cost, the results show that the optimal concentration for fabrication of CdSe/ZnS LSC PV is around $3.0\mu\text{M}$.

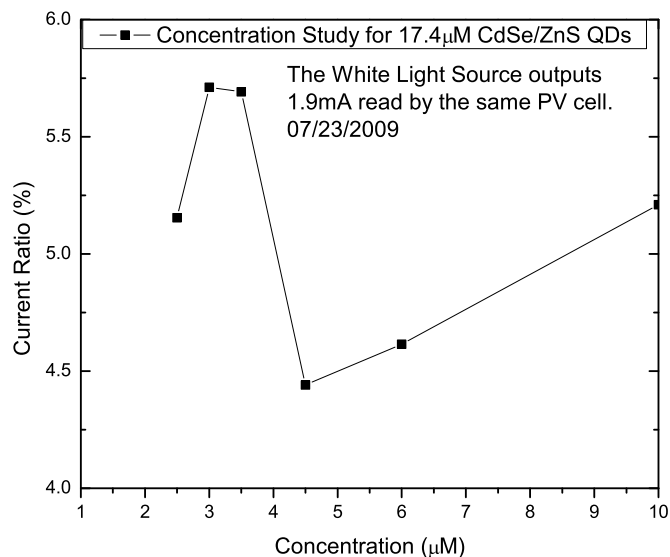


Figure 3.18: For CdSe/ZnS QD LSC PV systems, the tested output current ratio as a function of concentration. Due to re-absorption, samples with higher concentration produce less power. The optimum concentration for this design is around $3\mu\text{M}$.

3.4.3 Concentration Study for PbS QD LSC PVs

For PbS QDs, the maximum concentration that we obtained from Evidot Company is $193\mu\text{M}$. We have fabricated the PbS QD LSC PV systems with the solvent we have by diluting it. The concentration of these samples changes from $10\mu\text{M}$ to $193\mu\text{M}$. The tested short circuit output current ratios from these systems are shown in Fig. 3.19. As you can see, the output current is not very stable. It drops very fast at the beginning, but it drops much slowly after 10 minutes.

In order to show the stability of the output current of the PbS QD LSCs, the current ratios are plotted in Fig. 3.20 as a function of sample concentrations.

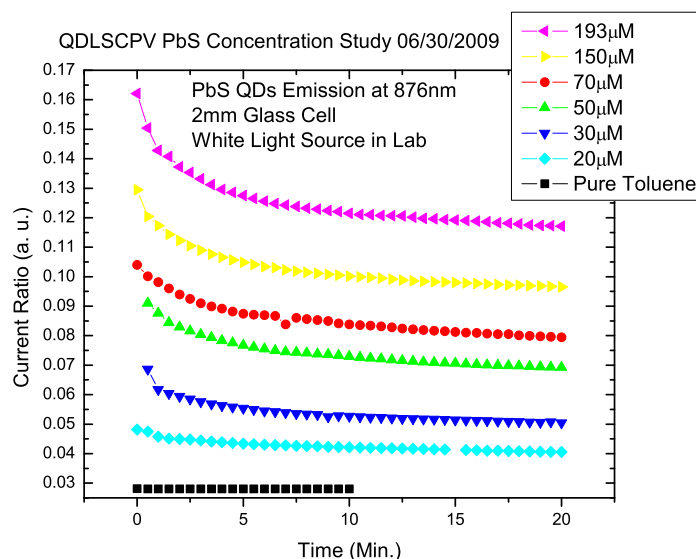


Figure 3.19: For the PbS systems at different concentrations, the tested output current ratio as a function of time. The output current is not very stable. (Samples at lower concentration are prepared by diluting from the $193\mu\text{M}$ PbS QDs from the vender.)

With the increasing of the concentration up to $193\mu\text{M}$, the current ratio has not reached a peak value, but become much flat. The results show that the optimum concentration for fabrication of LSC PV by using PbS Qds can be larger than $193\mu\text{M}$.

The testing results in Fig. 3.20 also show that for concentration up to $193\mu\text{M}$, the higher the concentration, the higher the output power for the fabricated LSCs.

3.5 Re-absorption Characterization

Because photons must usually travel a large distance before reaching the collection edge, overlap of the absorption and emission bands is a serious impediment for high efficiency LSCs. By partially illuminating the surface of the LSC through an aperture that slides along the length of the LSC and thus increasing

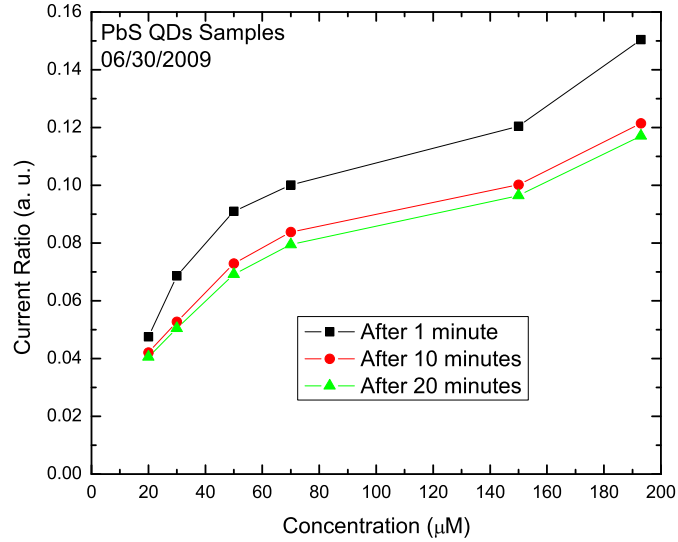


Figure 3.20: The tested output current ratio as a function of PbS QDs concentrations. The higher the PbS concentration, the higher the absorption. The output current drops much slowly after 10 minutes.

the source/detector distance, the path length of the emitted photons increases. This increases the probability of re-absorption. In this section, we characterize the re-absorption properties of the PbS QD LSCs, and compare the properties with visible QDs.

For $10\mu\text{M}$, the re-absorption study results are shown in Fig. 3.21 as a function of the source detector distance or excitation distance.

It shows the emission spectra tested by using UV-VIS spectrophotometer for $10\mu\text{M}$ PbS QDs LSC. The sample is excited by 408nm blue laser. The excitation distance is defined as the distance between the spectrometer detector and the excited laser point. From this emission spectra, we can see that with the increasing of the excitation distance, the intensity drops very quickly due to the loss of the emitted light when traveling from the excitation point to the spectrometer detector. The peak intensity from the $10\mu\text{M}$ PbS QDs LSCs as a function of the excitation distance (changing from 4mm to 26mm with each step increasing 2mm) is shown

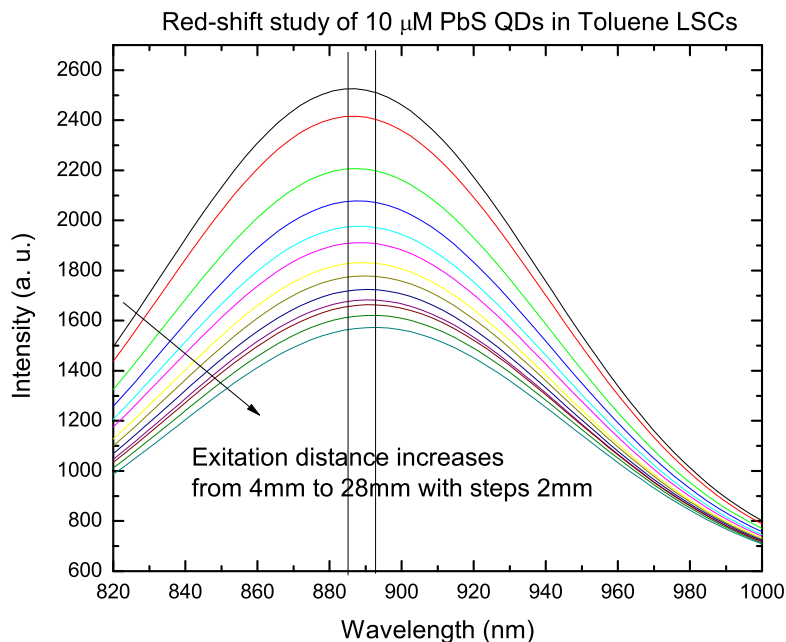


Figure 3.21: The emission spectra from the $10\mu\text{M}$ PbS QDs LSCs as the function of the excitation distance changing from 4mm to 28mm with steps 2mm. The excited wavelength is 408nm from a blue laser.

in Fig. 3.22.

If the loss is due to reabsorption, then the peak wavelength should increase. The reason is because if the emitted photon is re-absorbed and then re-emitted, the re-emitted photon will have lower energy, or with emission peaks centering at longer wavelengths. From Fig. 3.21, we see that the wavelength at peak emission of PbS QDs in this sample centers at 890nm, and the red-shifted range of the peak wavelength is less than 10nm with the increasing of the excitation distance.

For the highest concentration $193\mu\text{M}$ PbS QD LSC, the normalized emission spectrum is also tested as a function of the excitation distance changing from 0mm to 22mm with each step increasing 2mm. The results are shown in Fig. 3.23. The peak emissions center at 930nm which red-shifts 40nm from the peak emission wavelength of the $10\mu\text{M}$ sample. For the $193\mu\text{M}$ PbS QD LSC, the peak emission wavelength red-shift about 10nm with the excitation distance changing 22mm. This shift is much smaller than the visible CdSe/ZnS QDs and laser dyes

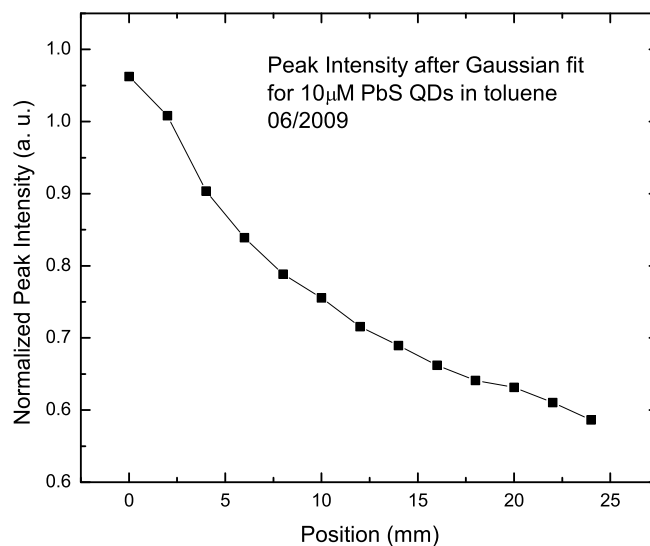


Figure 3.22: The intensity at peak emission from the $10\mu\text{M}$ PbS QD LSCs as the function of the excitation distance changing from 4mm to 26mm with each step increasing 2mm. The excited wavelength is 408nm from a blue laser.

tested in reference [SOC07].

One way of reducing the amount of red-shift is to control the amount of absorption/emission band overlap during synthesis of the materials [GLS⁺11]. The general profile of the bands and the general position of the peak of the bands are determined by the electronic structure of the materials. The width of the bands is also related to the distribution of dot sizes: the larger the distribution of dot sizes, the wider the bands. Hence a large distribution of dot sizes leads to larger absorption/emission band overlap and larger redshifts. Therefore, control over the distribution of dot sizes in quantum dot samples would lead to smaller redshifts and thus higher performance of fabricated LSCs.

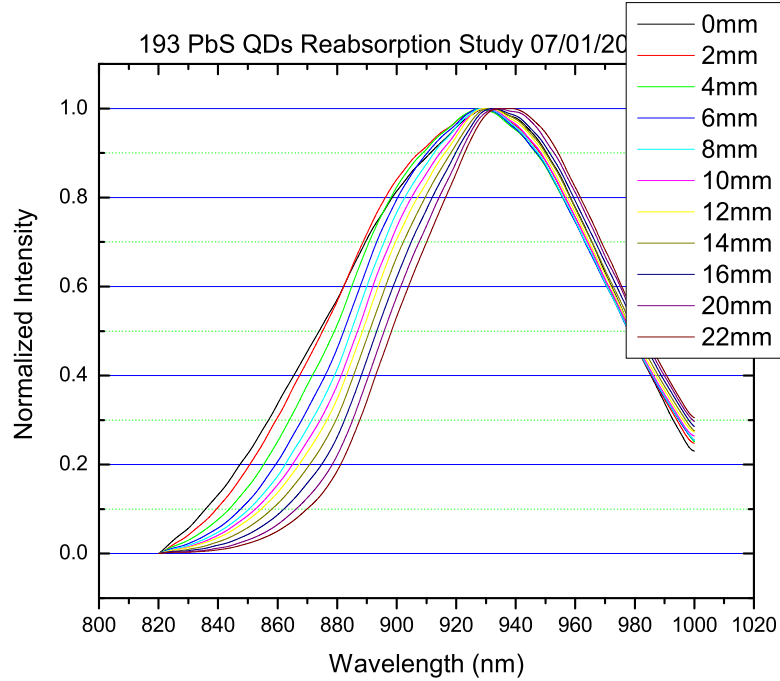


Figure 3.23: The normalized emission spectrum from the $193\mu\text{M}$ PbS QDs LSC as the function of the excitation distance changing from 0mm to 22mm with each step increasing 2mm. The excited wavelength is 408nm from a blue laser. The emissions centers on 930nm.

3.6 Electrical Characterization

3.6.1 Current Ratio Measurements

For comparison study, we have tested the output current ratio from the near infrared PbS QD LSCs, and compared with the visible CdSe/ZnS QDs and Rhodamine B laser dye LSCs fabricated at their optimum luminescent material concentration. The results from these three kinds of LSCs are plotted in Fig. 3.24.

PbS QD LSC perform the best although it is not very stable due to photo-bleaching, which is related to the high irradiation power density and photo oxydation of QDs. If protected by nitrogen, the decay should be very slowly [vSFB⁺02]. During the test,

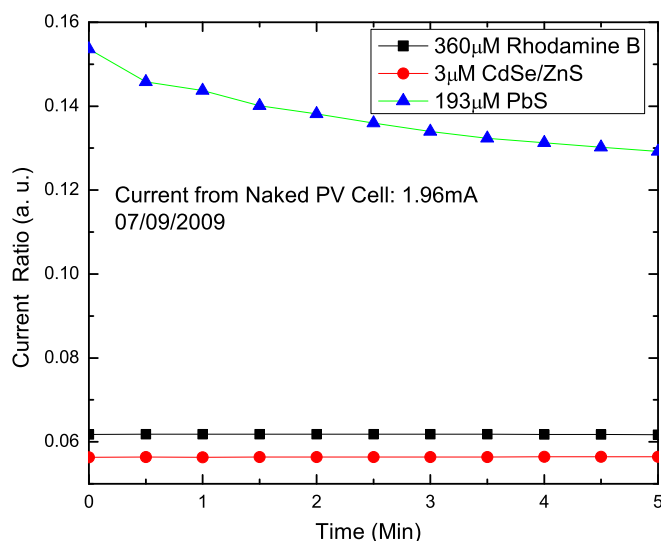


Figure 3.24: Output current ratio from the PV cell attached at the edge surface of LSCs fabricated with near infrared QD PbS, visible QD CdSe/ZnS, and organic laser dye Rhodamine B respectively.

(1) The white light source we used had about 11% of the flux output of sunlight.

(2) CdSe/ZnS QDs and Rhodamine B dye's concentration are 3 μ M and 360 μ M respectively, at which we have shown experimentally that LSCs yield the maximum output current from the LSC PV system for the 2mm glass cell.

(3) The 193 μ M of QDs we used is from Evidot with emission at 850nm.

(4) All study below of Sample 2 is done in 2mm Glass Cells.

LSC PV with PbS QDs yields much higher energy conversion efficiency. This is because of the spectral match of emitted radiation from the PbS QDs to the maximum conversion efficiency of the Si solar cells at approximately 850nm. The performance of the Rhodamine B LSC sample is better than that of the visible QD LSC sample since the quantum yield of the dye is much higher.

3.6.2 Optical Efficiency Analysis

From the tested output current for the LSCs with near infrared QD PbS, visible QD CdSe/ZnS, and organic laser dye Rhodamine B, we further estimated the output power conversion efficiency. As in the test we used the same glass (Quartz) box for the electrical characterizing; their geometrical concentration C_g is the same, which is about 10. Then, for the 360 μ M Rhodamine B LSCs, $R_I = 6.8\%$, and

$$\eta_{opt} = \frac{R_I}{C_g} = 0.68\%. \quad (3.1)$$

For the 3 μ M CdSe/ZnS QDs LSCs, $R_I = 5.71\%$,

$$\eta_{opt} = \frac{R_I}{C_g} = 0.57\%. \quad (3.2)$$

But for the PbS QDs LSCs, the current ratio can be higher than $R_I = 15\%$, and

$$\eta_{opt} = \frac{R_I}{C_g} \approx 1.5\%. \quad (3.3)$$

Based on the experiments, we can say that the near infrared PbS QDs are likely to be a good candidate in improving the LSC PV systems' efficiency.

Based on the power conversion efficiency of the PV cell we used, we can further estimate the power conversion efficiency for these fabricated LSC PV systems. And the estimated values may be too low as our purpose of this section is to identify the near infrared QDs as a new luminescent material for LSCs comparing with other available luminescent materials. Optimal structure designs for the LSCs can further improve the the solar energy conversion efficiency.

3.7 Output Power Stability Characterization

In the above sections, we characterized properties of near infrared PbS QD LSC PV systems, and showed that the PbS QDs are not very stable when we exposed them to the air. In this section, we further study the stability problem.

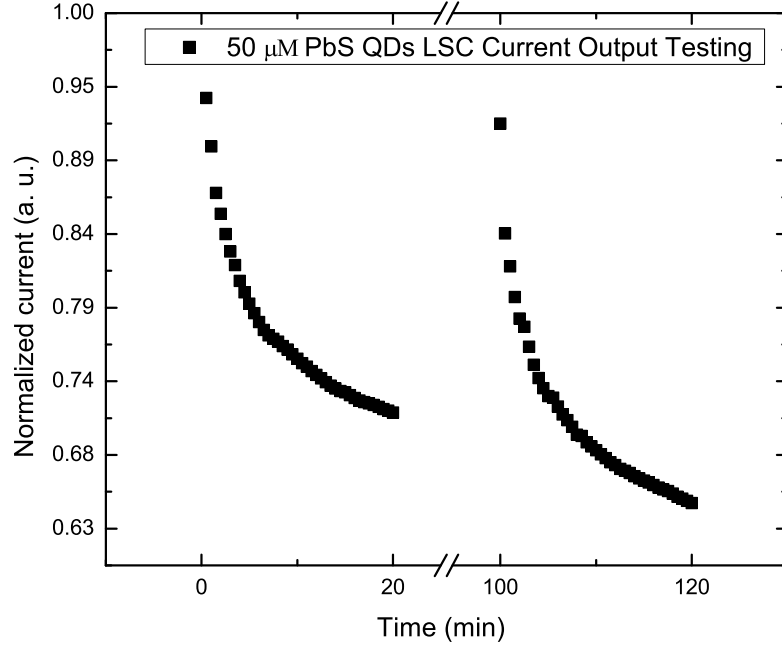


Figure 3.25: For the PbS QDs LSC at $50\mu\text{M}$, the tested output current as a function of time up to 120 minutes. After 20 minutes of testing, the sample was put into the dark, then retested at 100 minutes, and continued testing until 120 minutes.

For the PbS QD LSC systems at $50\mu\text{M}$, we tested the output current as a function of time. We first exposed the sample to the light source in 20 minutes. After that we kept the sample into the dark, and then exposed it to light source for testing from the 100 minutes to 120 minutes. The tested results are as shown in Fig. 3.25. We found that the output current is recovered due to quantum blinking [vSFB⁺02], and then the output current begins to drop again due to the photo-oxidation, and this decrease is not recovered.

For PbS QD LSCs at different concentrations, we found the same result under sunlight at Merced, California, on a typical sunny day. The tested results are as shown in Fig. 3.26. The output current for QDs at higher concentration drops slower than that for lower concentration samples. This is due to the photo-bleaching at higher irradiation power density. Also, compared with Fig. 3.20, we found that under sunlight, the output current drops faster than at room temper-

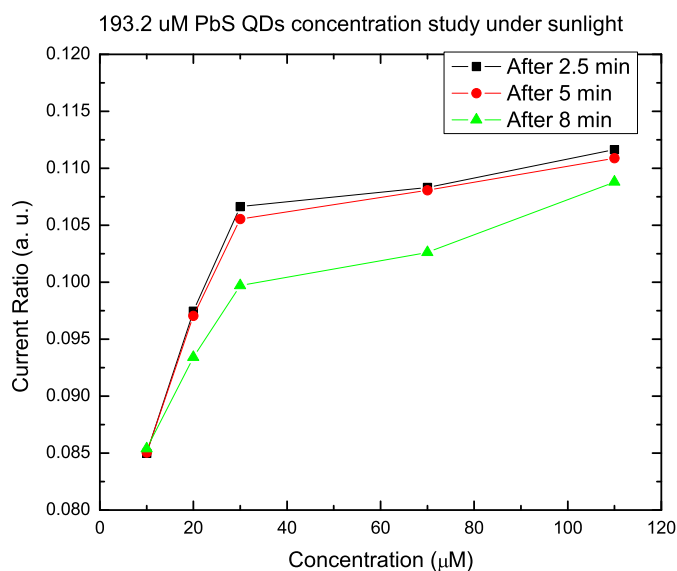


Figure 3.26: The outdoor testing of the current ratio as a function of PbS QD concentration. The higher the PbS concentration, the higher the absorption. The output current drops much slower after 10 minutes.

ature exposure to a light source with 11% of sunlight intensity.

The result shows the importance of stabilizing the output current of the PbS QDs for the application in LSC PV systems.

3.8 Optical Enhancement for Quantum Dots Thin Film LSCs

In this section, we propose several methods to optimize the design of the LSC structure and further improve the system efficiency. Toluene is used as a solvent for the quantum dots LSC fabrication. The fabricated LSCs need to be sealed very well or it evaporates in the air very quickly. Because of this, We first apply the following proposed optimization methods to laser dye LSCs since both of the dye and the solvent are very stable during the characterization process. We then applied these optimization methods to QD in thin film LSCs since we have

successfully fabricated thin film QD LSCs by embedding QDs into PMMA plastic materials.

3.8.1 Optimization Methods

The proposed methods for optimizing the design of the LSC structure and further improving the system efficiency are as follows:

(1) From the bottom, we can use a white diffuser attached at the bottom of the glass box. The white diffuser is to reflect back or diffuse the transmitted light to the LSCs and then to increase the absorption of luminescent materials.

(2) From the edge surfaces, we can attach mirrors or silver reflective tapes at other LSC edge surfaces to increase the to increase the output efficiency.

(3) From the edge surfaces, we can amount optical gel between glass cells and attached PV cells. The optical gel can be used to reduce the reflective light and match the refractive index to increase the absorption of the concentrator.

3.8.2 Optimization for Liquid Dye LSCs

In our experiments, the Rhodamine B samples show very stable output power properties. We apply our proposed optical efficiency enhancement methods to a Rhodamine B dye LSC first. Table 3.1 shows the results of applying optical gel, white diffusers and reflective silver tapes with polished quartz cells tested under sunlight from the short edge surface of LSCs.

From Table 3.1 and Fig. 3.27, we can see that for case **B**, applying optical gel to the system can improve the output performance by 91%, combined with using a white diffuser attached at the bottom, we obtained 182% of improvement shown by case **C**. For case **D**, we applied optical gel and a reflective silver tape at the other edges of the LSC. The reflective silver tape performs like a mirror. As a result, we got the improvement of the output current ratio $2.18\times$. For case **E**, we attached a PV cell at one edge of the dye LSC, but applied reflective silver tapes

	Current(mA)	Current Ratio (%)	Improvement
A	2.45	13.6	
B	4.46	24.8	1.91×
C	6.90	38.3	2.82×
D	5.34	29.7	2.18×
E	8.45	46.9	3.45×

Table 3.1: For the 400 μM Rhodamine B LSC PV system, the tested output current, calculated current ratio and the improvement by applying different optimization methods. **A.** Only Cells; **B.** Optical Gel (at the edges); **C.** Gel (at the edges)+ White Paper(at the bottom); **D.** Gel (at the edges) + Reflective Silver Tape (at other edges); **E.** Gel (at the edges)+ Reflective Silver Tape (at other edges) + White Paper (at the bottom).

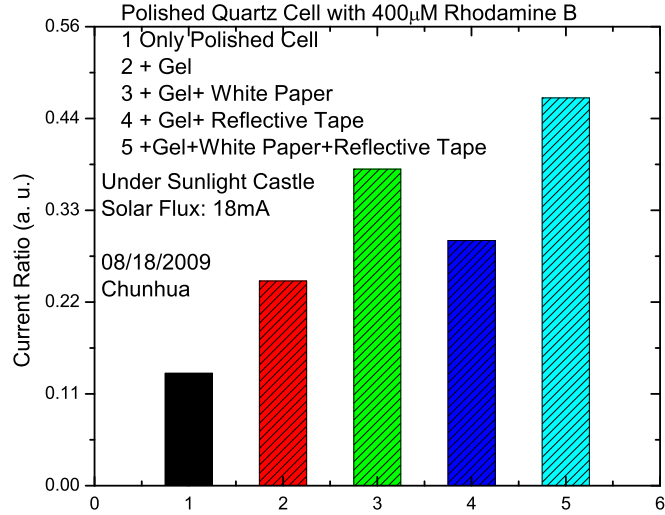


Figure 3.27: Optimum results for polished quartz cells filled with 400 μM Rhodamine B, testing under sunlight.

at the other edges of the LSC. Together with the white diffuser, we obtained a further improvement of 3.45× from Case **A**.

Since the geometrical gain of the system is about 5, for case **D**, with optical gel and silver reflective tape, ideally, we can get about 5 times of improvement on the output current ratio from case **B** (only applying optical gel). However, we

only got 1.2 times of the improvement. Further improvement is necessary. One possible reason why the improvement was not as expected is from the re-absorption of the dye. Most of the light reflected back by the silver reflective tape may be re-absorbed during the process of transporting to the edge surfaces where PV cells are attached. Another reason may be related to the attaching method, such that the silver reflective tape has not been attached very tightly to the cell. As a result, some light may be reflected into other directions rather than into the LSC system.

We also optimized the performance of the fabricated LSCs from their long edges. The testing configuration is shown in Fig. 3.28. During the test, the PV cell with dimensions 12mm by 3.2mm is attached at one long edge of a tested LSC, and is moved along the long edge with each step increasing 0.5mm.

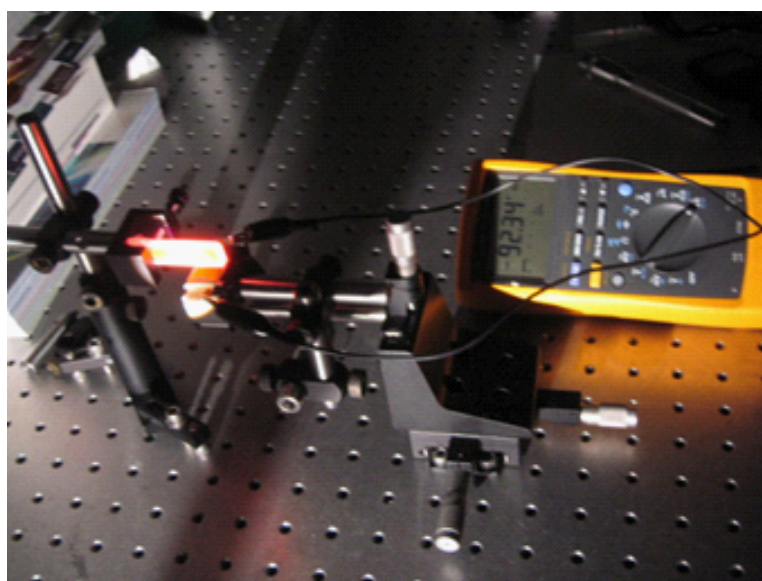


Figure 3.28: Testing configuration by using PV cell from the long edge of the fabricated LSC. The PV cell with dimensions 12mm by 0.3mm is attached and moved along the long edge with each step increasing 0.5mm.

The testing result is shown in Fig. 3.29. The whole effective length of the tested LSC is 36mm. First, the current distribution along the long edge is approximately symmetric. The middle position of the LSC long edge is located at 9mm of the position of the PV cell in Fig. 3.29, and the maximum output

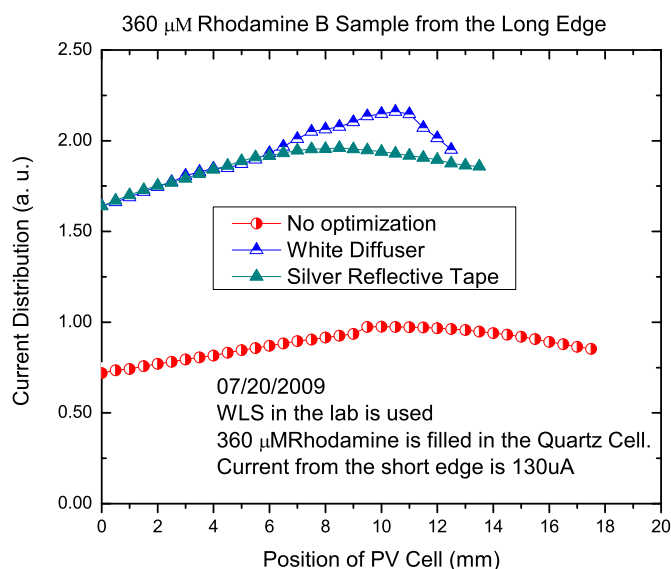


Figure 3.29: The current distribution along the long edge of the glass box without optimization (normalized), and optimized by white diffusers and silver reflective tapes.

current from the attached PV cell at this middle position is $124.2\mu\text{A}$ without any optimization. Further optimizing the system by attaching a white diffuser at the bottom surface, we got the increase by $2.15\times$; but optimizing by the silver reflective tape attaching at the bottom of the LSC, the increase is only $1.95\times$. The increase by the white diffuser is much higher than the silver reflective tape. It is mainly because a white diffuser can effectively reflect and diffuse the transmitted light into the LSC while the silver reflective tape can only effectively reflect light into the LSC.

3.8.3 Optimization for QDs Thin Film LSCs

We have embedded the visible and near infrared emission QDs into PMMA films, and made solid QD LSCs. One fabricating method is (1) mixing the PbS QDs in toluene with MMA solution, and then (2) polymerizing the solution by

heating the solution at certain temperature. The second fabrication method is (1)Mixing the PbS QDs in toluene with PMMA powder, and then (2)Casting the mixture on a piece of glass or plastic substrate to make QDs LSC thin films.

The concentration of the fabricated PbS QD thin film LSCs changes from $20\mu\text{M}$ to $60\mu\text{M}$. They have the size 2.54cm by 7.62cm by 0.4cm. Fig. 3.30 shows their performance. From this figure, we can see that applying a white diffuser, the output current can be strongly enhanced. And the enhancement is about $4\times$. Also, the higher the concentration of the QDs we embedded, the higher the output current ratio from the thin film QD LSCs.

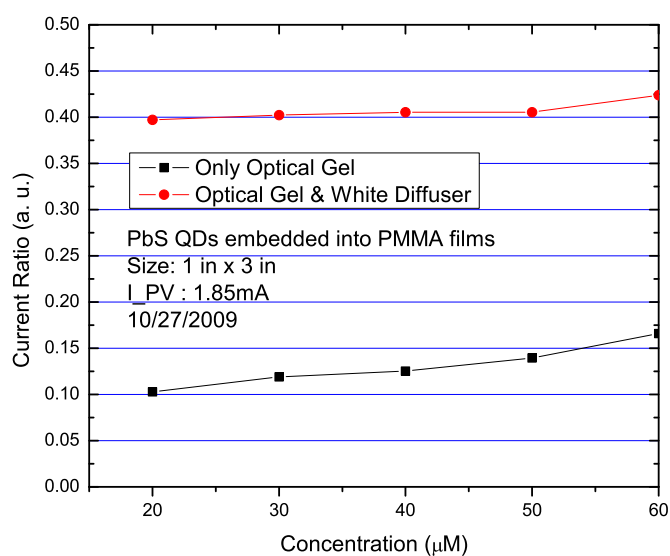


Figure 3.30: Optimization by using a whiter diffuser for PbS QD thin film LSCs at different concentrations changing from $20\mu\text{M}$ to $60\mu\text{M}$.

We have applied the same optimization methods to thin film CdSe/ZnS QD LSCs with the same dimensions. The results are shown in Fig. 3.31. The improvement from the white diffuser for these samples is between $3\times$ to $4\times$. The result shows that the CdSe/ZnS QD LSC at $3\mu\text{M}$ performs the best. This concentration is also the optimal concentraiton for liquid CdSe/ZnS QD LSCs.

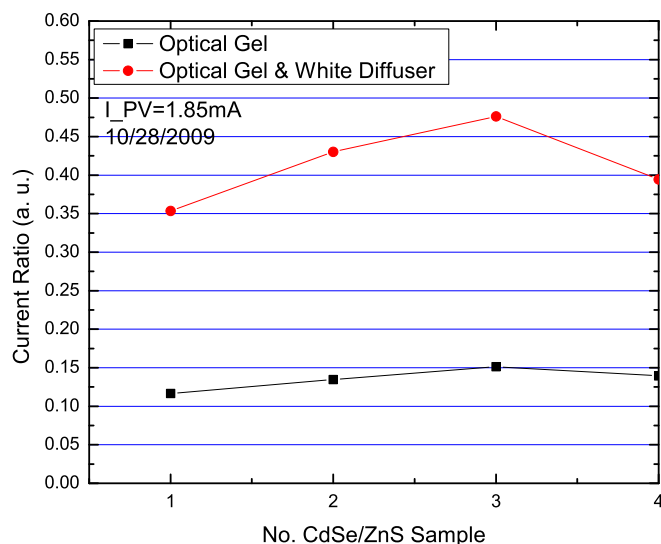


Figure 3.31: Optimization by using a whiter diffuser for CdSe/ZnS QD thin film LSCs at different concentrations changing from $1\mu M$ to $4\mu M$.

By applying both optical gel and white diffusers, the fabricated LSCs yield the highest output performance. For the thin film PbS QD LSCs with 2.54cm by 7.62cm and 0.4cm, only with the optical gel and a white diffuser, we obtained $2.7\times$ improvement for PbS QDs at lower concentration of $50\mu M$ and $3.1\times$ improvements for CdSe/ZnS QDs LSCs. For higher concentration samples, we can get higher output current ratio improvement.

3.9 Summary

In this chapter, we described the experimental fabrication and characterization process for nano-structured QD LSCs. Focusing on luminescent materials characterization, we compared properties of the near infrared PbS QDs, visible CdSe/ZnS QDs and Rhodamine B organic laser dye as luminescent materials for LSCs. The results show the great potential of improving LSC efficiencies by apply-

ing the near infrared QDs due to their broaden absorption spectrum, near infrared emission and weak re-absorption properties.

We investigated effects of luminescent material concentrations on the LSC efficiency for each luminescent material, and proposed their suitable concentrations in fabrication process to balance the absorption of sunlight and re-absorption of re-emitted light. The results show that although there are optimum concentrations for visible CdSe/ZnS QDs and laser dye LSCs at $3\mu\text{M}$ and $360\mu\text{M}$ respectively, we can increase the molar concentration of PbS QDs up to $193\mu\text{M}$ to get the higher output current. The experiments on testing the red shifting of peak emission wavelengths under various excitation distances also show a weak re-absorption of the PbS QDs. This results show that the efficiency of PbS QD LSC systems can be further increased by increasing the molar concentration of the PbS QDs.

The electrical characterization experiments show that although there is degradation due to photo-oxidation, optical efficiency of PbS QDs LSCs is much larger than that of other materials. The power output stability problem of the near infrared quantum dots is examined and further characterized, which proposed the challenge for further applications of infrared PbS QDs for LSCs.

We proposed and applied several LSC efficiency improvement methods to thin film QD LSCs from their bottom surfaces and their edge surfaces. We also observed a great improvement on the output power from these methods. By only apply the optical gel and white diffusers, we obtained $3.1\times$ improvement for CdSe/ZnS QDs LSCs, and $2.7\times$ improvement for PbS QDs at lower concentration at $50\mu\text{M}$.

In conclusion, our research on the near infrared QDs shows that PbS QDs LSCs could potentially be used in high efficiency and low cost LSCs, and for them to become practical in the market, increased stability is required.

3.10 Acknowledgements

Parts of the work is published in *Appl. Phys. Lett.* **96**, 191901 (2010); doi:10.1063/1.3422485 and in *Proc. SPIE* 7772, 77720G (2010); doi:10.1117/12.860094

Chapter 4

Organic Luminescent Solar Concentrators

4.1 Introduction

Generally, an organic LSC is a piece of highly transparent plastic or glass material containing luminescent organic dyes. Photovoltaic (PV) solar cells are used to attach at one or more edge surfaces of the LSC. The schematic of an organic LSC is shown in Fig. 4.1. Light comes into this system, and is absorbed by the organic dye molecules. The absorbed light then is re-emitted from the dye luminescent molecules at longer wavelengths in all directions. A large portion of this re-emitted light can be guided and concentrated at the edges of the LSC by total internal reflection. The attached PV cells will collect and convert the light from the edges into electricity.

Organic luminescent materials are used in this concentrated PV systems for lower solar energy concentration applications, which is very attractive. This is mainly because the system can concentrate both direct and diffuse light without tracking at potentially very lower material cose [vSBS⁺08]. They can also reduce the cost since less PV materials can be used comparing with the larger area of

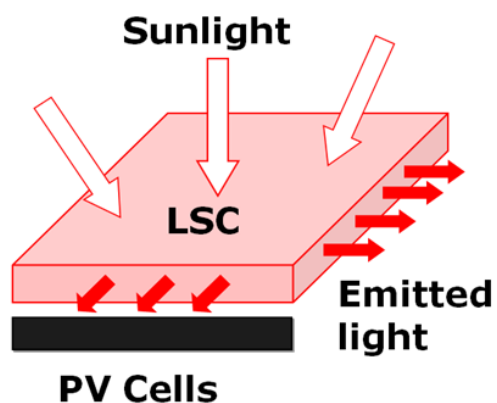


Figure 4.1: Schematic of an organic luminescent solar concentrator (LSC).

expensive solar cells required in a standard flat-plate PV panel[Rei10].

Fig. 4.2 shows some organic LSC samples in our lab. They are fabricated by embedding different organic dyes into plastic materials. They show different colors mainly due to the properties of the contained different dyes.

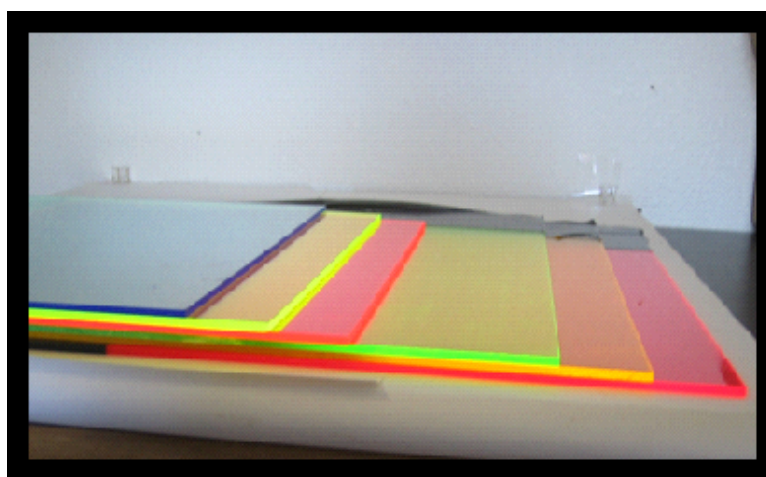


Figure 4.2: Organic LSC samples fabricated by embedding dyes into plastic materials.

For these systems, the predicted theoretical value of the concentration factor

is a function of the Stokes shift of luminescent materials, and this value can be very high if the Stokes shift is large [CMH⁺08, PKHG09]. For a typical red dye, the power conversion efficiency is estimated to be 102 with Stokes shift 33nm [SRWY90].

The experimental power conversion efficiency of organic LSC PVs is much lower than the value predicted theoretically. As we know, the reported power conversion efficiencies for LSCs are less than 10% [PKHG09]. The best result reported for an LSC with four GaAs cells is 7.1% measured at European Solar Test Installation laboratories with the geometrical concentration factor 2.5 [SBB⁺08]. Comparing with the theoretical prediction, there is a large potential in improving the power conversion efficiency of LSC PV systems.

Although much work is now focused on identifying effective luminescent materials for LSCs [Row07, BLH⁺07, DVN⁺11], it's equally important to optimize the designed structure to further enhance the power conversion efficiency [DTK⁺09]. Also, the sizes of the LSCs in previous studies are limited, and size-dependence of the optimization methods needs to be studied for LSCs with reasonable sizes.

In this chapter, we study the performance of the organic LSCs with the purpose of improving the output power conversion efficiency of LSCs from optical design. The design methods include: (1) using refractive index matched optical gel between the surfaces of LSC edges and attached PV cells; (2) using a white diffuser at the bottom of the LSC surface; (3) applying multi-layer LSCs (Dyes in each layer utilize the solar spectrum at different wavelength ranges); (4) Covering the top surface of the LSC with wavelength selective films.

We also investigate the LSC size and structure dependence of the efficiency enhancement by applying these design methods. For our fabricated prototypes, the thickness and the concentration of contained dyes are already optimized in the fabrication process. We will characterize the performance of LSCs by changing the size or geometrical gain of LSCs under sunlight. The largest LSC we have studied has a length of 120cm. This is the largest LSC we know of to date. And this is

large enough for applications in buildings as windows.

Although in our experiments we use LSCs fabricated with organic laser dyes, the research results are very useful in the optimization of LSCs fabricated with other luminescent materials.

The fabrication process and experimental setups are described in Sec. 4.2. In Sec. 4.3, we optically characterize properties of organic dyes for LSCs. We have tested two groups of organic dyes. In this section, the new dye materials for LSCs are identified, and absorption and emission spectrum properties of these dyes in LSCs are characterized.

We also characterize the electrical properties of LSCs for PV technologies by applying the above optimization methods for different sizes and different shapes. The results are shown in Sec. 4.4. In this section, we mainly study the size and shape dependence of the optical efficiency enhancement for one layer LSCs. We have obtained the LSC concentration factor of $4\times$. In Sec. 4.5, we study the size and shape dependence of the optical efficiency enhancement for multilayer LSCs.

Since we can further apply wavelength selective films on the top of the LSC surfaces to improve the output efficiency of the system, a wavelength selective film is fabricated and applied to our fabricated LSCs, and the results are shown in Sec. 4.6. The energy balance analysis method for LSCs is given in this section. With this method, we show the dependence of system dimensions on energy loss from LSC PV systems.

Stability properties of LSCs are very important for collecting solar energy, which can be improved by selecting proper organic dyes [DCM⁺85, ERFS10]. We tested the stability properties of a group of LSCs fabricated with fluorescent plates. The tested results are shown in Sec. 4.7.

Since LSCs can be applied as “smart” windows by integrating into buildings to collect and convert solar energy into electrical power, in Sec. 4.8, prototypes of LSC PV systems at practical sizes for such application is fabricated. The concentration properties of these prototypes for both direct and diffuse lights are

characterized and compared. The conclusion of this chapter is given in Sec. 4.9.

4.2 Experiments

In this section, we briefly describe our prototype fabrication processes and the experimental setups for the study on the performance of organic LSCs. The matrix materials for the organic LSC PV systems we fabricated and tested are PMMA plastic. This material has been tested with very good stability for solar energy applications [vSBS⁺08]. These LSCs are fabricated by embedding the organic dyes (Lumogen dyes) into the plastic material. All the fabricated samples have the same thickness $\frac{1}{8}$ in or 0.32cm. We cut them into different shapes with the longest size in length 120cm.

We have tested two groups of organic LSC samples. These two groups of LSCs mainly differ in dyes' stability properties from the vender. The out put power from one group of LSCs with the embedded organic dyes is supposed to be more stable than the other group, but is not commercially available. We call this group outdoor using samples in this dissertation and expect that they will be used for collecting solar energy in the near future. We then call the other group the indoor use sample.

We first characterized optical properties of these samples. The Perkin-Elmer Lambda 35 UV - VIS spectrophotometer is used for the absorption and transmittance testing. This is a double-beam instrument, meaning that the monochromarized lamp output is split into two beams, one beam passing through the sample cell of the sample compartment and the other through the reference cell of the sample compartment. The instrument then calculates the ratio between the intensity of light after passing through the sample cell and the intensity after passing through the reference cell. The base ten logarithm of this ratio gives the absorbance of the sample.

The Perkin Elmer LS 55 luminescence spectrometer or fluorimeter is used

for the emission testing. It consists of a xenon lamp producing broadband UV-VIS excitation light, an excitation monochromator that selects a narrow frequency range of light produced by the lamp, a sample holder that contains the sample to be measured, optics to collect the light emitted by the sample, an emission monochromator that selects a narrow frequency range of the light emitted by the sample, and a photomultiplier that detects the intensity of the emitted light. During the emission testing, the wavelength of the light emitted by the sample is scanned. The transmission ability of the samples is also tested by using PV cells.

For the electrical characterization under sunlight, we have fabricated prototypes with different sizes. In the test, by using a solar tracker, we have been able to change the pointed direction of the tested samples. The configurations of horizontal, vertical to the ground, as well as normal to the coming sunlight directly are tested. The experimental set up is shown in Fig. 4.3.

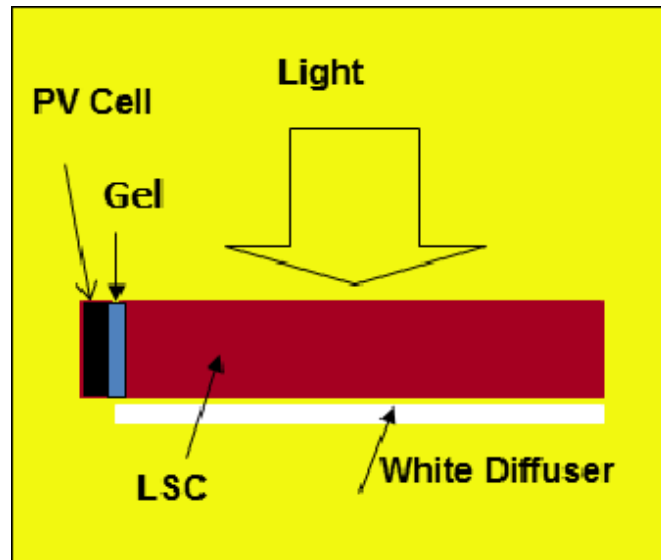


Figure 4.3: Schematic of experimental setup for optical enhancement of LSCs by attaching a white diffuser at the bottom of the LSC and adding refractive index matched optical gel between LSC edges and the attached PV cells.

In order to improve the output power, the optimization methods are applied, as shown in Fig. 4.3. A white diffuser is applied at the bottom of the tested LSC.

Optical gel is applied between the surfaces of the attached PV cell and the LSC edge surfaces.

To further improve the output performance, the stacked structure is applied

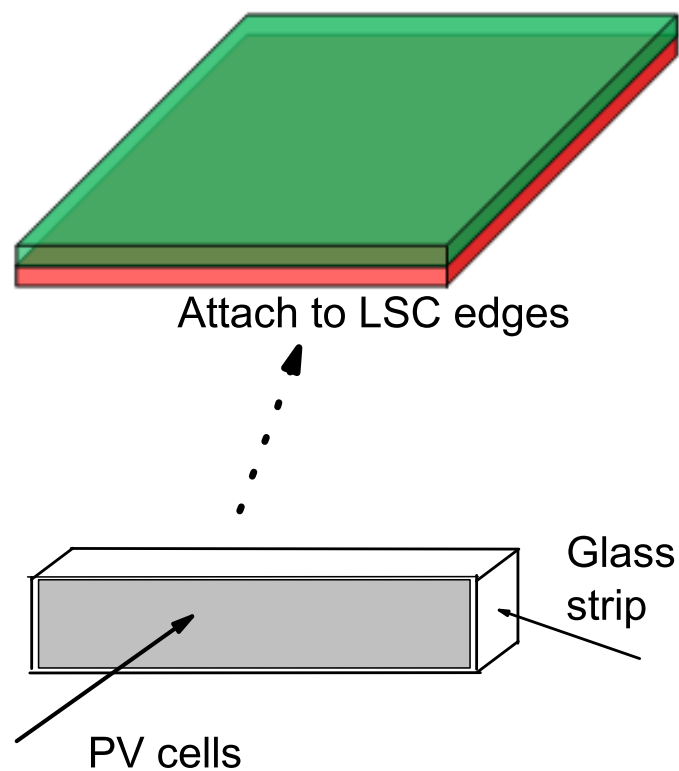


Figure 4.4: The two layered stacked LSC plates for photovoltaics with the green LSC on top of the red LSC. Glass strips are used between surfaces of PV cells and the LSC edges.

attached are connected in series at edges of the LSC. The size of silicon PV cells we use is 12.7cm in length and 0.64cm in width. The fill factor of these PV cells is 72% and the efficiency is around 16.9%. The maximum length available is 6in.

As shown in Fig. 4.5, in the fabrication, because the thermal expansion of

PV cells and the LSCs are different, we inserted a strip of glass between the LSC plate and PV cells in the experiments. They are cut with exactly the same size

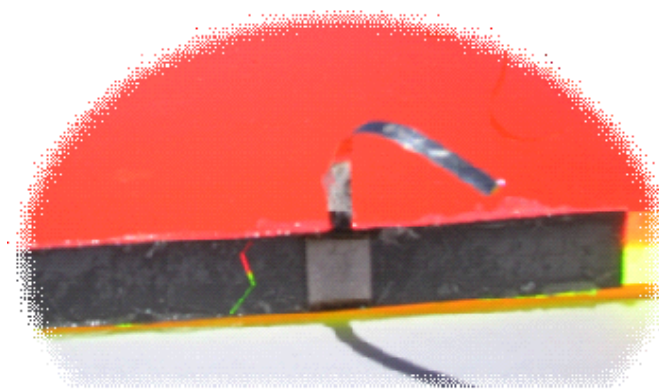


Figure 4.5: Without applying glass strips shown in Fig. 4.4 between PV cells and LSCs, PV cells attached at the edge of the LSCs break due to different thermal expansion properties.

of our PV cells and are glued with RTV silicone clear Caulk as also shown in Fig. 4.4. These glass strips are used to protect fragile PV cells from breaking. Without applying them in our first prototype, several attached PV cells at the edge surfaces were broken as shown in Fig. 4.5 when we exposed the prototype to the sunlight. However, after applying the glass between the LSC edges and the attached PV cells, we have not seen the PV cells fail by exposing the fabricated prototype to intense sunlight. For the two “smart” windows, window frames are also added to protect the dyes from degradation. We can fabricate LSC “smart” windows with different shapes and sizes. By putting them on top of a solar tracker, we can easily change the direction of the sample to sunlight, as seen in Fig. 4.6.

In the experiments, for testing the concentration for diffuse light, the stacked structure is used without any optical gel and white diffusers for optimization [DTK⁺09]. This is to decrease the influence from them on the results. We have tested the performance of LSCs from each of their edges. In the test, PV cells with 12.7cm by 0.64cm are used as detectors and are attached at the middle position of each edge surface. In the test, one LSC PV system with black background is

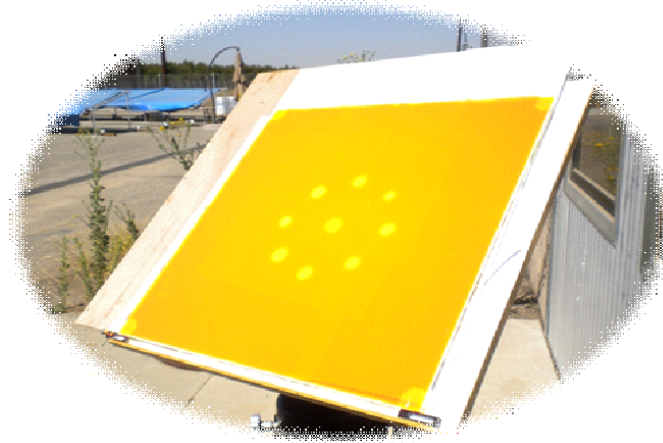


Figure 4.6: The prototyped “smart” window of stacked LSCs with PV cells attached at all edges in series. It is put on a solar tracker.

placed vertically to the ground, and is pointed south at Castle, UC Merced, California. This is for testing the performance of the LSC PV as “smart” windows on concentrating global lights. The other LSC PV system with black background is placed vertically to the ground, and is pointed toward north at Castle. This is to test the concentration effect for diffuse light on the output power. Data are recorded every half hours from 8:00AM to 6:00PM during a sunny day.

In order to estimate the optical efficiency of different LSCs with different sizes, we define the geometric gain G as

$$G = \frac{A_{top}}{A_{edge}}, \quad (4.1)$$

where A_{top} is the area of the top surface of LSCs illuminated by a light source, and A_{edge} is the area of the collecting edges. The current ratio is defined as

$$R_I = \frac{I_{edge}}{I_{SC}}, \quad (4.2)$$

where I_{edge} is the short-circuit current of the PV cell attached the LSC edges under illumination of a light source and I_{SC} is the short-circuit current measured from the same solar cell under direct illumination of the same light source instead of attached at the edge of LSCs. Under sunlight, the open-circuit voltage V_{OC} of the

PV cell and the fill factor f only change slightly [12]. In our experiments, values of V_{OC} are around 0.55V, and values of f are around 0.72. So the current ratio can be considered as the output electrical gain, or concentration factor. The optical efficiency can be estimated by

$$\eta_{opt} = \frac{R_I}{G} = \frac{I_{edge}A_{edge}}{I_{SC}A_{top}}. \quad (4.3)$$

As shown by Batchelder et al [Bat81], the optical efficiency decreases with an increase on geometric gain, and a geometric gain on the order of 10 shows a good balance between a large geometric gain and a high optical efficiency [SOC07]. The power conversion efficiency can be estimated as

$$\eta_{power} = \eta_{opt}\eta_{PV}, \quad (4.4)$$

where η_{PV} is the power conversion efficiency of the attached PV cell. In our experiment, η_{power} mainly depends on the η_{PV} . So we draw the current ratio for our testing, which should be able to reflect the performance of the LSC PV systems.

4.3 Optical Characterization of Organic LSCs

The luminescent materials should absorb a broad portion of the solar spectrum and emit efficiently [RWR08]. For a typical laser dye Rhodamine B (Rh. B) in ethanol glycol, we have tested its absorption and emission spectra as shown in Fig. 4.7.

This dye absorbs light effectively only approximately from 500nm to 600nm over the broad solar spectrum. Similar to these spectra, organic laser dyes usually have very narrow absorption range over the solar spectrum. The emission peak is at 582nm with Stokes shift 29nm. The overlap between the absorption and emission spectra often results in the strong re-absorption. These optical properties also emphasize the necessity of optical enhancement of the LSC performance by optical designs. Similar spectra properties can be observed from other kinds LSCs with dyes contained either in liquid solvents or in solid PMMA or glass materials.

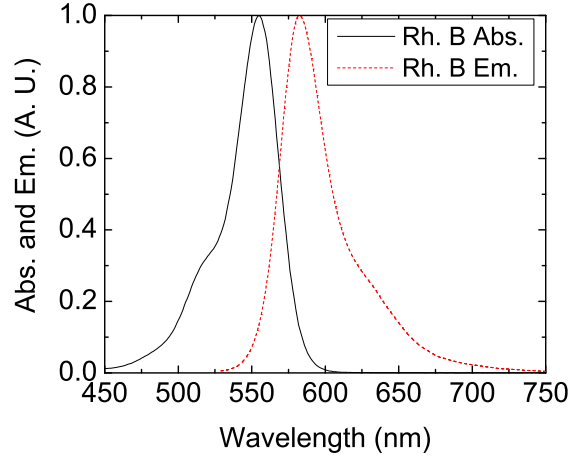


Figure 4.7: Steady state absorption (Abs.) and emission (Em.) spectra properties of the normally used high quantum yield Rh. B dye for LSCs.

For the indoor use samples, in Fig. 4.8 (a) and (b), we show the absorption and emission spectra of the tested green and red color emission organic dyes in PMMA plastic materials. PMMA as matrix material, has been proved very stable in solar energy collection [RWR08].

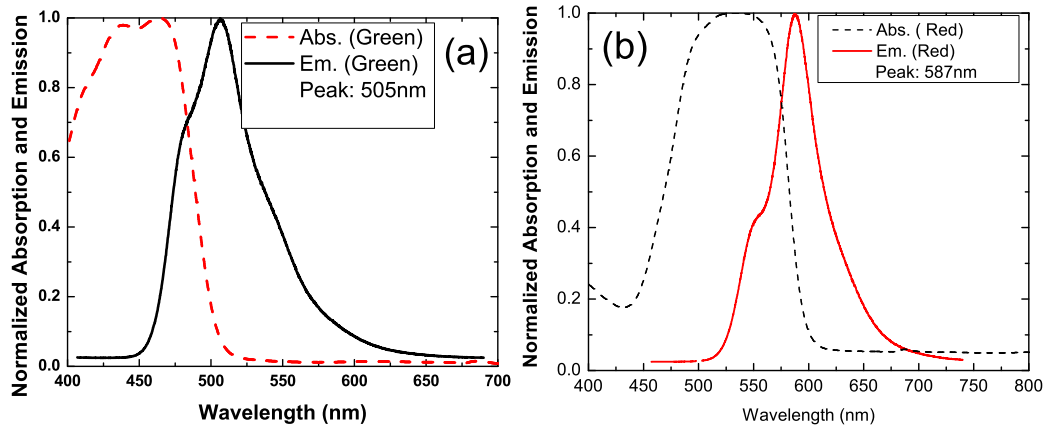


Figure 4.8: Absorption and emission spectra of the tested (a) green and (b) red color emission organic dyes in plastic.

From Fig. 4.8 (a) and (b), we see that for both of these dyes, the absorption spectra become narrow compared with the broad solar spectrum. They center at 450nm and 570nm respectively. And there exists overlaps between the absorption and emission spectrum, which will result in the self-absorption problem. After

embedding these dyes into PMMA, depending on the concentration of the dyes, the peaks of the absorption and emission spectra may shift a little bit, and as the distribution of the size of the molecules may change, the spectrum may be broadened.

By stacking these green and red LSCs together, the absorption spectrum can be effectively expanded over the solar spectrum from 400nm to 600nm. And they emit in different wavelength ranges with emission peaks of the two dyes separated by 82nm. Since the efficiency of LSCs strongly depends on the absorption and emission properties, the absorption efficiency should be greatly improved by stacking these two sheets together. Consequently, the power conversion efficiency should be enhanced. This is demonstrated in our experiments by comparing the performance of individual layers of green and red emission LSCs with the performance of the stacked double layered LSCs.

As analyzed above, if we identify proper dyes and fabricate stacked LSCs with different layers that different layers of LSCs effectively utilize different parts of the solar spectrum, the power output of the LSC PVs can be further improved. Using the group of outdoor use dyes, we have fabricated the outdoor use samples. Fig. 4.9 and Fig. 4.10 show their transmittance and emission of the Lumogen red 305, yellow 083 and orange 240 organic dyes in plastic materials. These three kinds of dyes are embedded into plastic plates respectively. By stacking them together, the absorbed wavelength range is effectively expanded to the range from 400nm to 600nm, which is the main part of the solar spectrum. As there are air gaps between the stacked LSCs, the emitted light from the green emission LSC will not be reabsorbed by the yellow emission LSC attached at its bottom. Similarly, the emitted light from the yellow LSC will not be absorbed by the red emission LSC at its bottom.

For LSC plates, we can also test their transmission abilities by using PV cells as detectors. In the experiments, the transmittance is estimated by the transmitted current ratio R_{tras} , which is defined as I_{Cover} over I_{PV} , where I_{PV} is the short-

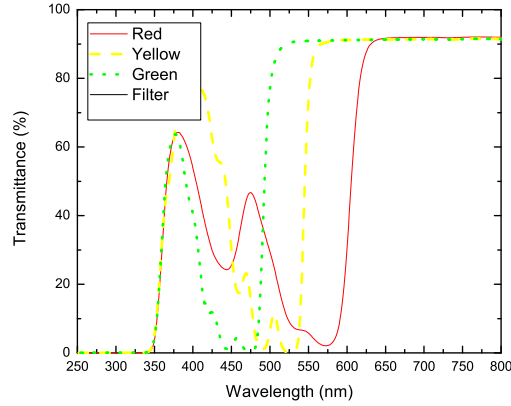


Figure 4.9: Transmittance of Lumogen red, yellow and green emission organic dyes in plastic materials.

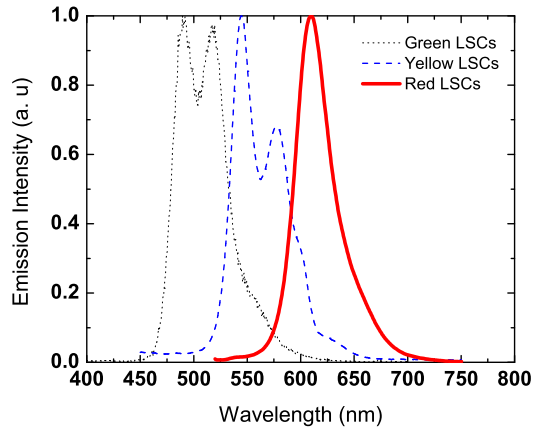


Figure 4.10: Emission spectra of Lumogen red, yellow and green emission organic dyes in plastic materials.

circuit current from a PV cell exposing to sunlight directly, and I_{Cover} is the short-circuit current from the same PV cell covered by the LSC on its top surface.

The tested transmitted current ratio for the indoor and outdoor use samples with the same thickness are shown in Fig. 4.11. They are very transparent. So it is still good enough for them to be used as “smart” windows. Comparing with the red sample for the indoor use, the lumogen Red F 305 sample can absorb 16.4% of more light.

Fig. 4.12 further shows the result if we stack them in different ways. Since the high transmitted current ratio means low absorption efficiency of the LSCs,

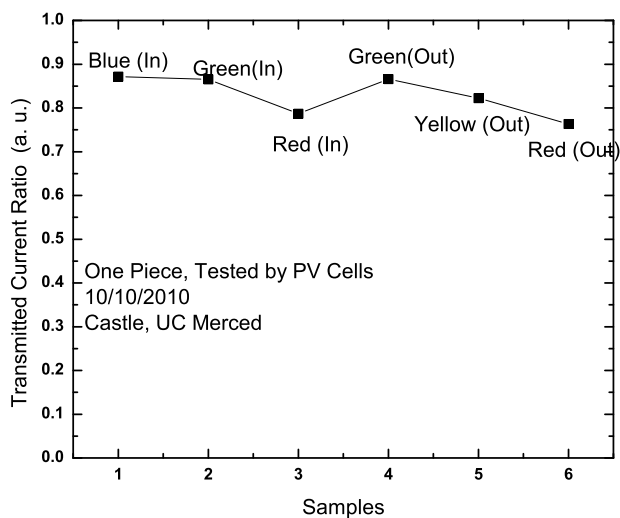


Figure 4.11: Transmitted current ratio of outdoor- and indoor- use LSC samples.

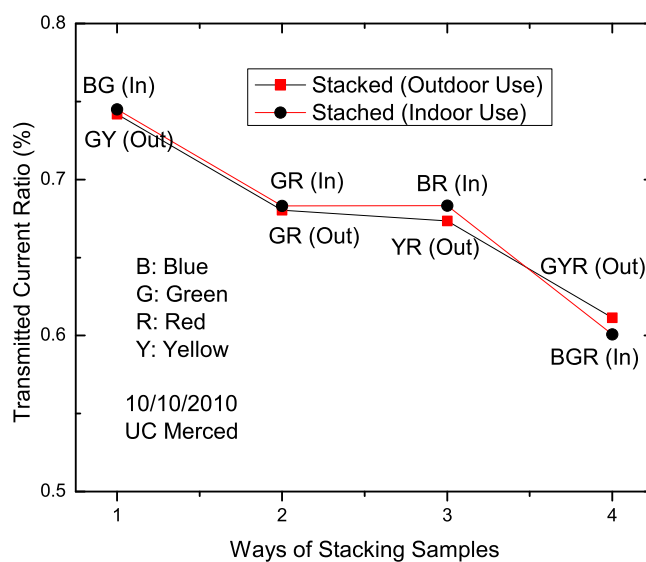


Figure 4.12: Transmitted current ratio of outdoor- and indoor- use samples by stacking in different ways.

the absorption of outdoor use dyes are higher than that of indoor use dyes. This result highlights the necessity of optical enhancement and efficiency enhancement.

4.4 Efficiency Enhancement and Optimal Design for Single Layer LSCs

In this section, for single layer LSCs, we investigated the size-dependent optical enhancement for laser dye LSCs by using optical gel and white diffusers. We tested LSCs with geometrical gain ranging from 1.2 to 62.5 under sunlight using a solar tracker. The largest tested LSC has length up to 120cm, which is as we know the larger reported size to date, and is large enough for a window in buildings. Although in our experiments, we mainly use LSCs fabricated with organic laser dyes as there are much cheaper, stable and with very good performance, the research result is also very useful for the optimization of other LSCs.

4.4.1 Optical Enhancement for Small Samples

The size dependent optical enhancement by white diffusers and optical gel can be seen clearly from testing a very small sample and a very large sample. We first test a very small LSC sample with size 4.5cm by 1.2cm by 0.32cm. It is fabricated by filling $600\mu M$ Rhodamine B solution in a polished glass cell. As show in Fig. 4.13, the output current increases 90% by adding index matched optical gel between attached PV cells and the short edge surface of the LSC. We get the improvement 50% by attaching a white diffuser at the bottom of the LSC. With both methods, the total enhancement is up to 190%. The geometrical gain G for this sample is 1.2 if we attache PV cells at all edges, and the current ratio is 40%. The calculated optical efficiency is estimated as 35% by using Eq. (4.2).

Since the obtained current ratios are less than 1, We have not seen the concentration effect of this LSC. The reason may partially because of the small size of the sample, the narrow absorption range and the strong re-absorption of the dye. As the size of the above tested LSC is much smaller for most practical applications, we then further tested LSCs with different sizes.

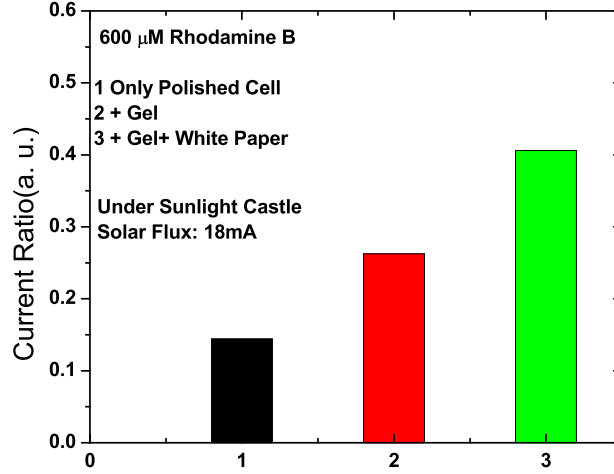


Figure 4.13: Current ratios by using different optimization methods for the small LSC sample with dimensions 4.5cm by 1.2cm by 0.32cm (Tested under sunlight).

4.4.2 Optical Enhancement for Larger Samples

The largest size we tested is 60cm by 120cm by 0.32cm with geometrical gain $G=62.5$. It is fabricated by casting red emission dyes into PMMA materials. As we know, this is the largest reported tested LSC to date.

By using the same optimization methods for this smallest sample, we obtained the current ratio results, as shown in Fig. 4.14. We can see that there is a huge improvement by using optical gel and white diffuser. Very excitingly, as shown in Fig. 4.14, we obtained the current ratios with the highest value 3.9 from the short edge and up to 2.8 from the long edge. This LSC shows a very higher concentration effect as a solar concentrator for photovoltaics.

For this largest LSC with geometrical gain 62.5, the optical enhancement by optical gel and white diffuser drops to 65% and 26% from 90% and 50% for the smallest LSC respectively, so this optical improvement is size dependent: the larger the size, the less the improvement. Also, the performance of the white diffuser drops faster than that of the optical gel, which means that the performance of the white paper is more sensitive to the LSC size. However, as the geometrical gain G increases from 1.2 to 62.5 (52 times), the calculated optical gain is 6.1%, which

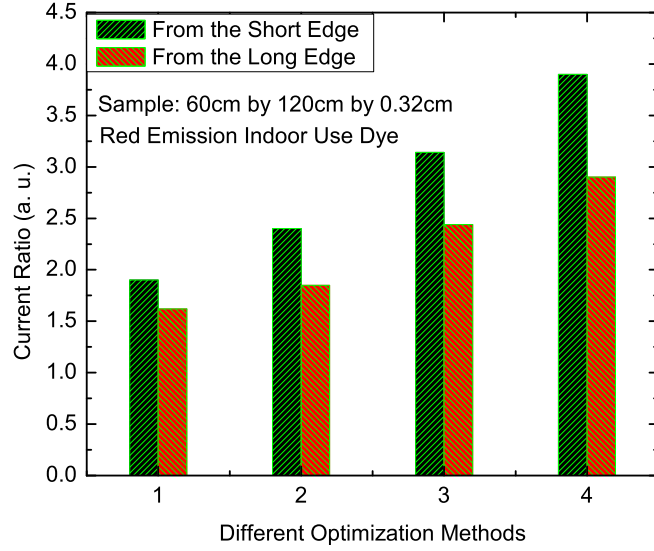


Figure 4.14: Current ratio of the largest tested LSC with 60cm by 120cm by 0.32cm. Optimization methods: 1. No optimization; 2. Only optimized with a white diffuser attached at the bottom of the LSC; 3. Only optimized with refractive index matched optical gel added between the edge of the LSC and the PV cell; 4. Optimized with a white diffuser and optical gel (Tested under sunlight).

only decreases 5.9 times. This drop is mainly due to the re-absorption. Although the size of the LSC is very large, the optical efficiency of the system may keep at a certain value.

4.4.3 Size Dependent Optical Enhancement

The size dependent enhancement of white diffusers is further tested as the white diffuser is more sensitive to the size of LSCs. The LSC we used is fabricated by casting the indoor use red emission organic dyes into PMMA material. The dimensions are 6 cm by 120 cm by 0.32cm. It has the same length and thickness with the largest LSC sample, but is narrow in width. In the experiments, PV cells are attached at the short edges without using the index matched optical gel. At

the first step, there is no white diffusers attached at the bottom of the LSC, so the background of the LSC is black. We first cover over the LSC completely with a dark cover from the top surface of the LSC, and then move the dark paper from one size to the other size of 2.54cm by 2.54cm until the LSC is completely uncovered. In this way, after each step, the length of the LSC increases 2.54cm. We did the same thing but attaching a white diffuser as a white background at the bottom surface of the tested LSC.

The corresponding values of current ratio R_I for both cases are shown in Fig. 4.15. Fig. 4.15 (a) shows that the longer the length, or the larger the size of the LSC, the larger the output current ratio, or the larger the electrical gain, and the stronger the concentrator effect of the LSC. Fig. 4.15 (b) shows that with the increase of the LSC size, the improvement by the white diffuser decreases from 78% and tends to plateau at 42% after the length is larger than 76cm. It can be explained by the following mechanisms. First, the white diffuser reflects the highly transmitted light back into the LSC for luminescent materials to utilize again. Also, the white diffuser reflects light directly towards PV cells attached at the LSC edges. When the size of the LSC increases, the enhancement from the second mechanism becomes weaker and weaker, which contributes to the slowly increase of the output current ratio in Fig. 4.15 (a) and the very flat enhancement ratio in Fig. 4.15 (b).

For this tested long strip LSC sample, without the refractive index matched optical gel, the current ratio is 1.5 as shown in Fig. 4.15 (a). It can be improved to 3 by applying optical gel. With the geometric gain calculated as 9, the optical efficiency is $\eta_{opt} = 16.7\%$. The power conversion efficiency of the PV cell we used in the experiment is approximately $\eta_{PV} = 17\%$. So the power conversion efficiency of the LSC with the attached PV cell can reach $\eta_{power} = 2.83\%$ from Eq. (4.4). With the refractive index matched optical gel, we estimate that the efficiency can be as large as $\eta_{power} = 5.4\%$.

The size of the LSC for optimization design of LSC can be selected based on

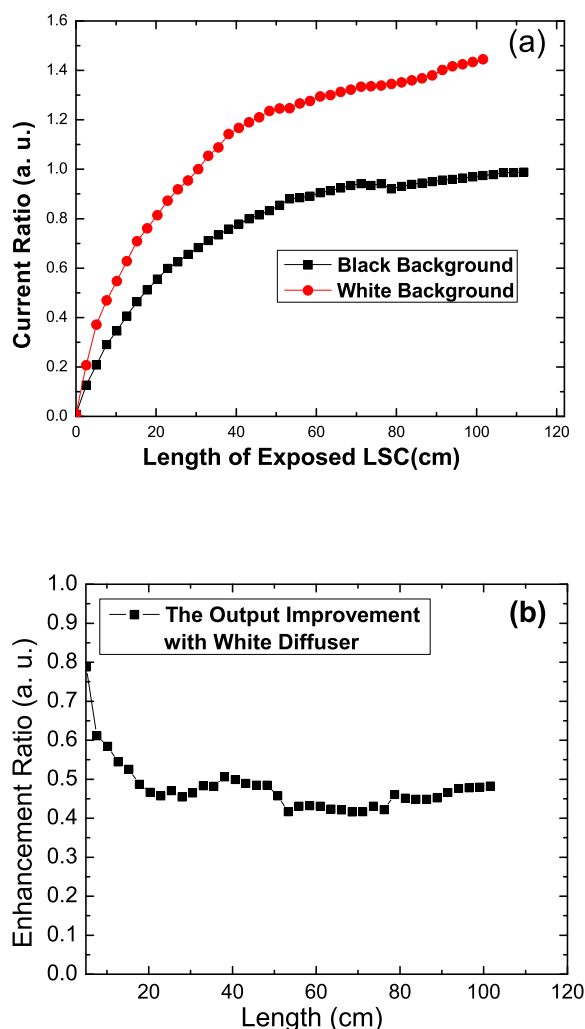


Figure 4.15: Size dependent optical enhancement by using a white diffuser for LSCs. The tested LSC has dimensions 6cm by 121cm by 0.32cm. In the test, it is partially covered to change the size of LSCs. (a) Output current ratio with (Diamond) and without (Square) attaching a white diffuser at the bottom surface as white and black backgrounds respectively; (b) The enhancement ratio by using a white diffuser with the change of the length of the exposed LSC (The change of the exposed size). The refractive index matched optical gel is not used in showing the size-dependent effect of the white diffuser on the current ratio.

a re-absorption testing. Contributions of different parts of the LSCs to the output photocurrent are different due to the re-absorption loss. If the emitted light is from

a part of LSC which is far away from the attached PV cell, it is easily absorbed by other dye molecules during the transport process. It may also escape from the transparent materials due to the top surface loss.

4.4.4 Size Dependent Re-absorption Loss

In order to estimate the contributions of different parts of a LSC to the output photocurrent due to re-absorption, we design and show the experimental setup in Fig. 4.16. The same LSC strip is used with dimension 120cm by 6 cm by

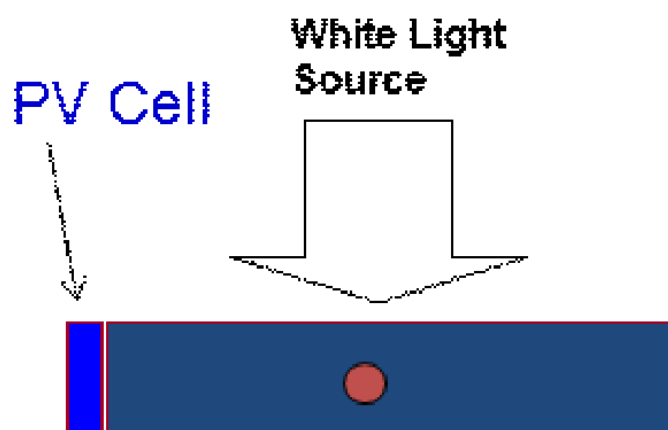


Figure 4.16: Experimental setup for testing the output power contributed by different parts of the LSC. The black paper with a hole is covered from the top surface of the tested red emission LSC. The output open circuit voltage and short circuit current from the attached the PV cell are recorded when the position of the hole changes.

0.32cm. The black paper with a hole is covered from the top surface of the tested LSC. The diameter of this small hole is 2.54cm. With the increase of the distance between the exposed hole of the LSC and the attached PV cell, the contribution of the small hole of the LSC is reduced. The output short circuit current from a PV cell attached at the edge of the Lumogen Red F 305 LSC is recorded by exposing the system to sunlight. The excited length is measured between the exposed hole and the attached PV cell. The output photocurrent drops approximately exponentially as a function of the excitation length as shown by the fitted curve in Fig. 4.17. As

a result, the size of the LSC for optimization design of LSC should be considered when we consider the increasing cost of the materials.

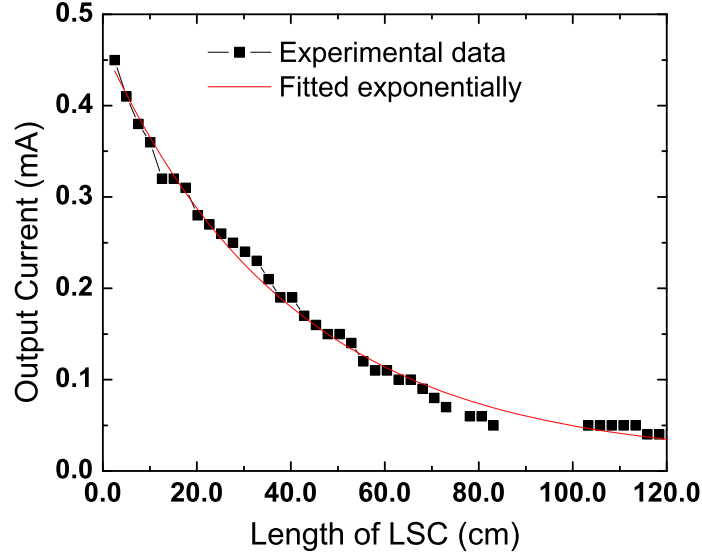


Figure 4.17: The output short circuit current from a PV cell attached at the red emission LSC strip by exposing it to sunlight. The LSC is with 121cm by 6 cm by 0.32cm. (Experimental setup is shown in Fig. 4.16).

4.4.5 Size Dependent Energy Loss from LSCs

The energy loss of LSCs is size dependent. In order to estimate this size dependence, we analyzed energy distributions from each surface of LSCs with different sizes and different geometrical gains.

In the experiments, we tested the red LSC sample with dimensions 60cm by 120cm by 0.32cm. The geometrical gain is 62.5. A silicon PV cell as a detector is 12.7 cm by 0.32cm. The open circuit from the reference PV cell is tested as 130mA. During the test, we have applied a white diffuser and optical gel for optimization. At the beginning, a black paper is used to cover the whole LSC. We then moved the covered black paper in increments of 2.5cm from the side with PV cells attached

until the LSC was completely uncovered. By moving the black paper cover, we changed the geometrical structure and the geometrical gains of the tested LSC. At each step, we recorded the output current from the tested LSC.

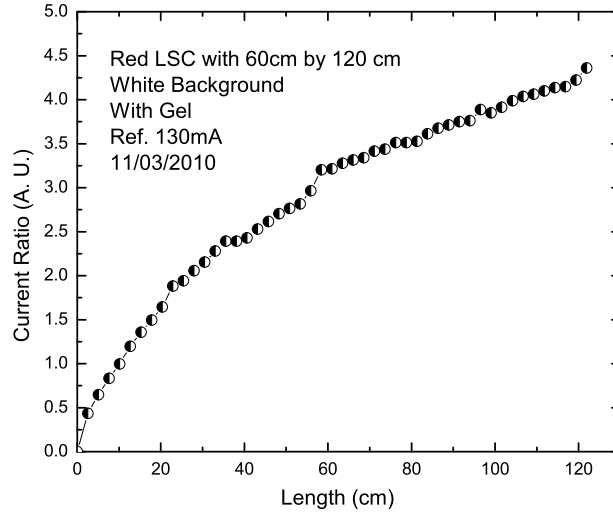


Figure 4.18: The concentration factor, or the current ratio, as a function of the length of a LSC.

The calculated current ratios from the edge of the LSC at different sizes are plotted in Fig. 4.19. Clearly, we see that the larger the length exposed to sunlight, the larger the size of the LSC, and then the larger the output current ratio, and the concentration factor.

We also note that the increase of the output energy is not linear with the increase of the length of the LSC. In order to analyze the energy distribution, we defined the percent of energy lost from the LSC system, η_{loss} , as

$$\eta_{loss} = 1 - \eta_{top} - \eta_{bottom} - \eta_{edge}. \quad (4.5)$$

For the LSC we tested, the escaped energy is 2% from the top surface, 78% from the bottom surface, so

$$\eta_{loss} = 1 - 2\% - 78\% - \eta_{edge}. \quad (4.6)$$

η_{loss} is the function of the LSC size which is described by the length of the LSC, L . If we fix the width of tested LSCs, the geometrical gain can then be calculated

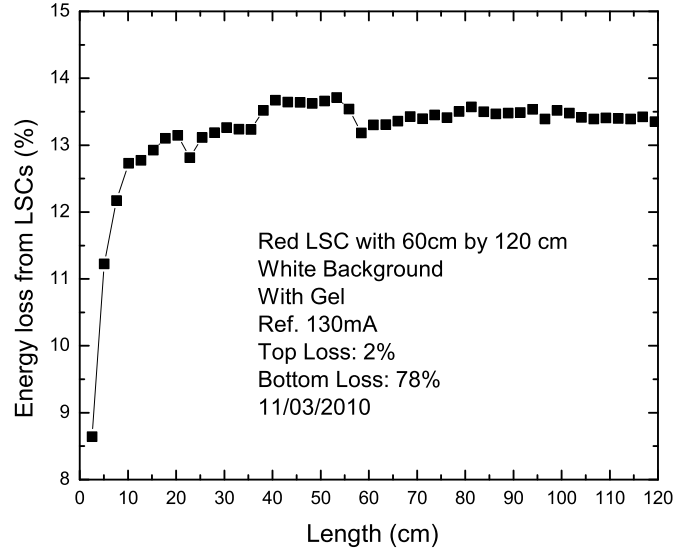


Figure 4.19: The energy loss from the system as a function of the length of the tested LSC.

as

$$C_{geometrical} = \frac{60L}{2 \times 0.32 \times (60 + L)} = \frac{93.8L}{60 + L}. \quad (4.7)$$

By changing the length of the LSC to 120cm and fixed the width to 60cm, we tested the current ratio and calculated the energy loss $loss$ as a function of the LSC length L . The tested result is shown in Fig. 4.19. When the size of the LSC is very small, the energy loss is also small, but this loss increases very quickly when the LSC becomes larger, and keeps at certain value with the increase of the LSC size.

As a result, when the size of the LSC is small, the energy loss is not very serious, but this energy loss increases very quickly with the increase of the size of the LSC. At certain size, this loss will drop very slowly. With this energy analysis method, we can find the optimal length for the optimal design of an LSC for photovoltaic technologies.

4.5 Efficiency Enhancement for Multilayer Organic LSCs

We have shown the absorption and emission spectral properties of organic dyes in optical characterization experiments. As we know, these dyes absorb solar radiation in different ranges of the solar spectrum. In order to utilize the whole solar spectrum, one of the methods is to design multilayered LSCs. The designed system can separate different portions of the solar spectrum like multi-junction cells to improve the absorption efficiency.

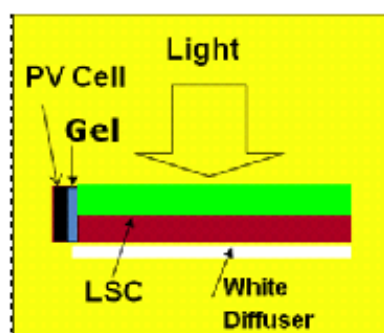


Figure 4.20: A schematic of the experimental setup for efficiency enhancement of LSCs by attaching a white diffuser at the bottom of the tested LSCs (Stacked two layers of LSCs in this figure), and by adding refractive index matched optical gel between LSC edges and the attached PV cells. In the test, a larger piece of PV cell with 1.2cm by 1.2cm is masked with black tape to match the thickness of the tested LSC edges.

As shown in Fig. 4.20, a white diffuser is attached at the bottom of the LSCs with an air gap to reflect and scatter the transmitted light back into the LSC to increase the output efficiency. As also shown in Fig. 4.20, the refractive index matched optical gel is added between the edge of the LSC and the attached PV cells.

With the stacked optical enhancement methods, the performance of a green emission and a red emission LSC both with 15.2cm by 15.2cm by 0.32cm are tested respectively, as shown in Fig. 4.21. First, the output current of red emission

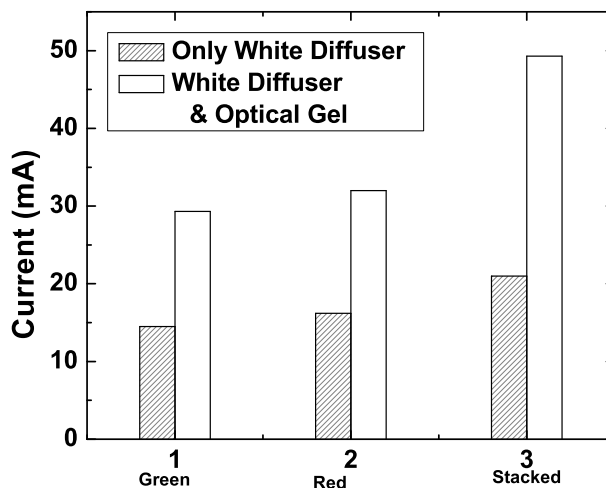


Figure 4.21: Output photocurrent for (1) Single green emission, (2) Single red emission and (3) Stacked green and red emission LSCs by using white diffusers and optical gel.

LSCs is higher than that of the green emission LSCs. Second, the output current increases almost 2 times for each of them individually by using the optical gel. However, the output current increases 2.3 times for the double-layer stacked concentrators after using the optical gel. This result shows that the efficiency enhancement methods by using a white diffuser and optical gel are more effective for stacked structures than for single layer LSCs. With such optimization, the optical efficiency for the stacked structure is 28%, which improves 87% from the single green emission layer LSCs and 76% from the single red emission layer LSCs respectively. So we get higher output current, higher optical efficiency, and higher power conversion efficiency with stacked structures.

We noticed that the current in Fig. 4.21 of the stacked samples is less than the sum of the green and red emission LSCs. This is mainly due to the partial overlap of the absorption spectra between red and green emission LSC samples.

As the dyes in the stacked green and red emission LSCs sheets mainly absorb different portions of the solar spectrum, we observed in our experiments that the order of stacked LSCs single layers can be reversed without reducing the output current.

The geometrical gain for the tested one layered LSC with dimension 15.2 cm by 15.2cm by 0.32cm, is 12, and is 6 for the tested stacked LSCs. For the stacked LSC sample $\eta_{opt} = 28\%$, $\eta_{PV} = 17\%$, the power conversion efficiency of the LSC with the attached PV cell is about $\eta_{power} = 4.8\%$ calculated from Eq. (4.4).

For a larger stacked prototype with the dimensions 60cm by 45cm by 0.64cm, the result shows that the optical efficiency drops to about 10.7%. So we can predict that the enhancement by using white diffuser and optical gel also is size dependent for stacked structured LSCs, and such dependence will not be very strong after a certain size.

From the above discussion, we can see that the stacked structure optimized with white diffusers and optical gel performed the best. Since the optical efficiency drops when the size of the stacked LSC increases, it is very necessary to study the size dependence of the output efficiency for stacked LSC structures. In the following part, we fabricated a stacked LSC with practical size, tested and estimated the output efficiency.

For the application of LSCs as windows or roofs of a building, the practical size in length is often around 0.5m or larger. As described in the experimental part, we have fabricated two such prototypes by stacking a green and a red emission LSCs together. They are fabricated by casting the green and red emission dyes into PMMA plastics materials respectively. And each of them is with 60cm by 60cm by 0.32cm. They are stacked together with PV cells attached at the LSC edge surfaces in series. The calculated geometrical gain is 24. In the testing, the whole system is put on a tracker and pointed to the sun with a white diffuser as background at Merced, California.

The tested output short circuit current from the PV cell is $I_h = 550mA$, and the corresponding open circuit voltage is $V_h = 9.3V$. Since for the same PV cell, we can get the short circuit current $I_{Ref} = 230mA$, the current gain is calculated

as $R_I = 550/230 = 2.2$, the optical efficiency is then estimated as

$$\eta_{opt} = \frac{R_I}{G} = \frac{2.2}{24} = 9.2\%. \quad (4.8)$$

Correspondingly, the power conversion efficiency is estimated as

$$\eta_{Power} = \eta_{opt} \times \eta_{PV} = 1.4\%. \quad (4.9)$$

In another way, we estimated the power conversion efficiency. The output power of this system is 4.09 W with the fill factor 0.72. The power input is between $0.6m \times 0.6m \times 1000W/m^2 = 360W$ since the solar constant at Merced is about $990W/m^2$ to $1050W/m^2$. As a result, if we use silicon PV cell, the power conversion efficiency will be 1.1%. This value is very close to 1.4%.

We have to note that although the efficiency of the whole system is low, the electric gain or current ratio we have is 2.2, which shows the performance of light concentrating.

In order to estimate the performance of the “smart” window systems in a year, the solar irradiance at UC Merced is estimated. We have estimated the monthly total solar radiation incident on the system with 1m² in kW-hrs at Merced and at Denver. These data are from the Program F-Chart. The monthly averaged output power of our LSC systems at Merced horizontally (0°) and at both Merced and Denver vertically (90° as normal windows) is shown in Fig. 4.22 with the estimated efficiency 4%.

We also fabricated LSCs by stacking three layers of fluorescent plates, and each layer utilize different parts of the solar spectrum. The stacked blue, green and red emission fluorescent plates are the indoor use dyes. In the experimental, the white diffuser is applied. We did the size dependent efficiency enhancement study by optical gel for the three layered LSCs. A smaller prototype is with three fluorescent plates in square and dimensions 30.48cm by 30.48cm by 0.32cm, A larger one is with three fluorescent plates in square and dimensions 60.96cm by 60.96cm by 0.32cm. The tested results are shown in Fig. 4.23. We can see that

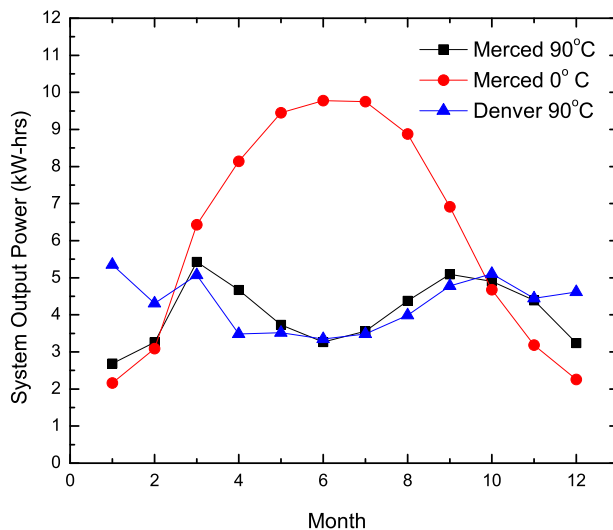


Figure 4.22: The monthly averaged total output power of the fabricated LSC system with vertical position at Merced and Denver (0°) and horizontal position (90°) at Merced.

the larger the size of the stacked LSC, the larger the output current. The results are pretty consistent.

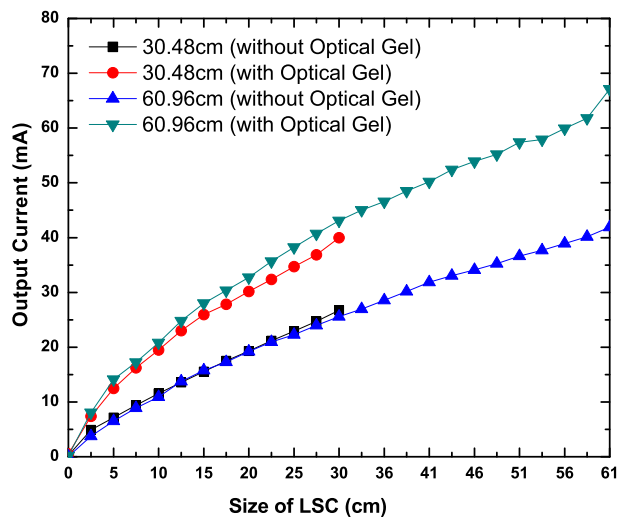


Figure 4.23: Photo luminescent current from blue, green and red emission fluorescent plates stacked LSCs.

The distribution of the output current along the LSC edges is also characterized for three prototyped stacked LSCs by using PV cells. The experimental

setup is shown in Fig. 4.24 and the tested output is shown in Fig. 4.25.

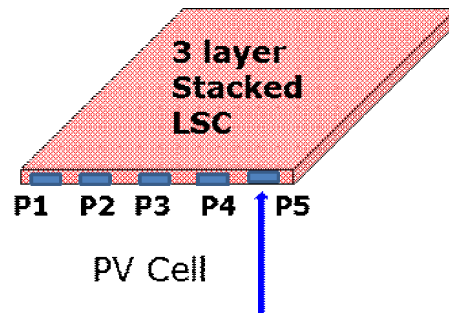


Figure 4.24: Experimental setup for characterizing the distribution of the output current along the stacked LSC edges by using PV cells.

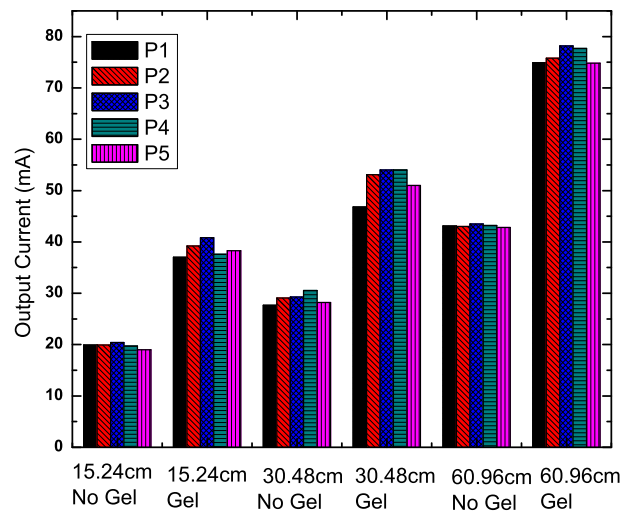


Figure 4.25: The output edge distribution of three layer stacked LSCs. There are blue, green and red emission fluorescent plates stacking from top to bottom in sequence. All of them are in square shape with length in 15.24cm (6in), 30.48cm(12in) and 60.96 cm (24in).

We characterized the output current edge distributions of these three layer stacked LSCs. They are with blue, green and red emission fluorescent plates stacking from top to bottom in sequence, and each of these florescent plates are in square shape with thickness 0.32cm (1/8 in). The 3 layer stacked LSCs are with length in 15.24cm (6in), 30.48cm (12in) and 60.96 cm (24in). The output current is slightly high from the middle position P3, but distributed very evenly at different posi-

tions. In addition, the enhancement by optical gel for these three configurations is around $1.6\times$.

4.6 Wavelength Selective Films for LSCs

4.6.1 Optimization principle

Due to total internal reflection, a large amount of the emitted light from luminescent materials can be transported to the LSC edges. However, the refractive index of matrix materials is around 1.5. As a result, about 25% of light will escape from the top surface of an LSC. In order to reflect back the escaped emitted light from the top surface, one of the optimization methods is to use wavelength selective films. By applying this film on the top of an LSC surface, the escaped emitted light from the LSC top surface can be reflected back into the LSC. At the same time, the wavelength selective film should not affect the absorption of the coming solar radiation. So the selective film has to be very transparent in the absorption range of the embedded dyes. The wavelength selective film acts like a “smart” mirror since they reflect and transmit light in different wavelength ranges [vSBS⁺08, DVV⁺10a, DVV⁺10b, DVR⁺08].

4.6.2 Spectral properties of 3M films

We have collaborated with 3M Company and produced wavelength selective films for organic LSCs. The tested transmittance of the produced 3M “smart” mirrors is shown in Fig. 4.26. The film reflects wavelengths very effectively from 600nm to 750nm, and are very transparent for wavelengths from 300nm to 600nm. By comparison the transmittance of the outdoor using fluorescent LSCs and the wavelength selective filter, we can see that this wavelength selective film is able to transmit the wavelength in the absorption range of the LSCs, and can be approximately used for the Lumogen Red F 305 Red sheets. It cannot be used for the

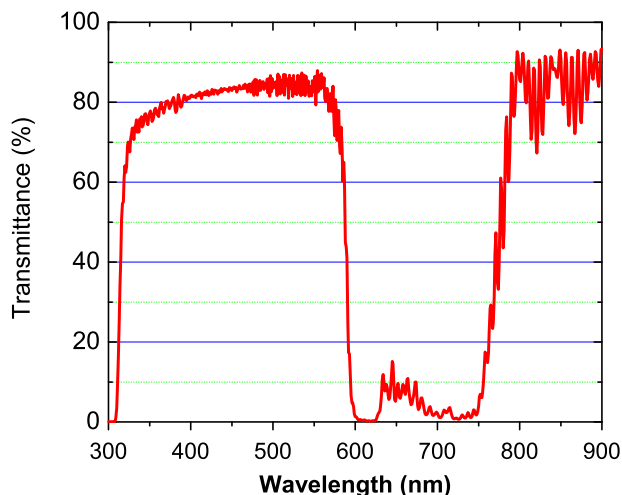


Figure 4.26: Transmittance of the 3M wavelength selective film. The film can reflect wavelength very effectively from 600nm to 750nm.

yellow and green emission LSCs as the emitted light cannot be reflected back into the LSC if applied.

4.6.3 Transmitted current ratio

We tested the transmittance properties of the 3M wavelength selective film. Using a silicon PV cell with dimensions 1.2cm by 1.2cm as a detector, the tested output current from the bare PV cell is 15.2mA, but is 9.3mA when we covered the same PV cell with the wavelength selective film. So the transmitted current ratio R_{Tran} is $9.3/15.2 = 61\%$. This result means that about 61% of light passes through the LSC with the wavelength selective film covered on its top surface. That 39% of light is either reflected back by the film or absorbed by the film and dyes in the LSC. We estimated that this is mainly due to the effective reflection of the film to light in 600nm to 750nm. In the testing, when we vertically aligned and exposed the LSC covered with the film to the ground, we still get the transmitted current ratio 63%.

4.6.4 Performance of LSCs with the wavelength selective film

In order to estimate the performance of the 3M film on our fabricated LSCs, two LSCs are tested. One is with dimensions 35cm by 35cm by 0.32cm and geometrical gain 28. The other is with dimensions 60cm by 120cm by 0.32cm and geometrical gain 62.5. The PV cell used as a detector is the silicon PV cell from Sunpower with dimensions 12cm by 0.32cm. During the test, we also considered the effect of a white diffuser and optical gel on the LSC output currents.

All the tests are done under sunlight. The tested results are shown in Table 4.1 for the first LSC. The output current from the reference PV cell is 15.2 mA.

LSC sample Surface	I_{output} without 3M Film (mA)	I_{output} with 3M Film (mA)
Top(No Gel)	0.05	0.05
Bottom(No Gel)	0.76	0.50
Edges (No Gel)	2.33	2.15
Edges (With Gel)	4.24	3.15

Table 4.1: Tested output current I_{output} for the LSC with geometrical gain 28 at white background.

First, from Table 4.1, we can see that by applying the 3M film, the output current decreased by $(4.24 - 3.65)/4.24 = 14\%$. Second, the optical efficiency is 15% without applying the wavelength selective film, but decreases to 13% when we applied the film. The decrease is mainly because the reflective range of this 3M film does not exactly match the emission spectrum of the tested LSC. Some of the escaped light from the tip surface of the LSC cannot be reflected back to the LSC by the film. The calculated power conversion efficiency for this system is $\eta_{power} = (0.13 \sim 0.15) \times 0.17 = 2.2\% \sim 2.6\%$. During the test, we also showed the effect of optical gel on the output current of the tested LSC. We found that without the application of the wavelength selective film, the optical gel can improve the output current $1.81\times$, but improves $1.70\times$ when we applied the wavelength

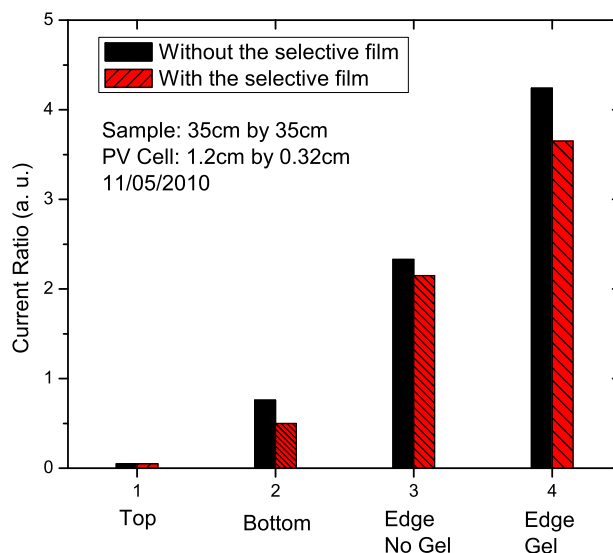


Figure 4.27: The current ratio from each surface of a LSC with dimensions 35cm by 35cm by 0.32cm, and geometrical gain 28. The detector is a silicon PV cell with 1.2cm in length and 0.32cm in width. It is fabricated with the outdoor use red emission dyes.

selective film. The results are also shown in Fig. 4.27. We obtained the current ratio 4.24, which means that concentration factor of this concentrator is 4.24. This result is much higher than any fixed concentrator based on geometrical optics.

We then analyzed the energy distribution from all surfaces. The result is shown in Fig. 4.28.

We found that most of the light escapes from the bottom surface. This is due to the narrow absorption spectrum of the embedded dyes. This analysis emphasizes the application of stacked structures and white diffusers.

We also tested the LSC with different sizes. The maximum size we tested is with dimensions 60cm by 120cm by 0.32cm with geometrical gain 62.5. The output current ratio is shown in Table 4.2 for the testing with a black background and Table 4.3 for the testing at a white background. Fig. 4.29 further shows the output current ratio from each surface of the LSC. Table 4.2 and Table 4.3 show that the output power did not increase. By further calculation, we see that the decrease by application of the 3M wavelength selective film is 4% without

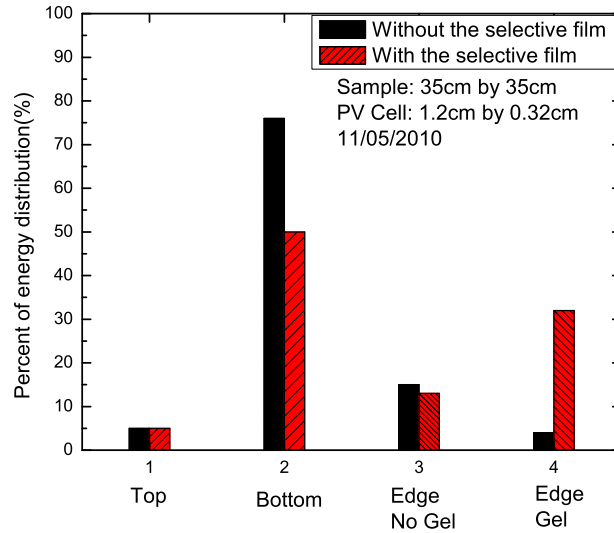


Figure 4.28: The energy distribution from each surface of the LSC with dimensions 35cm by 35cm by 0.32cm, and geometrical gain 28. The detector is a silicon PV cell with 1.2cm by 0.32cm.

LSC sample Surface	I_{output} without 3M Film (mA)	I_{output} with 3M Film (mA)
Top(No Gel)	0.02	0.02
Bottom(No Gel)	0.74	0.49
Edges (No Gel)	1.90	1.76
Edges (With Gel)	3.16	3.01

Table 4.2: Tested output current I_{output} for the LSC with geometrical gain 62.5 at a black background.

application of optical gel at the edge surfaces and 3% if applied optical gel at the edge surfaces.

Although the size of the LSCs increases more than twice from the one with geometrical gain 28, the effect of the optical gel on the output is still about $1.6\times$ either at the black background or at the white background.

The calculated optical efficiency of this LSC for black background, is 4.7% with the application of the 3M film, but is 4.9% without the application of the 3M film. If we use a white diffuser, which applied a white background for the LSC, the optical efficiencies are 6.6% and 6.4% with and without the application of the

LSC sample Surface	I_{output} without 3M Film (mA)	I_{output} with 3M Film (mA)
Top(No Gel)	0.05	0.02
Bottom(No Gel)	0.74	0.49
Edges (No Gel)	2.63	2.53
Edges (With Gel)	4.23	4.10

Table 4.3: Tested output current I_{output} for the LSC with geometrical gain 62.5 at a white background.

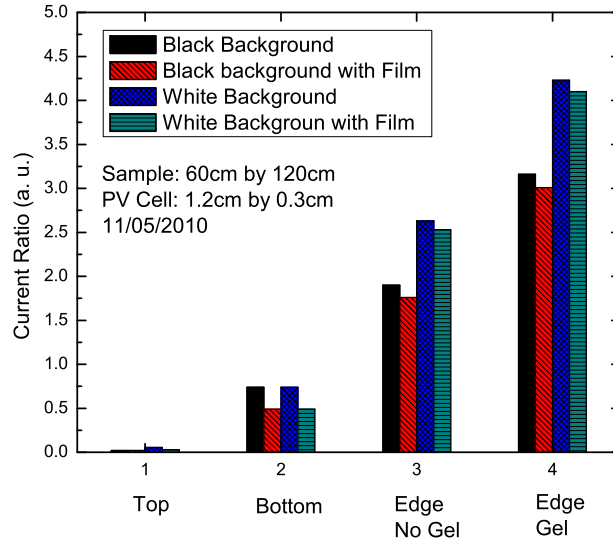


Figure 4.29: The current ratio from each surface of a LSC PV system with dimension 60cm by 120cm by 0.32cm and geometrical gain 62.5.

3M film respectively.

The efficiency does not enhanced by applying the wavelength selective film mainly because the reflective range of the 3M wavelength selective film does not match the whole emission wavelength range of the dye material of the tested LSCs. We can obtain the enhancement by applying the wavelength selective film if the film reflects most wavelengths in the dyes' emission range. The energy balance analysis from each surfaces of this LSC is given in Fig. 4.30, which also clearly shows that most of the energy escapes from the bottom surface limited by the narrow absorption spectra of the applied dyes. When we applied the 3M wavelength selective film, a large amount of energy is absorbed or reflected to the sky by the

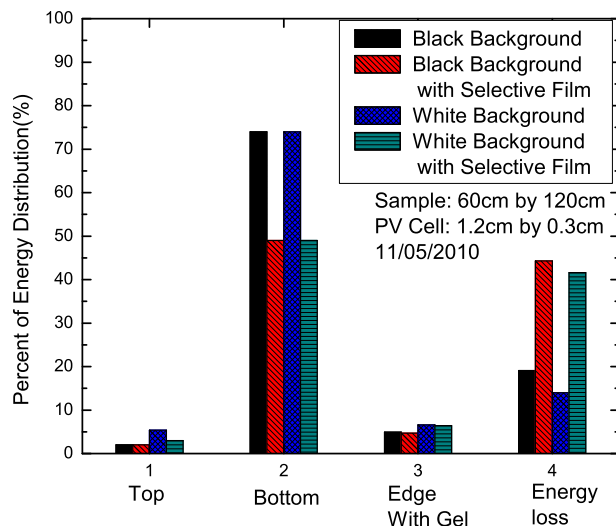


Figure 4.30: The energy distribution from each surface of the LSC with dimension 60cm by 120cm by 0.32cm and geometrical gain 64. The detector is a silicon PV cell with 1.2cm by 0.32cm.

3M film.

When we compare the optical gain of these two LSCs, we found that although the concentration gain of the smaller prototype with outdoor use dyes is 28, it yields almost the same current ratio 4.24 with the largest tested LSC prototyped with indoor use dyes. Also, the optical gain of this system is 15% without applying the 3M film, and is $2.67\times$ of the largest tested LSC. This results show that the performance of the outdoor use sample is very encouraging.

By applying the energy balance analysis method to other LSCs, we can get the energy distribution among each LSC surface. This will be beneficial for the optimum LSC designs.

4.7 Stability Properties of Organic LSCs

Stability properties are very important for LSCs in applications of LSC for photovoltaic technologies. The plastic Plexiglas material tested by the Evonik Company has shown the unsurpassed UV stability and superb weather ability,

which makes this material the logical choice among plastic materials for outdoor and artificial lighting applications. When dyes are embedded into these plastic materials, it is very necessary to further test the system stability properties by characterizing their optical and electrical properties under the real weather conditions.

We have done the experiment for LSCs with the group of indoor and outdoor use dyes, and we assume that the stability properties of dyes for outdoor use should be better than that of the indoor use dyes. In our experiments, the optical and electrical properties of the samples are characterized for comparing the stability properties.

The experimental process is described as follows:

a. Preparing LSCs: We prepared 3 groups of LSCs for testing. Each group contains a piece of red emission LSC and a piece of green emission LSC. During the test, the first group is kept into dark; the second group is exposed outside with black board attached at their bottom surfaces as black backgrounds; and the last group is exposed outside with a white board attached at their bottom surfaces as white backgrounds. The sample is shown in Fig. 4.31. All the red or green

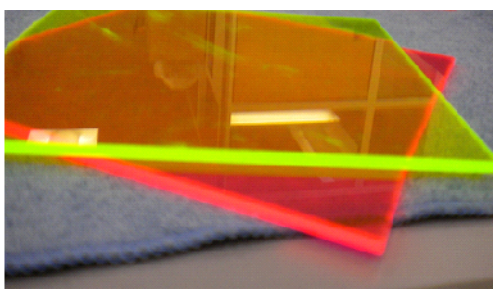


Figure 4.31: Picture of one group of LSCs for the stability testing. For each group, there are a LSC fabricated with green emission dyes and a LSC fabricated with red emission dyes. There are three such groups: the first group is kept in the dark; the second group is exposed to sunlight with black board attached at the bottom as black background, and the third group is exposed to sunlight with white board attached at the bottom as white background.

emission LSCs are cut from the same large piece of LSC. All the samples have the

same dimensions 15.24cm by 15.24cm by 0.32cm.

b. Comparing the optical properties: the absorption and emission properties are tested. After each testing, we immediately put the samples back to the experimental conditions.

c. Comparing the output power for PV technologies: the output current from Si PV cells attached at the edge surfaces of the LSCs is tested with the position normal to sunlight's incident direction. After each testing, we immediately put the samples back to the experimental conditions.

The output current and the spectra from these samples are tested weekly, and have characterized for two months.

The tested current ratio from these three groups are plotted in Fig. 4.32. In this figure, we can see that the output current ratio or the concentration factor

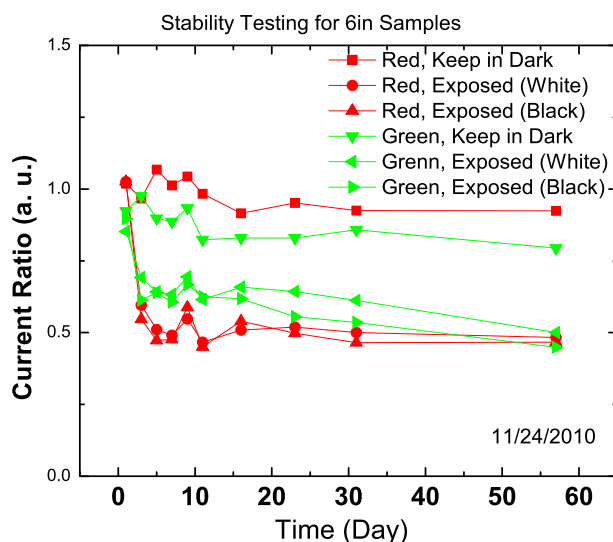


Figure 4.32: The stability testing results for the three groups of LSCs fabricated with red and green emission dyes.

from samples exposed to sunlight drops very fast at the beginning, but drops much slower after the first week. Also, for the group kept into dark, the red LSC performs better than the green LSCs. While for the groups exposed under sunlight, the drop of the current from the red LSCs is faster than that from the green LSCs.

In addition, the LSCs exposed under sunlight with black background drop faster than the LSCs exposed under sunlight with white background.

After two months, the transmittance and the emission properties of green LSCs are tested and plotted in Fig. 4.33 (a) and (b) respectively.

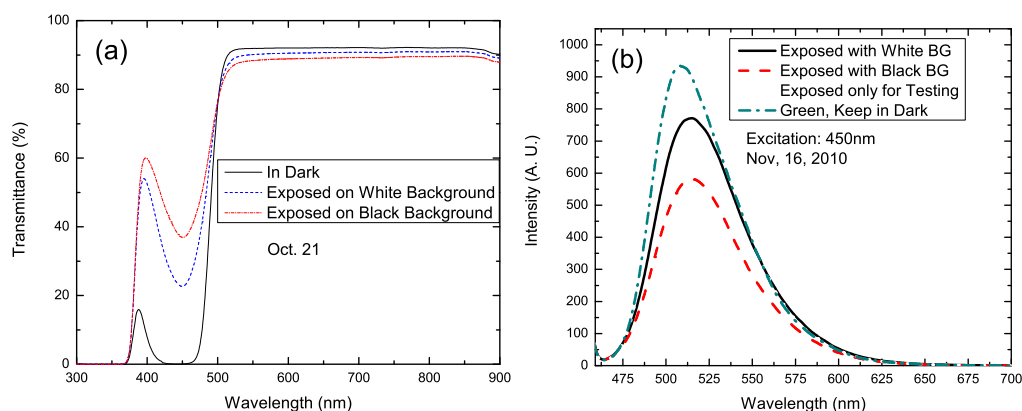


Figure 4.33: (a) Transmittance and (b) emission spectra of green emission LSC for stability testing. The samples have been exposed to sunlight or kept in dark for two months.

The sample kept in the dark absorbs more sunlight than the samples exposed under sunlight, and emits with the strongest emission intensity. It means that the absorption efficiency and the emission efficiency of the sample kept in dark are the best. Also, LSCs exposed under sunlight with white background have better absorption and emission abilities than LSCs exposed under sunlight with black background.

Similarly, the transmittance and the emission properties of red LSCs are tested and plotted in Fig. 4.34 (a) and (b) respectively. Although the transmittance of these samples has not changed a lot, LSCs kept in the dark emit with the strongest emission intensity, and LSCs exposed under sunlight with white background have better absorption and emission ability than that under sunlight with black background. The testing results show that the absorption efficiency of the red LSC has not decreased too much while the emission efficiency dropped more obviously in two months.

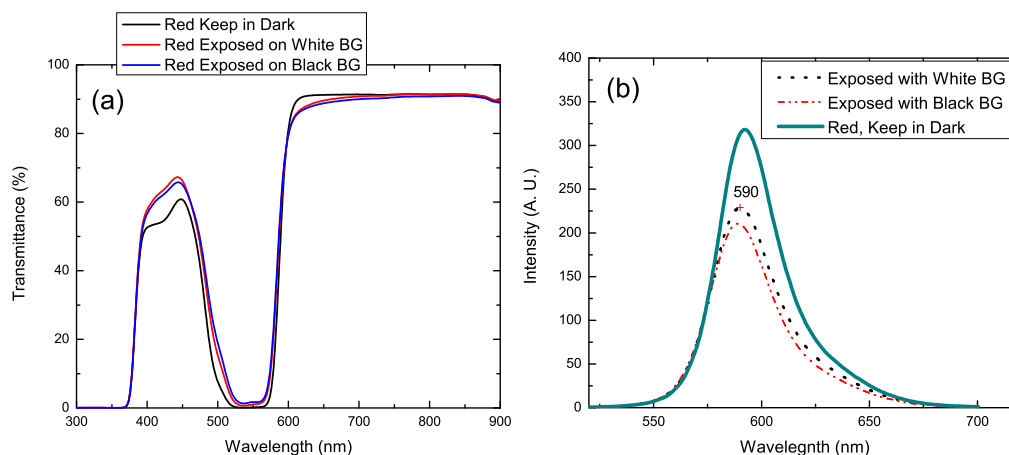


Figure 4.34: (a) Transmittance and (b) emission of red LSCs for stability testing. The samples have been exposed to sunlight or kept in dark for two months.

4.8 Concentration Performance for Diffuse Light

An LSC is known as a non-tracking system. One of the advantages of the LSC is to concentrate both direct and diffuse light effectively without tracking. In order to test the performance of our samples as "smart" windows, we fabricated two stacked LSC PV systems. The attached high efficiency mc-Silicon PV cells are strips with size 12.7cm by 0.63cm.

The experiments are described as follows.

(1) LSCs: There are two layers for the stacked LSC PV system. Each layer is with the size 30cm by 30cm by 0.3cm. Luminescent materials in the top and bottom layers are green and red organic dyes respectively.

(2) PV Cells: At the four edges of the LSC, four pieces of PV cells are attached at the middle respectively. They are not wired together, and optical gel has not been used for optimization.

(3) Locations: To concentrate the global light that comes into the LSC PV system, the first stacked system is vertically aligned to the ground with the top side toward the south and the bottom side toward the north with black cover. (Applying this background is to avoid light coming into the system from the bottom). To



Figure 4.35: Experimental set up for the performance of LSCs in collecting global and diffuse light. Prototypes of LSCs are fabricated by stacking green and red LSCs together.

concentrate the diffuse light, the second LSC is also vertically aligned to the ground but with the top side toward to the north. The bottom side is also covered with black cover to avoid light coming into the system. We call them “smart” windows because we can get electric from them if they are integrated into buildings as windows. The setup is shown in Fig. 4.35.

(4) Data recording: The output current is recorded every half hours from 8:00AM to 6:00PM during a sunny days.

(5) Weather: We selected a typical sunny day for our testing at Atwater, California. We tested the performance of the LSC PV systems for both global and diffuse light.

The tested current ratio from each attached PV cells at the four edges of the prototype for global and diffuse light are shown in Fig. 4.36. We show the change of the concentration factors of LSCs from 4 edges for the collection of global light in Fig. 4.36 (a) and for the collection of diffuse light in Fig. 4.36 (b). In

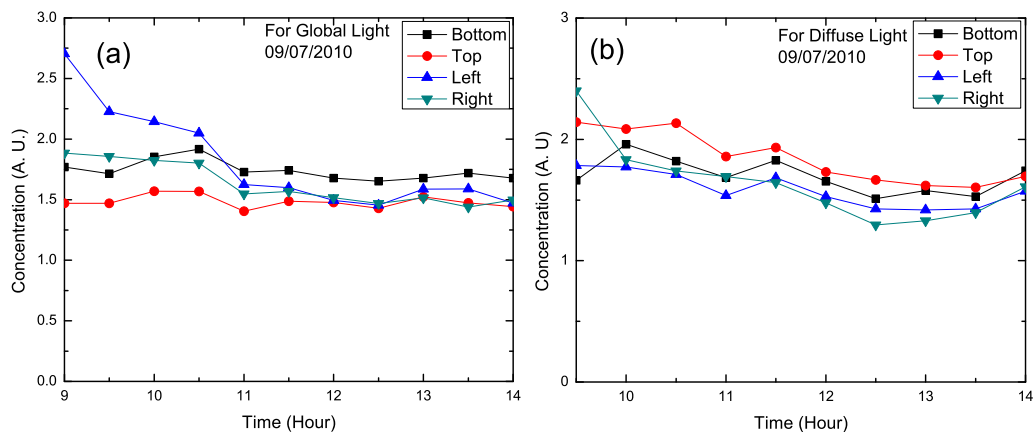


Figure 4.36: The concentration factors of LSCs from 4 edges for (a) global light and (b) diffuse light as function of the time in hours on 09/07/2010 without any optimization. (The background of the tested LSC is black and no optical gel has been applied.)

the test, we have not applied any optimization in order to get the results more accurately. So the background of the tested LSCs is black and no optical gel has been applied. From the four edges, the concentration factors change between 1.5 to 2.5. The comparison of the concentration factors for both global and diffuse light are shown in Fig. 4.37 recorded from earlier 8:00AM to later 2:00PM, Sep. 7, 2010. The output current is recorded at every half hours. Fig. 4.37 shows that the LSC performs very well for both global and diffuse light. And in the morning, LSC PV system performs better for the diffuse light. Our results proves the advantages of LSCs in concentrating diffuse light.

4.9 Summary

Organic LSCs have been widely investigated due to their potential in dramatically decreasing the LSC cost. In this chapter, we designed, fabricated organic luminescent solar concentrators and investigated their properties. The size dependent output efficiency enhancement methods for the LSC PV are explored.

We identified two groups of organic laser dyes: indoor use and outdoor use.

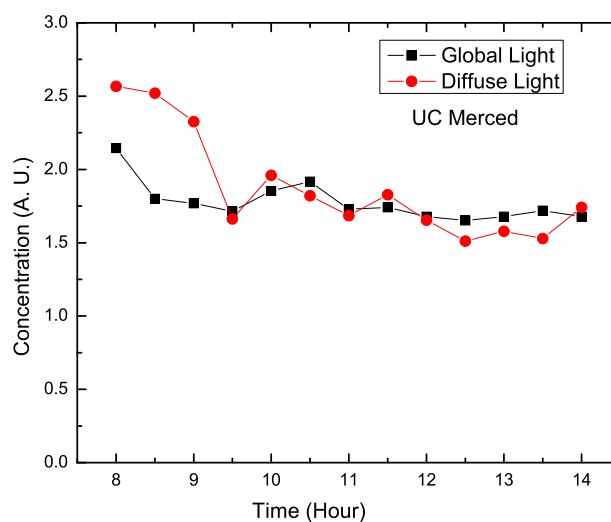


Figure 4.37: Concentration factor of stacked LSC PV systems for concentrating both global and diffuse light during a typical sunny day at Merced, California from 8:00AM to later 2:00PM, Sep. 7, 2010.

They are embedded into transparent plastic materials and fabricated into LSCs. For these prototyped LSC PV systems, we optically and electrically characterized their concentrating properties. The absorption and emission spectra of the embedded dyes are characterized by using spectrophotometers and fluoreimeters. The transmission of the LSCs is also characterized by using silicon PV cells as detectors.

We found that for the dyes we used, the absorption ranges are narrow compared with the overall solar spectrum. Different dyes have different absorption ranges, which show the advantage of using stacked structures to effectively utilize more parts of the solar spectrum for optimizing the LSC structures. Also, the outdoor use dyes perform better than the indoor use dyes for LSCs.

For LSCs fabricated by casting organic dyes into PMMA materials, we investigated size dependent efficiency enhancement methods for LSCs with single layer and multi-layer structures. The efficiency of the organic luminescent solar concentrators has been greatly enhanced by attaching white diffusers at the bottom surface of LSCs and by adding refractive index matched optical gel between the LSC edges and the attached PV cells.

The geometrical gain of the tested LSCs ranges from 1.2 to 62.5. And the largest size with geometrical gain 62.5 has dimensions 60cm by 120 cm by 0.32cm fabricated with indoor use dyes. This is the largest LSC we know of to date. It shows a very strong concentration effect. The yielded electrical gain from it by testing under sunlight is 4.23. This concentrator is much larger than any fixed concentrators based on geometrical optics. And the optical efficiency is still as high as 6.6%.

For LSCs fabricated with outdoor using dyes, the largest tested size is 35cm by 35cm by 0.32cm. Although the concentration gain of this prototype is 28, it yields almost the same current gain 4.24 with the largest tested LSC prototyped with indoor use dyes. Also, the optical gain of this system is 15% without applying the wavelength selective film, which is $2.67\times$ of the largest tested LSC. This results show that the performance of LSC with outdoor use organic dyes is very promising. Although the size of the LSCs increases more than twice from the one with geometrical gain 28, the effect of the optical gel on the output is still about $1.6\times$ either at the black background or at the white background.

The performance of LSCs by applying the white diffuser is more size dependent than the performance of LSCs by applying the optical gel. The enhancement from the white diffuser drops and then tends to plateau with increasing geometrical gain of LSCs. The corresponding re-absorption characterization shows that parts of LSCs closer to PV cells dominate the output photocurrent. This can be applied in designing optimal structures of LSCs.

We have not seen the strong concentration effects because our fabricated wavelength selective films do not exactly match the emission spectra of the dyes, and some of the emitted light cannot be effectively reflected back to the LSC.

The comparison study for single layers and stacked structures shows that the efficiency enhancement is higher for stacked structures than that for single layers. The optical efficiency is enhanced by stacking green and red emission LSCs. For both one layered LSCs and multi-layered LSCs, our experiments show that the

larger the size of the LSC, and then the larger the output current ratio, or the concentration factor. And the output from their edges distribute very evenly, this is beneficial to PV cells connecting in series.

The stability test shows that the output current ratio, or the concentration factor for samples exposed to sunlight drops fast in the first week, but drops much slowly after the first week. Also, for the group kept into dark, red emission LSC performs better than green emission LSCs. While for the groups exposed under sunlight, the drop of current from red emission LSCs is faster than that from green emission LSCs. In addition, the LSCs exposed under sunlight with a black background drop faster than the LSCs exposed under sunlight with a white background. For red emission LSCs, although the absorption efficiency has not decreased too much, the emission efficiency drops very obviously by the tests in two months. Future work can focus on the weather ability of outdoor use dyes with the expectation that they may perform better.

The study proves the advantage of the LSCs in concentration solar radiation without tracking. The fabricated “smart” windows performs equally well for both global and diffuse light. And in the morning, LSC PV system performs better for the diffuse light. These results can be applied to optimize the design of LSCs.

4.10 Acknowledgements

Part of this work is published in the following papers:

Chunhua Wang, Roland Winston, Weiya Zhang, Dave Pelka, and Sue Carter, “Size- and structure-dependent efficiency enhancement for luminescent solar concentrators”, *J. Photon. Energy*. **1**, 013502 (2011); doi:10.1117/1.3534864.

Chunhua Wang, Roland Winston, Weiya Zhang, Lun Jiang, Dave Pelka, Sue Carter, “Performance of organic luminescent solar concentrator photovoltaic systems”, *CPV-7 Las Vegas* (2011).

Chunhua Wang, Roland Winston, Weiya Zhang, Dave Pelka, Sue Carter,

“Optical enhancement for luminescent solar concentrators”, *Proc. SPIE* **7785**, 77850D (2010); doi:10.1117/12.863250.

And some manuscripts on “Comparison of nano-structured quantum dots and organic dyes as active materials for luminescent solar concentrators”, are in preparation.

Chapter 5

Liquid Crystal Dye Alignment for New Generation Luminescent Solar Concentrators

5.1 Introduction

To improve the power conversion efficiency of Luminescent Solar Concentrators (LSCs) PVs, suitable luminescent materials, optimal LSC design structures, and appropriate waveguide materials are required [RWR08]. In Chapter 3, we studied properties of available luminescent materials, including nano-structured quantum dots emitting in near infrared and visible wavelengths. We have shown the great potential of applying infrared QDs to LSCs. In chapter 4, we investigated optimal LSC design methods. We took organic LSCs as examples as they have the potential to lower the cost of PV systems with cheaper materials and expected ease of large-scale manufacturing.

Different waveguide materials for LSCs have been investigated [KBD09, Row07]. Their refractive indices are normally around 1.5. Ideally, the dyes re-emit the absorbed light into waveguide modes that are coupled to the solar cells; but

some photons are always lost, and re-emitted through the surface of the LSC and coupled out of the waveguide due to the lower refractive index of the waveguide materials. This loss can be further decreased by employing high refractive index waveguide (matrix) materials or employing wavelength selective mirrors. However, higher refractive index materials are normally expensive. The subject of selective mirrors has recently been addressed by several other groups and is clearly an important topic in the study of LSCs [DVV⁺10a, DVV⁺10b]. Dielectric mirrors require many layers to achieve omni-directional reflectivity at luminescent wavelengths and high transmission for broadband solar excitation at all incident angles. The fabrication of such mirrors may prove costly.

If we can align the embedded dyes into a certain direction using liquid crystalline host materials, the lost re-emitted light through the surface will be reduced, and then the power conversion efficiency of the LSC will be improved. Since materials with high refractive indices are also typically dipolar dye molecules, aligning dye molecules may be the most promising path to higher efficiency LSCs [VKH⁺09], [MRV⁺10]. In this chapter, we introduce our work on this efficiency improvement method for LSC PV systems. This is considered the new generation of the LSC PV technologies [FY11].

As we know, LSC performance depends on the absorption efficiency η_{abs} , photo-luminescent efficiency or quantum yield η_{PL} , and the trapping efficiency η_{trap} , which is the fraction of photons confined within the waveguide. Certain dyes are limited by their structures, making the absorption efficiency hard to improve further, and several dyes already have an η_{PL} almost equal to 1. For η_{trap} , however, large efficiency improvement is possible since the theoretically predicted value is about 75% for a conventional waveguide.

Previous work on this subject has been done by a group at MIT [MRV⁺10]. The results show that Coumarin 6 dye can be aligned by using a homeotropic polymerizable liquid crystal mixture. In the fabrication process, the solution of liquid crystalline host UCL018, laser dye Coumarin 6, surfactant FC-4430, and

toluene are mixed and spin-cast on glass substrates. In this paper, they also demonstrates an increase in the trapping efficiency from 66% for LSCs with no dye alignment to 81% for a LSC with vertical dye alignments when both samples absorb 40% of incoming light.

Other research groups also demonstrate the alignment using a guest-host dye-doped liquid crystal sandwiched between conductive glass slides [MCCS10]. The result shows that application of a potential, while illuminating through a narrow edge caused a drop in the intensity of luminescence escaping from the large top surfaces, and an increase in the intensity of light escaping from the narrow edges of the system. They explained these results in terms of alignment of the dipoles of the dye. The applied potential causes the alignment of the dipole of the luminophore along the waveguide surface normal, directing the maximum possible proportion of luminescence into waveguide modes.

In their experiments, *N-N-Bis(2,6-dimethylphenyl)perylene-3,4,9,10-tetracarboxylic diimide* (PDI), was chosen for a near-unity quantum yield from a single optical transition, good solubility, high photostability and, crucially, emission anisotropy along the long molecular axis. The main shortcoming of PDI is a small Stokes shift.

In this chapter, we study material properties of liquid crystals and dyes, and identify suitable dyes and liquid crystal materials for LSC PV systems. Particularly, we investigate the properties of Coumarin 6 and Lumogen Red F 305 dyes in different matrix materials; study the effects of UV light cross linking and the specific alignment coating layers on the properties of the fabricated thin films. We focus on experimental fabrication of anisotropic liquid crystal films and their characterization for LSC PV systems.

The dyes we tested are Coumarin 6 [YST09] and Lumoen F Red 305 [vSBS⁺08] laser dyes with very high quantum yields. We select Coumarin 6 mainly because of its high quantum yield and absorption spectrum around 500nm, a wavelength close to the peak of solar spectrum. This dye can be used as the first layer in

the designed stacked structures. As Mulder et al [MRV⁺10] has already tested the properties of the Coumarin 6 dye, it is very helpful for us to use this dye to begin our work on the experimental part. There are two main reasons for us to select the Lumogen F Red 305 laser dye. First, this dye has very high quantum efficiency and very good stability. Second, the center wavelength of the emission spectrum is around 600nm which is favored by the silicon solar cells based on their spectral response. We can use it as the second layer for LSCs with stacked structures.

The liquid crystal as a matrix material and a dye alignment material should have very high transmittance and low absorbance over the solar spectrum. It is very important to note that it should be able to align dye molecules in certain directions. We have characterized and compared several liquid crystal materials, and finally selected the polymerizable UCL018 liquid crystal mixture from Dai Nippon Ink and Chemicals Inc. This liquid crystal is a mixture of a polymerizable nematic liquid crystal, homeotropic dopant molecules, and a photo-initiator. The tested phase transition sequence of this material is from the crystal phase to a liquid crystal phase, and then from the liquid crystal phase to an isotropic liquid.

In Sec. 5.2, we describe principles of liquid crystal dye molecular alignment method and give the theoretical predicted efficiency improvement value of using this method. As a proof of principle project, we focus on experimental characterization. We describe properties of liquid crystals and organic dyes for producing LSCs in Sec. 5.3 and 5.4, respectively. In Sec. 5.5, we describe experimental techniques we used in preparing liquid crystal dye aligned anisotropic LSCs and PMMA isotropic LSCs. In Sec. 5.6, we optically characterize spectral properties of these fabricated prototypes, and compare anisotropic LSC samples with isotropic LSC samples. We also give phase transition properties of the liquid crystal after mixing with dye molecules, and characterize the alignment properties of anisotropic samples with differential scanning calorimetry (DSC) and polarized optical microscopy (POM) methods. Finally, we conclude our work on this project and discuss the future work on further improvement in Sec. 5.6.2 and 5.6.3.

5.2 Theoretical Analysis

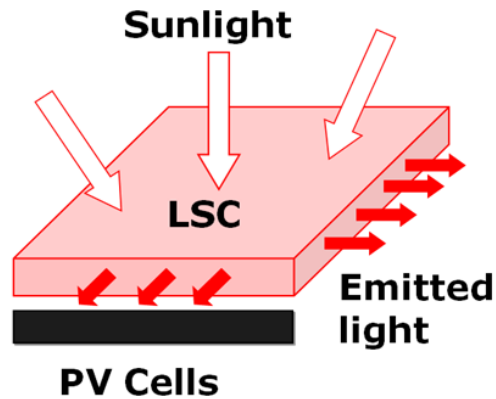


Figure 5.1: Schematic of a LSC, the embedded luminescent materials can be dispersed isotropically or anisotropically.

A schematic of a LSC is shown in Fig. 5.1. Typically, it is a sheet of transparent waveguide materials with luminescent materials dispersed or cast inside. The transparent waveguide materials can be glass or plastic (matrix materials) etc, and the dispersed luminescent materials can be organic dyes, organic semiconductor polymers (active materials) or nano-structured quantum dots [RWR08]. The structure can also be a layer of planar waveguide with a thin-film coating on the face. Ideally, incident solar-energy is absorbed by the dispersed organic luminescent materials and reemitted into the waveguide, and then transported to the edges for collection by the solar cells as shown in Fig. 5.1. However, as shown in Fig. 5.2, photons re-emitted within the escape cone cannot be trapped in the waveguide by total internal reflection, and then cannot be guided to the edges of the plate.

For an LSC with an isotropic emitter, the inside luminescent materials are not aligned, as shown in the left part of Figure 5.3 (a), so the emission profile is

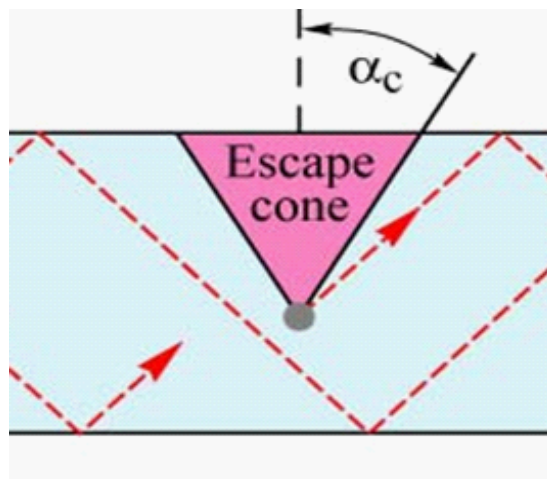


Figure 5.2: Escape cone of a waveguide, where α_c is the critical angle. This angle is related to the refractive index of the waveguide material. Emitted light in this angle will escape from the LSC.

uniform as shown in the right part of Figure 5.3 (a). If the refractive index of the waveguide material is 1.5 (typical PMMA plastic materials), 25% of the light is emitted and escapes through the critical angle α_c . For each repeated absorption and emission process, this light loss happens. This means that even if the quantum efficiency of the organic dye is very high, the optical concentration may still be seriously reduced.

Alignment of dye molecules with polymerized liquid crystals can greatly diminish the magnitude of the luminescence escape and improve the absorption efficiency of the LSC PVs. The key idea is to exploit the polarization properties of the organic dyes when they are aligned in a certain sequence by liquid crystals to greatly reduce the luminescence lost to the escape.

We first explore the polarization effect of identified dyes for alignment. There are certain rod-shaped organic dyes, which are also luminescent materials. If they are isotropically distributed in the matrix material, glass or plastic, there is no special direction selection for the emission spectrum distribution. Taking the refractive index as n , and θ as the angle between the normal of the surface and the

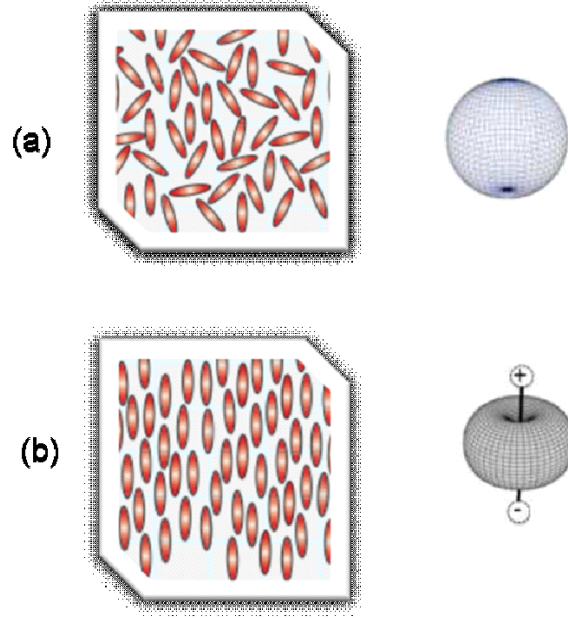


Figure 5.3: Emission profiles of (a) an isotropic distribution of dyes in an LSC and (b) an anisotropic dye distribution in an LSC.

orientation of a Hertzian dipole, a brief calculation by

$$\eta_{Trap,Iso} = 1 - 2 \frac{\int_1^{\cos \alpha_c} d \cos \theta}{\int_1^{-1} d \cos \theta} = \cos \alpha_c, \quad \sin \alpha_c = \frac{1}{n} \quad (5.1)$$

shows that the trapping efficiency is about 75% for $n=1.5$. So 25% of the emitted light will escape. However, if dye molecules are aligned in a certain order, such as vertical to the wave guide plane, as shown in the left part of Fig. 5.3 (b), the emission from these dye molecules has a certain direction selection. The emission power distribution becomes anisotropic, acting like anisotropic dipoles. The emission profile of the anisotropic dipoles is shown at the right part of Figure 5.3 (b), it can be characterized by a $\sin^2 \theta$ profile, with no power emitted along the long axis of the dipole molecule. Specifically, at the direction vertical to the aligned direction, or parallel to the surface of the waveguide, the emission is the strongest. A brief calculation by

$$\eta_{Trap,A} = 1 - 2 \frac{\int_0^{\alpha_c} \sin^3 \theta d\theta}{\int_0^{\pi} \sin^3 \theta d\theta} \quad (5.2)$$

shows that for $n = 1.5$, $\theta_c = 42^\circ$, the theoretical trapping efficiency is 91%, then only 9% of the light escapes. This alignment improves the trapping efficiency by 21%. If the refractive index of the matrix material is larger, the improvement will be even stronger. So it is very important to explore the polarization effects of the organic dye alignment on improving the trapping efficiency for LSCs with larger size.

5.3 Properties of Liquid Crystals as Matrix Materials

In this section, we investigate suitable liquid crystals for aligning the luminescent dye molecules. There are certain liquid crystal polymers which have a nematic liquid crystal phase. Dyes can be dispersed inside and aligned vertically to the surface of glass or plastic substrates. Theoretically, the liquid crystal as matrix material should have the following properties:

First, low incident light and emitted light absorption, or being transparent: The liquid crystal should absorb the least emitted light as possible. This property is very important for transporting the emitted light to the edge surfaces of the LSCs without being absorbed by the liquid crystal material.

Second, vertical alignment of organic dye molecules to the top surface of a LSC, especially in larger area of a LSC. This is because with vertical alignment, the trapping efficiency will be maximized. It is also because LSCs, as normal windows, should be practically at reasonably large size to collect solar energy effectively. Dyes are aligned by the liquid crystal material having its direction axis normal to the surface of the LSC. This results in alignment of dyes vertical to the surface of the LSCs.

Third, suitable phase transition temperatures to satisfy the requirement of solar concentrators. The phase transition of the mixture of liquid crystal materials

and dyes may be different from the pure liquid crystal materials.

Finally, in the liquid crystal phase, after the dye molecules are aligned, the alignment, or orientation anisotropy would have to be locked. Considering the re-absorption issue, optimal dye concentration and the phase sequence have to be investigated very carefully. These required properties of liquid crystal materials for dye molecule alignment need to be addressed in the research, and it is worthwhile to examine this numerically and experimentally. We tried different kinds of liquid crystals, and finally identified UCL018 from Dai Nippon Ink, and Chemicals, Inc for the dye molecules alignment. We initially aligned Coumarin 6 dyes with the selected liquid crystal mixture, and explored the alignment for other organic luminescent materials in it. UCL018 is polymerizable homeotropic liquid crystal host mixture. It includes a polymerizable nematic liquid crystal, homeotropic dopant molecules, and a photo-initiator.

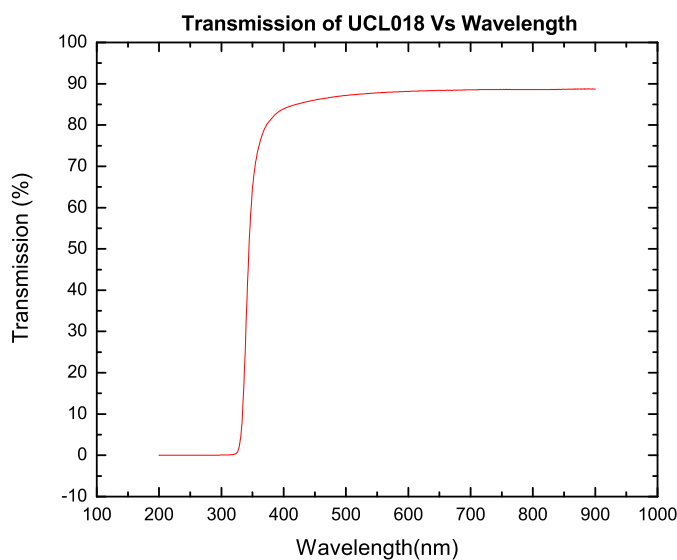


Figure 5.4: Transmittance of the UCL018 sample by casting a very thin layer on a glass substrate. It is up to 90% for wavelengths from 350nm to 900nm.

UCL018 is very transparent. As shown in Fig. 5.4, the transmittance is about 90% for wavelengths between 300nm to 900nm. The phase transition is characterized by optical polarized microscopy. A typical picture is given in Fig. 5.5.

During the cooling process, we observed the dark areas expanding, which means

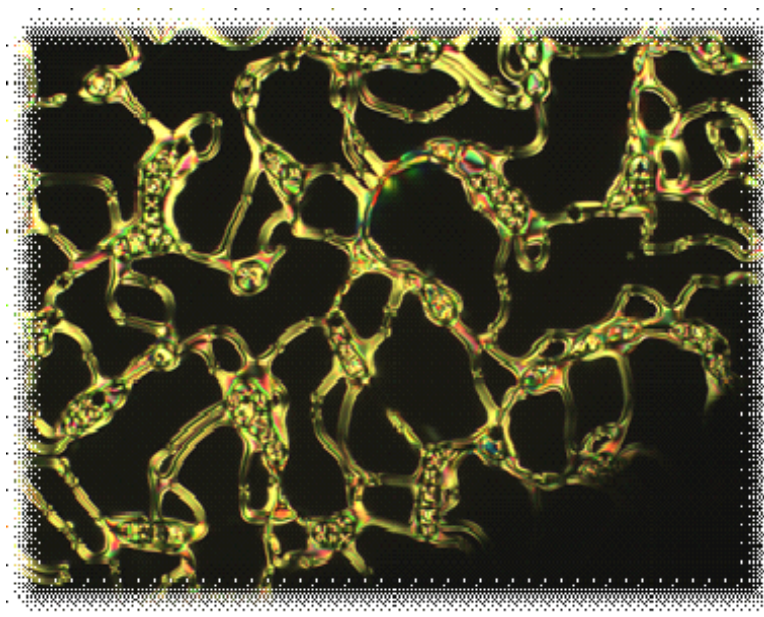


Figure 5.5: Polarized Optical Microscopy picture for UCL018 liquid crystal. Refractive index varies in different direction. We observed the dark area expanding when UCL018 is well aligned vertically to the glass surface.

that the molecules of UCL018 were well aligned vertically to the surface of the glass substrate. We further tested the phase transition properties by using differential scanning calorimetry (DSC). The result is shown in Figure 5.6. In this figure during the heating process, there are two peaks at 48°C and 66°C respectively. The material changes from crystal phase to liquid crystal phase and then changes to liquid phase, while there are no such peaks for pure PMMA powder. In the super cooling process, there is only one peak.

5.4 Properties of Organic Dyes for Alignment

In this section, we briefly investigate properties of dyes for the liquid crystal alignment. We initially selected Coumarin 6 organic dye for identifying suitable organic luminescent materials, as shown in Fig. 5.7. The powder of the dye looks

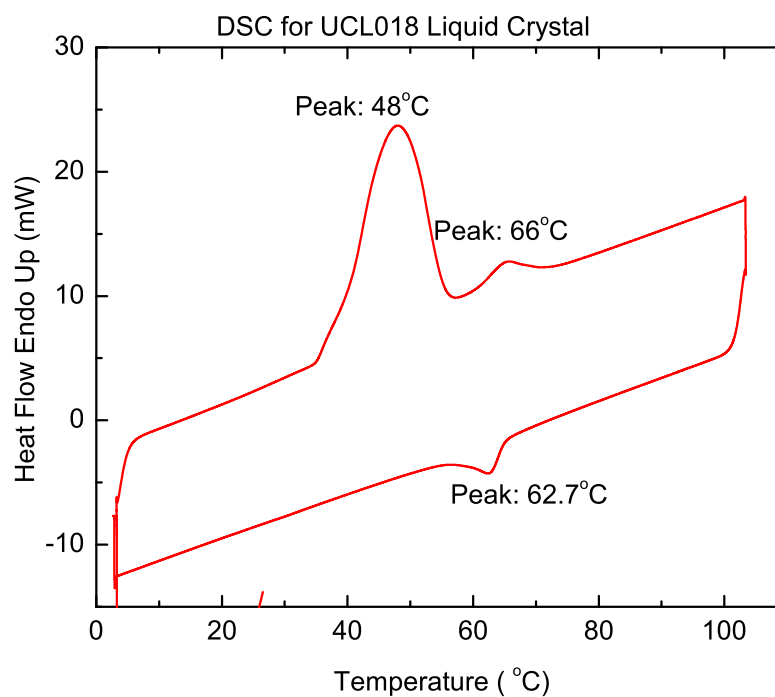


Figure 5.6: Phase transition sequence characterization for UCL018. The phase transition sequence is from crystal to nematic liquid crystal and nematic liquid crystal to isotropic transitions with the temperature peaks at 48C and 66C respectively



Figure 5.7: Coumarin 6 dye powder.

red, but becomes a green color when dissolved into solutions or contained in liquid crystal and PMMA plastic materials. Coumarin 6 effectively absorbs light from 400nm to 500nm over the solar spectrum as shown in Figure 5.8. Coumarin 6 is characterized by a large Stokes shift, which makes this dye especially suitable in

an LSC [MRV⁺10]. Coumarin 6 also has a very high photoluminescence efficiency (measured to be 78%), and is known to possess a relatively high dichroic ratio [MRV⁺10].

The absorption and emission spectral properties of this dye in toluene are tested, and shown in Fig. 5.8. The tested sample is made by filling Coumarin 6 dye with toluene solution into a quartz cuvette. The concentration of this sample is less than 10 10 μ M The cuvette has dimensions 1cm by 1cm by 3cm. With absorption and emission peak wavelengths at 439nm and 480nm respectively, we can see that the Stokes shift of this dye is 480nm - 439nm = 41nm.

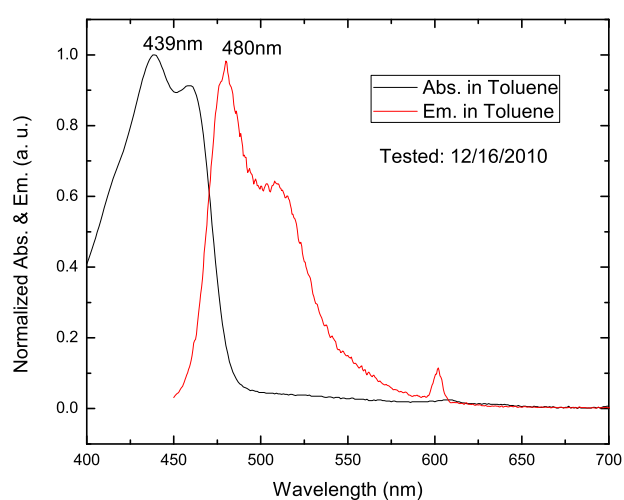


Figure 5.8: The normalized absorption and emission of Coumarin 6 dye in toluene solution.

We also selected Lumogen Red F 305 organic dye for alignment as this dye emits in the red, is very stable and has high quantum yield. The absorption and emission of the Lumogen Red F 305 organic dye in toluene solution is shown in Fig. 5.9. The Stokes shift of the Red F 305 dye in solution is 27nm with absorption and emission peak wavelengths at 573nm and 600nm respectively.

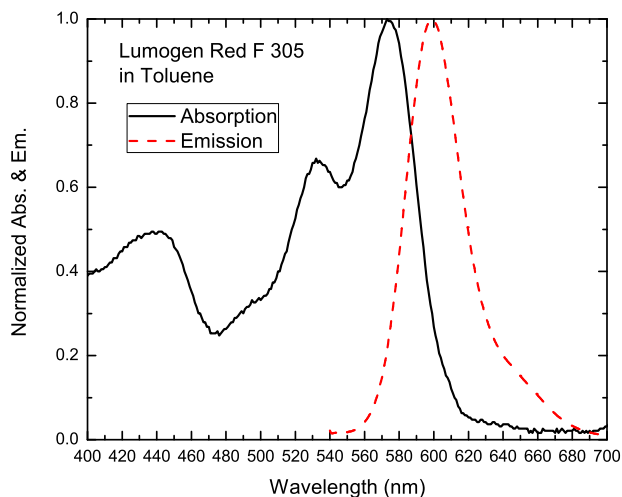


Figure 5.9: The absorption and emission of Coumarin 6 dye in toluene solution for the Lumogen Red F 305 organic dye.

5.5 Experiments

For the application of LSC PV systems, we aim to develop a device design that is compatible with existing screen-printing and glass manufacturing lines with sufficient lifetime and efficiency to enable rapid deployment by manufacturers. The key process for the prototype is to make a uniformly distributed anisotropic LSC with practical size. The organic dyes can be vertically aligned by liquid crystal materials to the top surface of the LSC, and the alignment is able to be fixed even at very high temperature.

For the study in the lab, we applied a spin-coating method to fabricate LSC samples. For anisotropic liquid crystal aligned prototypes, a typical process is:

- (1) Cleaning the glass substrate with acetone, ethanol, methanol and DI water,
- (2) Mixing dye and liquid crystals in toluene according to the following weight:

UCL018 liquid Crystal: 42%

Dye (Coumarin 6): 0.4%

FC-4430 surfactant: 0.4%

- (3) Stir and filter the mixture prepared by (2)
- (4) Spin coating thin film LSCs on the cleaned glass substrates

- (5) Dry the spin coated film on a hot plate
- (6) Cross link the sample by UV light.

To fabricate isotropic samples in PMMA, a typical process is:

- (1) Cleaning glass substrate with acetone, ethanol, methanol and DI water
- (2) Preparing the mixture of dye, PMMA into toluene with PMMA: 150mg/ml and dye: 1.5mg/ml.
- (3) Heating at 70°C, stirring and filter the mixture
- (4) Spin coating to thin film LSCs on the cleaned glass substrates
- (5) Heating and Drying

After fabricating these prototyped LSCs, the differential scanning calorimetry is used to obtain the phase transition properties, then polarized optical microscopy is used for characterizing the alignment of the dye molecules in the fabricated films.

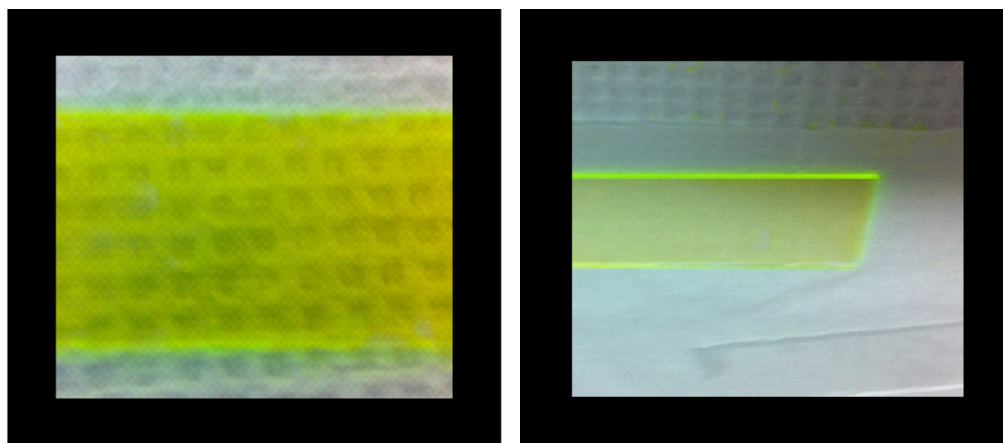


Figure 5.10: Coumarin 6 UCL018 liquid crystal spin coated samples at higher concentration (left) and lower concentration (right). The size is 2.54cm by 7.62cm (1in by 3in).

We have fabricated samples for Coumarin 6 dye and Lumogen Red F 305 dye. Fig. 5.10 shows pictures of the anisotropic LSC samples with Coumarin 6 dye at higher and lower concentrations respectively. Fig. 5.11 show pictures of anisotropic LSC samples with Lumogen Red F 305 dye at higher and lower

concentrations respectively. All of these samples are fabricated by using the spin coating methods on glass substrates with dimensions 2.54cm by 7.62cm.

Due to the re-absorption problem, we see that there is an optimum concentration at which the LSC yields the maximum power output. Before we obtain that optimum concentration, and do the electrical characterization [?], it is very important to show alignment properties at lower dye concentrations. Also at low dye concentration, short optical distance or small samples size, the effect of re-absorption is very weak.

In addition, for a comparison study of the alignment properties, we have prepared LSC samples with special thin glass cells. The inside top and bottom surfaces of these glass cells have specific the coatings, and the size of coated area from these glass cells is 1cm by 1cm. Molecules in the specific coatings are aligned either vertical to the surface of the glass substrate or horizontal in the plane of the glass substrate. After preparing the solution mixture of liquid crystal UCL018 and dyes, we then diffused the mixture into these glass cells. The properties of these samples are tested when they are dry.

For all of these samples, this alignment can be locked or cross-linked into the liquid crystal phase by UV-light.

5.6 Results and Discussion

5.6.1 Spectrum properties of dyes in different matrix materials

In this section, we focus on characterizing optical properties of the fabricated prototypes by spectrophotometry. We will also compare optical properties of anisotropic LSC samples with isotropic LSC prototypes.

To characterize spectral distributions of dyes, it is very important to compare the absorption and emission spectra of dyes in pure toluene, in PMMA and

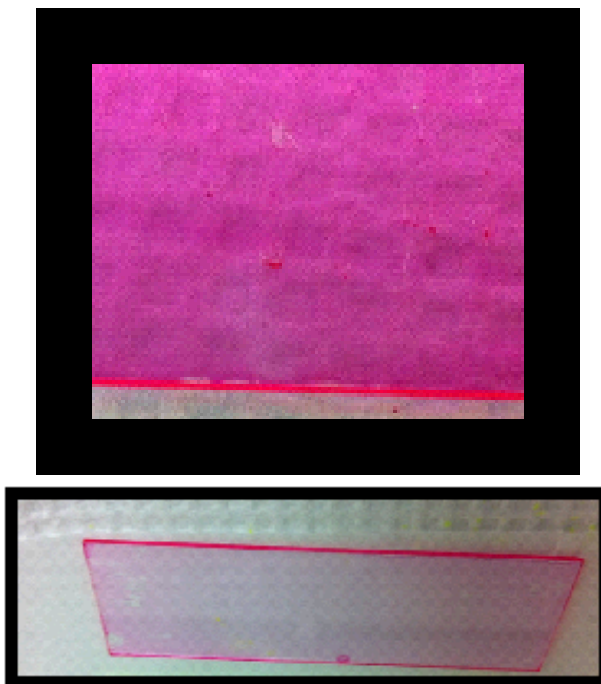


Figure 5.11: Red F 305 UCL018 liquid crystal spin coated samples at higher concentration (upper) and lower concentration (lower). The size is 2.54cm by 7.62cm.

toluene liquid mixture, in liquid crystal and toluene liquid mixture, in PMMA films and anisotropic in liquid crystal films. This is very important because in the fabrication process, we use toluene as a solvent to mix dyes with PMMA plastic powder or liquid crystal materials to make isotropic or anisotropic films. If the properties of the matrix materials change, the activities of the dye molecules will be affected. As a result, the spectral distribution of the dyes will change.

We will show the absorption and emission properties of Coumarin 6 dye in different matrix materials. The matrix materials characterized are (a) solid materials including PMMA and liquid crystal polymers, (b) liquid matrix materials including pure toluene solutions, PMMA polymer containing liquid mixture and liquid crystal contained liquid mixture. It is noted that to test the spectral properties of the dye in toluene, the solution is diluted to such a low concentration that it makes it hard to see the green color from the solution with the naked eye. Concen-

tration of dyes in PMMA and liquid crystal solutions are very high for preparing films.

a. Spectral Properties of Liquid Mixtures and Liquid Crystal Films

Fig. 5.12 (a) and (b) show the normalized absorption and emission spectra of Coumarin 6 dye in ULC018 liquid crystal films. Due to the high concentration of dyes in PMMA and liquid crystal solutions, the absorption and emission spectra are saturated which shows flat shapes at some wavelengths.

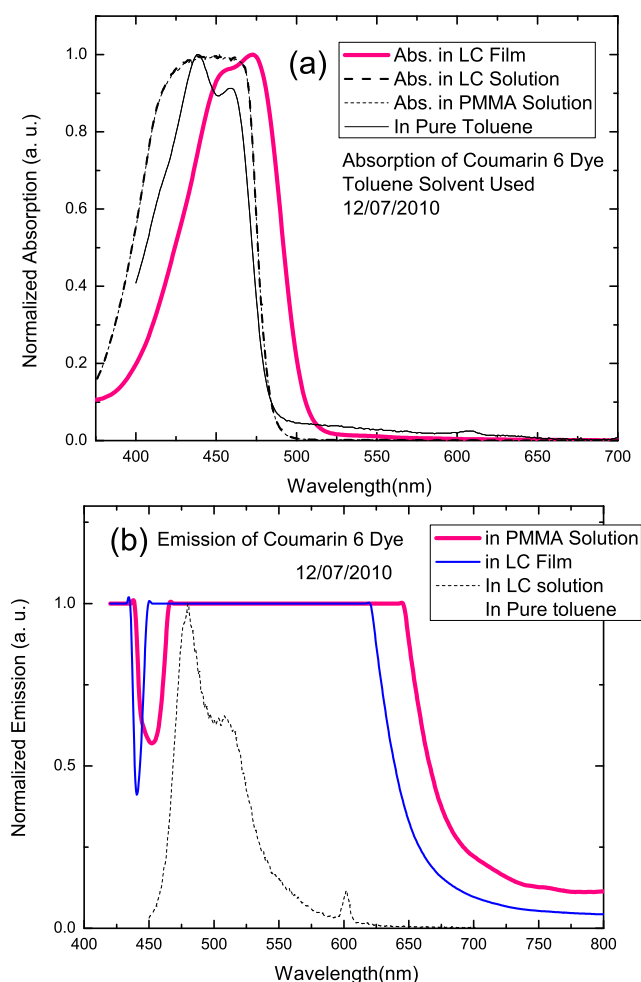


Figure 5.12: Normalized (a) absorption and (b) emission of Coumarin 6 dye in a spin casted liquid crystal film compared with absorption and emission of the same dye in PMMA powder contained liquid mixture and in LC contained liquid mixture.

The absorption and emission spectra of the dye in the liquid crystal solid films are shifted to longer wavelengths and the peak wavelength from the emission spectrum shifts more than the peak wavelength from the absorption spectrum. This is due to shorter distances between molecules in solid films than in liquid solutions. Also, as the concentration increases, the re-absorption problem becomes serious, and then the red shift of the spectra becomes more obvious possibly due to dye aggregation. In pure toluene solution, both the absorption and emission spectrum are very narrow as the size distribution of molecules is more uniform. It is noted that this wavelength shift of the spectrum is favored by the silicon PV cells in LSC applications.

In addition, the absorption and emission spectral distributions of the dye in PMMA toluene solution and in liquid crystal toluene solution are almost the same since we use the same dye concentration, and in liquid phase, the liquid crystal molecules are not aligned.

b. Spectral Properties of Liquid Solutions and PMMA Films

To prepare PMMA isotropic dye films, we first prepare the solution of the Coumarin 6 dye in ethanol. A pure PMMA plastic square film with dimensions 2.54cm by 2.54cm by 0.32cm is then submerged into the prepared solution. After 2 weeks, we take out the sample, and totally clean its surfaces with ethanol. We can obviously see that the color of the previously clear pure plastic piece becomes green. This is because the contained dye emits green light. The change of the color is due to the diffusion of the dye molecules in the solution into the PMMA plastic piece. Using this diffusion method, we have successfully fabricated dye containing PMMA films.

The absorption and emission spectra of the dye in the PMMA film are shown in Fig. 5.13 respectively by comparing with the absorption and emission spectra of the dye in toluene solution. We can see that there is a red shift for both of the absorption and emission spectra of the dye in PMMA films comparing

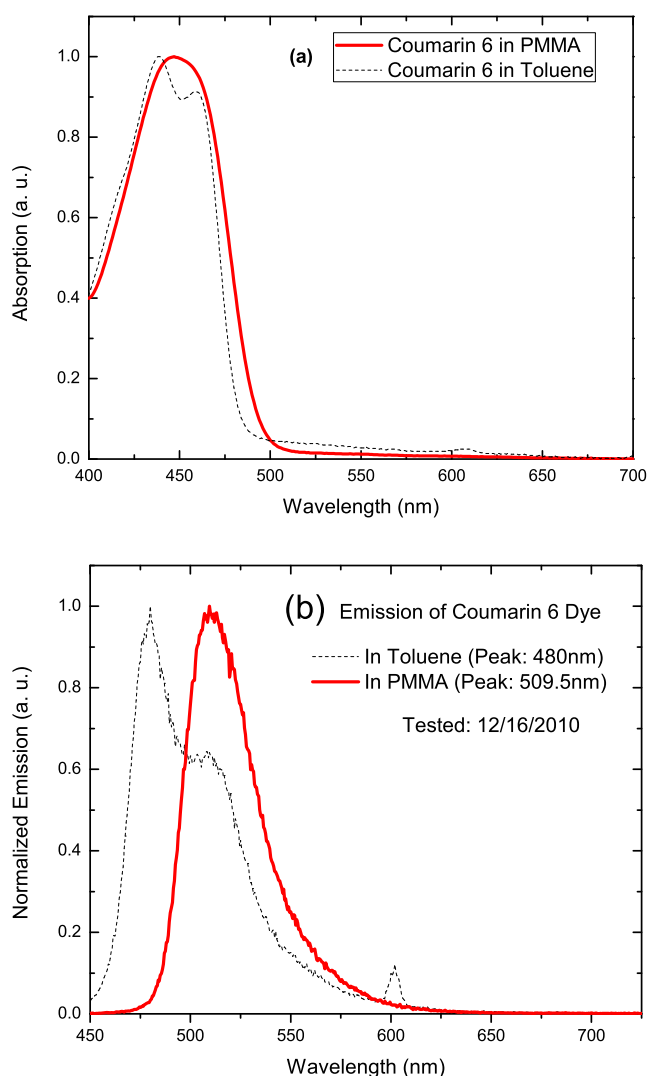


Figure 5.13: Normalized (a) absorption and (b) emission spectra of the Coumarin 6 dye in pure toluene solution and in a plastic sheet. Comparing the absorption of the dye in diffused PMMA plastic films and in Toluene solution.

the absorption and emission spectra of the dye in pure toluene. The peak of the absorption spectrum of the dye shifts from 439nm in toluene solution to 445nm in diffused PMMA plastic film. The wavelength of the peak emission from the diffused PMMA film shifts from 480nm in toluene solution to 510nm in diffused PMMA plastic films, which is about 30nm. Although the absorption spectrum does not change too much, the emission red-shifted a lot. As a result, due to the

lower concentration, the area of the overlap between the absorption and emission spectra becomes smaller for the diffused plastic film, which is shown in Fig. 5.14, and then the re-absorption problem is not very serious. It is worthwhile to note that the red-shift of the spectrum in solid films is favored by silicon PV cells in LSC applications.

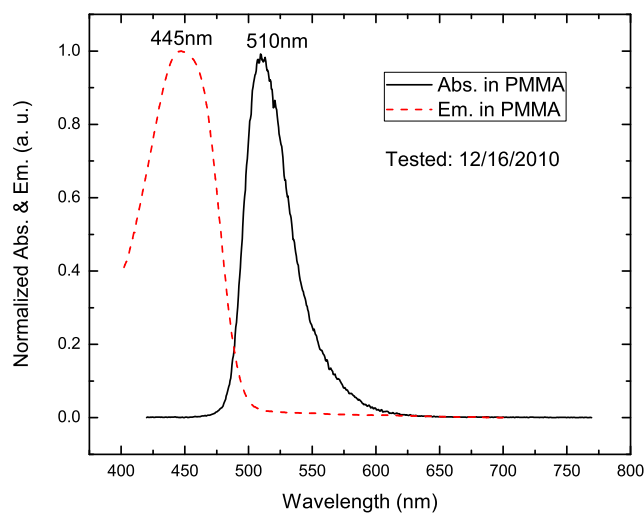


Figure 5.14: Normalized absorption and emission properties of Coumarin 6 dye in diffused plastic films.

c. Spectral Properties of Anisotropic and Isotropic LSC Films

In this part, we investigate and compare the spectral properties of dyes in anisotropic films and in isotropic films. We have fabricated LSC films by spin coating on glass substrates, and by filling in glass cells. For the glass cells, the inner top and bottom surfaces are coated with specific alignment coatings. For fabricated anisotropic films, we further compare spectral properties before and after cross-linking. We also study the effects of alignment coatings on the properties of these fabricated films.

From Fig. 5.15, comparing the absorption of the same dye in pure toluene shown in Fig. 5.12 (a), we can see that there is a red shift for the absorption spectra in solid films. The peak of the absorption spectra of the Coumarin 6 dye for these

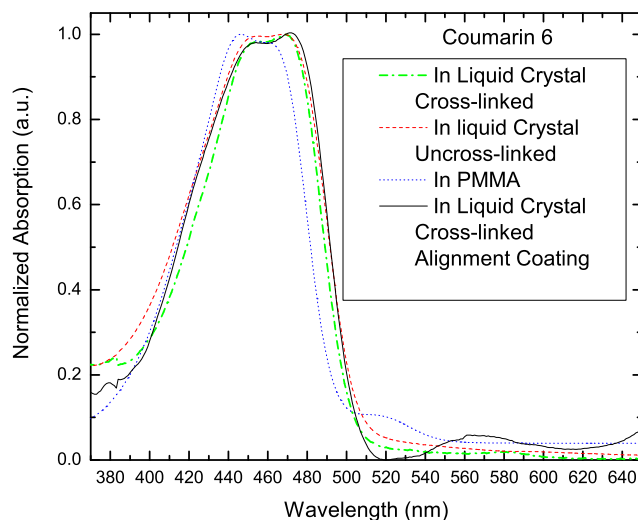


Figure 5.15: Normalized absorption properties of Coumarin 6 in anisotropic cross linked and uncross linked liquid crystal films by spin coated on glass substrates, in isotropic PMMA films spin coated on glass substrates, and in anisotropic liquid crystal films filled in glass cells.

films centers at 455nm, but centers at 439nm in toluene solution. The red-shift is smaller for dyes in PMMA films. Also, the cross-linking in short time only slightly blue shifted the absorption spectrum of the dye. The specific alignment coatings on the inner surfaces of the glass cell have not obviously changed the absorption spectrum of the dye.

In Fig. 5.16, we compare emission properties of Coumarin 6 in anisotropic cross linked liquid crystal films spin coated on glass substrates with emission properties of the same dye in isotropic PMMA films by spin coated on glass substrates. The difference of the peak wavelengths from the emission spectra is about 30nm, which shows that the emission properties of the dye can be very sensitive to matrix materials.

Similarly, we explore the absorption (in Fig. 5.17) and emission (Fig. 5.18 and Fig. 5.19) properties of Lumogen Red F 305 dyes in anisotropic cross linked and uncross linked liquid crystal films and in isotropic PMMA films spin coated on glass substrates. We also show the spectral properties for the same dyes in cross linked anisotropic liquid crystal films filled into glass cells.

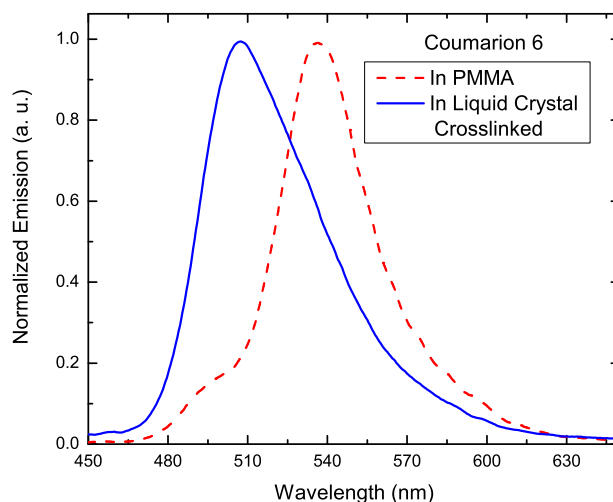


Figure 5.16: Normalized emission properties of Coumarin 6 in anisotropic cross linked liquid crystal films spin coated on glass substrates, in isotropic PMMA films spin coated on glass substrates.

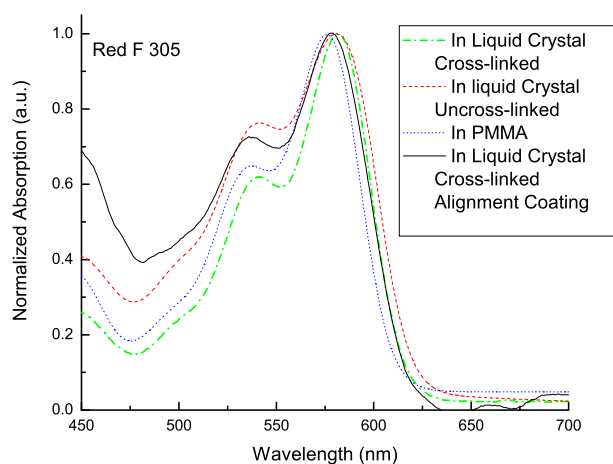


Figure 5.17: Normalized absorption properties of Lumogen Red F 305 in anisotropic cross linked and uncross linked liquid crystal films spin coated on glass substrates, in isotropic PMMA films spin coated on glass substrates, and in anisotropic liquid crystal films diffused in glass cells. The top and bottom surfaces of the glass cells are coated with specific alignment coatings.

For anisotropic LSCs, cross linking by UV light only slightly blue-shifted the absorption spectra as shown in Figure 5.23, since we only apply the UV light for a very short time. Correspondingly, the emission spectra also blue shifted a little bit after cross-linking by UV light. Dye molecules are aligned before cross-linking,

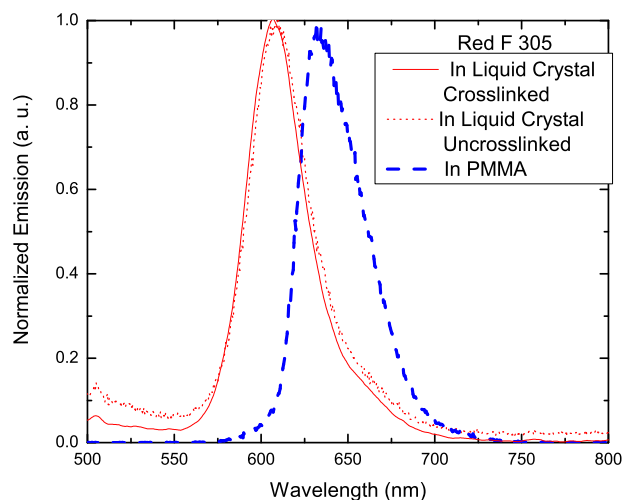


Figure 5.18: Normalized emission properties of Lumogen Red F 305 in anisotropic cross linked and uncross linked liquid crystal films spin coated on glass substrates, in isotropic PMMA films spin coated on glass substrates.

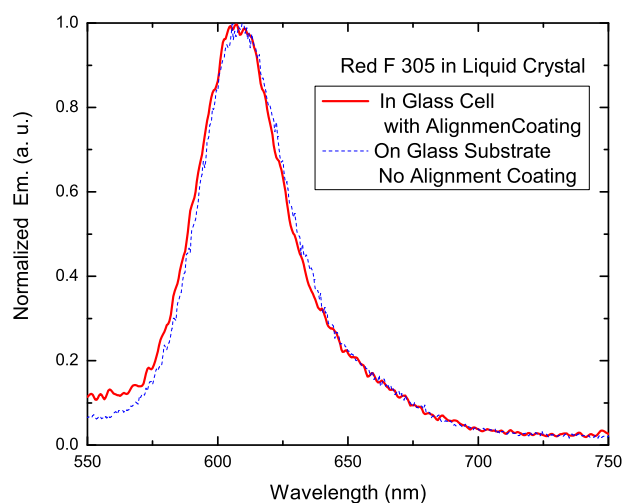


Figure 5.19: Normalized emission properties of Lumogen Red F 305 in anisotropic cross linked liquid crystal films spin coated on glass substrates, and in cross linked anisotropic liquid crystal films diffused in glass cells. The top and bottom surfaces of the glass cells are coated with specific alignment coatings.

and the alignment is fixed after cross-linking. UV light may cause photo-oxidation of the dye molecules, which leads to this blue shift. For the anisotropic films fabricated in glass cells, we see the same result shown in Fig. 5.19. The alignment with the help of the specific coating slightly blue-shifts the emission spectrum

of the dye. We further show the normalized absorption and emission spectra of Lumogen Red F 305 anisotropic liquid crystal aligned LSC films fabricated in glass cells in Fig. 5.20. Future work can focus on reducing the overlap of the absorption

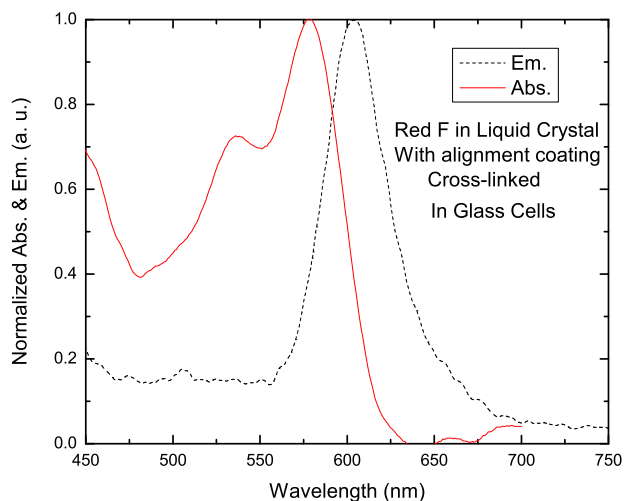


Figure 5.20: Normalized absorption and emission spectra of Lumogen Red F 305 anisotropic LSC films fabricated in glass cells.

and emission spectra.

In conclusion, the experimental results show the differences of the Stokes shift of the dye in different matrix materials. The Stokes shift is larger in solid matrix materials than that in liquid solutions. For Coumarin 6 dye, it is 65nm in PMMA plastic, which is 24nm broader than in pure toluene solution. More importantly, the experimental results also show that both the absorption and emission spectra shift to longer wavelengths for solid matrix materials. This red-shift is favored by the silicon PV solar cells for the LSC PV applications. The cross-linking and specific alignment coatings do not obviously change the spectral properties of the dye molecules, which means that our fabrication process does not affect the optical absorption and emission spectral properties of the dyes.

5.6.2 Phase transition properties of liquid crystal materials

The purpose of this part is to study phase transition properties of fabricated anisotropic LSC films. The alignment order of the dye molecules by the liquid crystal is fixed or cross-linked by UV light. We do not expect a phase transition when applying high temperature to the samples since the order of the liquid crystal molecules does not change after cross-linking. The phase transition properties can be checked by DSC.

a. Experiments on sample preparation

Samples for this study were prepared with liquid crystal UCL018 contained Coumarin 6 dye molecules. Steps for preparing the sample are as follows:

- (1) A mixture is prepared by mixing Coumarin 6, UCL018 dye, surfactant and toluene together.
- (2) A drop of the solution is casted on a clean glass substrate.
- (3) The sample from step (2) is exposed to the air in a fume hood at room temperature for 24 hours or longer until it is dry.
- (4) UV light with wavelength 350nm is used to cross-link the sample for 2 to 5 minutes.

b. Phase transition properties tested by DSC Scanning

The sample for the DSC testing is cut from the prepared cross-linked sample. It is about 4.1mg. The scanning process is in the following, which is the same for pure UCL018 liquid crystal:

Switch the Gas to Nitrogen at 20.0 ml/min.

Start the Run:

- (1) Heat from 0.00°C to 100.00°C at 10.00°C/min.
- (2) Hold for 1.0 min at 100.00°C.
- (3) Cool from 100.00°C to 0.00°C at 10.00°C/min.

(4) Hold for 2.0 min at 0.00°C.

The result for the heating process is shown below in Fig. 5.21. The scanning result for this liquid crystal without dyes shows two peaks at 48°C and 66°C respectively in Figure 5.6. Compared with this result, we see that there are no peaks at 48°C and 66°C respectively. The alignment of the molecules in these films is fixed, and therefore there are no phase transitions even when the temperature becomes higher in the sample after cross-linking 30°C to 90°C.

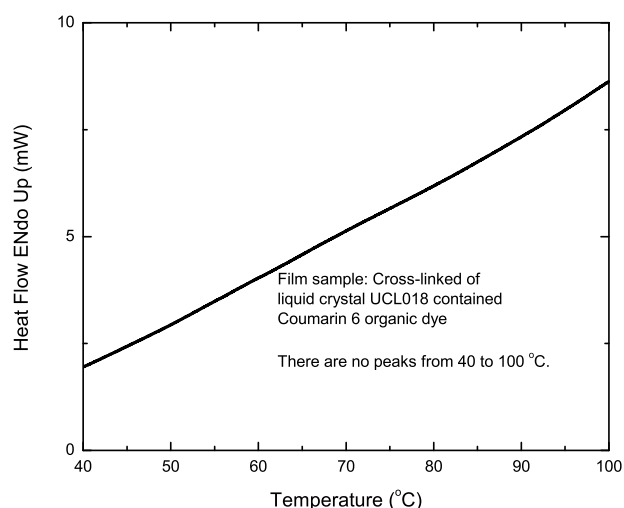


Figure 5.21: Phase transition for cross-linked liquid crystal UCL018 contained Coumarin 6 dye. There are no peaks observed.

No phase transition observed up to 150°C. This temperature range is suitable for the application of the LSC PVs. There is no phase transition for isotropic LSC films using PMMA (Sigma Aldrich) as the host matrix material under 100°C. We have done the same experiments for Lumogen Red F 305 dye, and obtained the same results.

5.6.3 Alignment and Birefringence Properties Tested by Polarized Optical Microscopy

By using polarized optical microscopy, we can visualize liquid crystal textures in the fabricated anisotropic dye containing LSC films. These textures depend on molecular alignment with respect to the optical axis and the polarizers.

As in the sample, molecules are vertically aligned to the glass substrate or the waveguide plane of the LSC. A black picture with some defect textures from the LSC films are expected. We have characterized the anisotropic LSC films fabricated by using glass cells with specific alignment coatings on the top and bottom surfaces. Typical polarized optical microscopy pictures are shown for the Lumogen Red F 305 dye and for the Coumarin 6 dye in Fig. 5.22 (a) and (b) respectively.

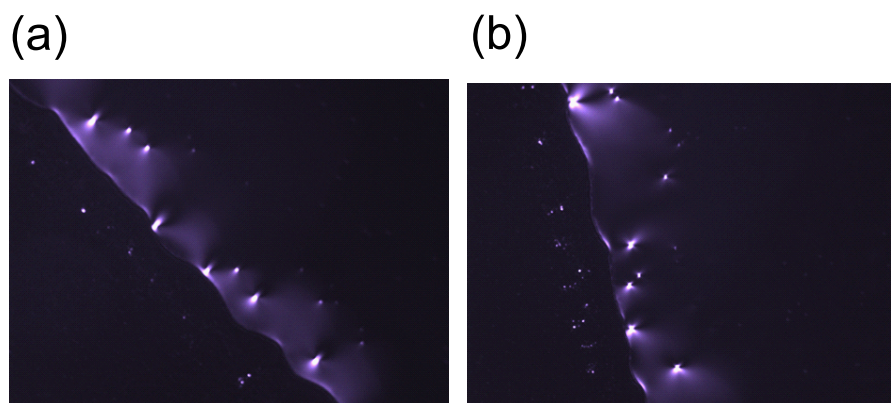


Figure 5.22: From the edge of the aligned (a) Lumogen Red F 305 and (b) Coumarin 6 samples (Glass Cells).

The selected areas are located at the edges of the LSC films. Except some bright defect textures at the edges shown in these two figures, we see that areas at both sides of the edges are black. At one left side of the edge, the dark is due to the anisotropic properties of the glass substrates, while for the other side of the edge, the dark is due to the vertical alignment of the dye molecules to the glass substrates.

5.7 Future Work

5.7.1 Alignment of Dyes for Stacked Structures

Since we have successfully aligned Coumarin 6 and Lumogen Red F 305 dye molecules by using polymerized liquid crystal materials, the future work will focus on characterizing the electrical properties of the films and comparing with isotropic samples under sunlight.

The environmentally-benign organic dyes with long lifetime and high conversion efficiency are to be identified to match different parts of the solar spectrum. These dyes need to be demonstrated that they can be aligned in a liquid crystal environment. The optical and electrical characterization and further mathematical modeling are very essential in evaluating the feasibility of such devices.

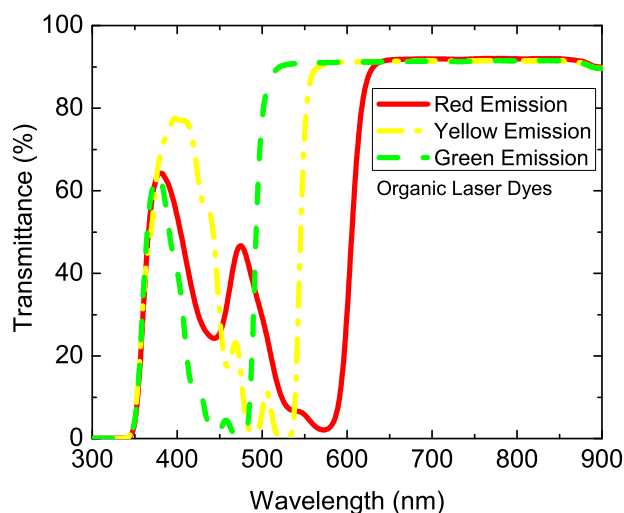


Figure 5.23: Transmittance of designed stacked LSCs with dyes aligned by liquid crystals. Fabricating anisotropic LSCs with these dyes, and then stacking these anisotropic LSCs into three layered structure, the absorption range of the stacked sample can absorb sunlight from 400nm to 600nm.

In addition, we characterized the Coumarin 6 green emission and Lumogen Red F 305 red emission dyes. We can further study stacking these two dyes together as a double-layered LSC. Furthermore, identifying other organic dyes which can cover more parts of the solar spectrum is always desired. For the organic dyes

we studied in chapter 4 for organic LSCs, the optical transmittance is shown in Fig. 5.23. Fabricating anisotropic LSCs with these dyes, and then stacking these anisotropic LSCs into three layered structure, the absorption range of the stacked sample can absorb sunlight from 400nm to 600nm, the peak of the solar spectrum. Research on aligning these dyes by using liquid crystal is very interesting and very challenging. The challenging part is also from the requirement of producing samples at reasonable large size.

5.7.2 Order Parameter Characterization

The method of charactering alignment properties of dye molecules by liquid crystal molecular for the anisotropic films needs to be further developed. The alignment of dye molecules is vertical to the surface of the glass substrate. When tested by polarized optical microscopy, we can judge the alignment by watching black areas expanding before cross-linking, and judging the alignment properties by characterizing defect textures in the film. To qualitatively characterize the order of the aligned dye molecules, it is very important to develop parameters for the anisotropic LSC films.

5.7.3 Stability Testing

Stability testing for anisotropic samples is an essential part for applications of the anisotropic LSCs for PV systems. The method or process for this testing needs to be developed. For organic anisotropic LSCs, we expect that the stability properties of these samples are excellent due to their development and use in OLEDs and dye lasers.

5.7.4 Further Design Optimization

Similar to isotropic LSCs, we can apply some optical enhancement methods to optimize the design and improve the output efficiency of the anisotropic

LSCs. For example, attaching a white diffuser at the bottom surface of an LSC, adding refractive index matched optical gel between the surfaces of PV cells and the LSC edges are expected to dramatically improve the output efficiency of the anisotropic LSCs. Since the energy escaping through the top surface dramatically decreases due to the alignment of dye molecules, the wavelength selective film becomes unnecessary to apply.

The future work involves the anisotropic samples' prototype fabrication, characterization and optimization for LSC PVs. If successful, this research will result in a great enhancement in non-imaging concentrator photovoltaic technology.

5.8 Summary

Controlling the orientation of dye molecules using a liquid crystalline host is a very promising way to improve the power conversion efficiency of LSC PV systems. LSCs fabricated this way are considered as the third generation LSCs. In this chapter, we theoretically show how much we can improve by this method to overcome the fundamental efficiency limit exerted by the small refractive index of LSC matrix materials of LSCs. For widely used plastic materials with refractive index 1.5, we show that the trapping efficiency can be improved from 75% to 91% if we vertically align dye molecules.

We analyzed the required properties of liquid crystals and dye materials for fabricating new generation LSCs. Liquid crystal materials for this application should have very high transmittance and very low absorbance over the solar spectrum. In addition, they are required to align embedded dye molecules in desired directions. We have characterized and compared several liquid crystal materials, and finally identified the UCL018 liquid crystal mixture from Dow Corning chemical company. The DSC results shows a peak at 48°C for the material changing from crystal phase to liquid crystal phase, and another peak at 66°C changing from liquid crystal phase to an isotropic liquid phase. This phase transition sequence is

verified by polarized optical microscopy method.

Using this liquid crystal material, we have successfully aligned Coumarin 6 and Lumogen Red F 305 dyes. For both the applied Coumarin 6 and Lumogen Red F 305 dyes, anisotropic LSC film samples are fabricated by spin coating on glass substrates or by filling dye mixtures into glass cells with specific alignment coatings on the inner top and bottom surfaces. The isotropic LSC film samples are fabricated either by spin coating on cleaned glass substrates or by soaking pure PMMA films in dye and toluene mixtures.

We investigated properties of these fabricated films, and compared anisotropic samples with isotropic samples. The spectral properties of the dyes are very sensitive to matrix materials. Red shifts of the absorption and emission spectra are very large when dyes are embedded into solid matrix materials compared to those in liquid materials. Also, the red shift is more obvious for isotropic materials. For both the Coumarin 6 dye and Lumogen Red F 305 dye, brief cross-linking in short time only slightly blue shifted the absorption and emission spectra of dyes. The specific alignment coatings on the inner surfaces of the glass cell affect the absorption properties of contained dyes very weakly.

The phase transition properties studied by DSC show that there is no phase transition from 0°C to 100°C after cross-linking the sample, therefore we assume that the fixed order in these samples does not change. This is favorable for outdoor applications of the luminescent solar concentrators.

This theoretical and experimental work is very valuable for us to characterize other organic luminescent materials for further aligning them into suitable liquid crystal polymers. It is also helpful for us to understand properties of luminescent materials and matrix materials for the LSC for long term applications and in improving system power conversion efficiency with lower cost and longer life time.

5.9 Acknowledgements

Part of this work is accepted by the SPIE 2011 Optics and Photonics conference.

And some manuscripts are in preparation.

Chapter 6

Conclusions

Luminescent solar concentrators as non-imaging solar concentrators are designed and developed for low concentration photovoltaics technologies with the potential of reducing PV materials cost and reducing infrastructure and time needed for manufacture.

6.1 New Luminescent Materials

In order to characterize proper luminescent materials, in Chapter 3, we compared properties of near infrared PbS QDs, visible CdSe/ZnS QDs and high efficiency Rhodamine B organic laser dye as luminescent materials for LSCs and show the potential LSC efficiency improvement by PbS near infrared QDs due to the broaden absorption spectrum and near infrared emission properties for PV solar cells.

We studied effect of luminescent material concentration in fabrication on LSC efficiency for each of the above luminescent materials, and proposed the proper concentration for each luminescent material to balance the absorption of solar radiation and re-absorption of re-emitted light. Our results show that although there are optimal concentrations for visible CdSe/ZnS QDs and laser dye LSCs, for PbS QDs, the output power increases by increasing the concentration up to

193 μ M. And the effect of the re-absorption problem is not very strong compared with other two luminescent materials based on the emission spectrum red-shift study. This red shift is a function of excitation distance. This result means that we can increase the system efficiency by increasing the concentration of luminescent materials, or the amount of seeded quantum dots in fabrication.

Although the output shows degradation due to mainly due to photo-oxidation, the concentration factor for the PbS QDs LSC can be 15%, which is almost twice of visible QDs and organic dyes.

The power output stability problem of the near infrared quantum dots is issued and further characterized, which proposed the challenge for the application of the infrared QDs in LSCs. In Chapter 3, we also proposed the following efficiency improvement methods for a LSC:

- (1). From the bottom surface, attach a white diffuser with an air gap.
- (2). From the edge surfaces, attach mirrors or silver reflective tapes to reflect light;
- (3). From the edge surfaces, apply optical gel between edge surfaces of LSCs and attached PV cells.

Applying these methods, we characterized the performance of the LSCs, and observed a great improvement on the output power. We also applied these methods for fabricated thin film PbS and CdSe/ZnS QDs LSCs with dimensions 2.54cm by 7.62cm by 0.4cm. By only apply the optical gel and white diffusers, we obtained 3.1 \times improvement for CdSe/ZnS QDs LSCs, and 2.7 \times improvement for PbS QDs at lower concentration at 50 μ M. We expect to get better optimization results for higher concentration samples. This is experimentally proved by the concentration study of PbS QDs as luminescent materials. This research on the luminescent materials shows that PbS QDs LSCs could be potentially used in high efficiency and low cost LSCs, and for them to become practical in the market, increased their output power stability is required.

6.2 LSC Optimal Structure Design

Since organic LSCs have been widely investigated due to their potential in dramatically decreasing the LSC cost, in Chapter 4, we designed and fabricated organic luminescent solar concentrators and investigated their properties. Taking organic LSCs as examples, we developed optical enhancement methods for LSCs in improving the power conversion efficiency.

We identified two groups of organic laser dyes: indoor use and outdoor use. They are embedded into transparent plastic materials and fabricated into LSCs. For prototyped LSC PV systems, we optically and electrically characterized their concentrating properties. The absorption and emission spectra of the embedded dyes are characterized by using spectrophotometers and fluoreimeters. The transmission of the LSCs is also characterized by using silicon PV cells as detectors.

We found that for the dyes we used, the absorption ranges are narrow compared with the overall solar spectrum. Different dyes have different absorption ranges, which shows the advantage of optimizing the structure for improving the absorption efficiency by using stacked structures to utilize more solar spectrum. Also, the outdoor use dyes can absorb more solar radiation than the indoor use dyes.

We developed size dependent efficiency enhancement methods for luminescent solar concentrators (LSCs) with single layer and stacked multi-layer structures. They are fabricated by casting two groups of organic dyes into PMMA matrixes. The efficiency of the organic luminescent solar concentrators has been greatly enhanced by attaching white diffusers at the bottom surface of LSCs and by adding refractive index matched optical gel between the LSC edges and the attached PV cells.

The geometrical gain of the tested LSCs ranges from 1.2 to 62.5. And the largest size with geometrical gain 62.5 has the dimension 60cm by 120 cm by 0.32cm. It is fabricated with indoor use red dye. This is the largest LSC we know

of to date. It shows a very strong concentration effect. The yielded electrical gain from it by testing under sunlight is 4.23. This concentrator is much larger than any fixed concentrators based on geometrical optics. And the optical efficiency is still as high as 6.6%. The effect of the optical gel on the output current can be more than 65%.

For LSCs fabricated with outdoor using dyes, the largest tested size is 35cm by 35cm by 0.32cm. Although the concentration gain of this prototype with outdoor use dyes is 28, it yields almost the same current ratio 4.24 with the largest tested LSC prototyped with indoor use dyes. Also, the optical gain of this system is 15% without applying the 3M film, which is $2.67\times$ of the largest tested LSC. This results show that the performance of LSC with outdoor use organic dyes is very promising.

Although the size of the LSCs increases more than twice from the one with geometrical gain 28, the effect of the optical gel on the output is still about $1.6\times$ either at the black background or at the white background.

The performance of LSCs by applying the white diffuser is more size dependent than the performance of LSCs by applying the optical gel. The enhancement from the white diffuser drops and then tends to plateau with increasing geometrical gain of LSCs. The corresponding re-absorption test shows that parts of LSCs closer to PV cells will dominate the output photocurrent. This property can be used to identify the optimal size of LSCs.

We have not seen the strong concentration effects because our fabricated wavelength selective films do not exactly match the emission spectra of the dyes, and some of the emitted light cannot be reflected back to the LSC.

The comparison study for single layers and stacked structures shows that the efficiency enhancement is very large for stacked structures than that for single layers. The optical efficiency is enhanced by stacking green and red emission LSCs. For both one layered LSCs and multi-layered LSCs, our experiments show that the larger the size of an LSC, and then the larger the output current ratio, or the

concentration factor of the concentrator. The output from their edges distributes very evenly.

The stability test shows that the output current ratio, or the concentration factor for samples exposed to sunlight drops fast in the first week, but drops much more slowly after the first week. Also, for the group kept into dark, red emission LSC performs better than green emission LSCs. While for the groups exposed under sunlight, the drop of current from red emission LSCs is faster than that from green emission LSCs since red emission dyes are more sensitive to photo oxidation. In addition, the LSCs exposed under sunlight with a black background drop faster than the LSCs exposed under sunlight with a white background. The reason is partially due to the higher temperature of the samples with a black background when exposed to sunlight. For red emission LSCs, although the absorption efficiency has not decreased too much, the emission efficiency drops very obviously by the test in two months. Future work can focus on the weather ability of outdoor use dyes with the expectation that they may perform better.

The study proves the advantage of the LSCs in concentration solar radiation without tracking. The fabricated “smart” windows performs equally well for both global and diffuse light. And in the morning, LSC PV system performs better for the diffuse light. These results can be applied to optimize the design of LSCs.

These results can be applied to optimize the design of LSCs.

6.3 New Generation LSCs

Controlling the orientation of dye molecules using a liquid crystalline host is a very promising way to improve the power conversion efficiency of LSC PV systems. LSCs fabricated by this way are considered as the third generation LSCs.

In chapter 6, we theoretically show how much we can improve by this method to overcome the fundamental efficiency limit exerted by small refractive index of matrix materials of LSCs. For the widely used plastic materials with

refractive index 1.5, we show that the trapping efficiency can be improved from 75% to 91% if we vertically align dye molecules.

We analyzed the required properties of liquid crystals and dye materials for fabricating new generation LSCs. Liquid crystal materials for this application should have very high transmittance and very low absorbance over the solar spectrum. In addition, they are required to align embedded dye molecules in desired directions. We have characterized and compared several liquid crystal materials, and finally identified the UCL018 liquid crystal mixture from Dow Corning chemical company. The DSC results shows a peak at 48°C for the material changing from crystal phase to liquid crystal phase, and another peak at 66°C changing from liquid crystal phase to an isotropic liquid phase. This phase transition sequence is verified by polarized optical microscopy method.

Using this liquid crystal material, we have successfully aligned Coumarin 6 and Lumogen Red F 305 dyes. For both the applied Coumarin 6 and Lumogen Red F 305 dyes, anisotropic LSC film samples are fabricated by spin coating on glass substrates or by filling dye mixtures into glass cells with specific alignment coatings on the inner top and bottom surfaces. The isotropic LSC film samples are fabricated either by spin coating on cleaned glass substrates or by soaking pure PMMA films in dye and toluene mixtures.

We investigated properties of these fabricated films, and compared anisotropic samples with isotropic samples. The spectral properties of the dyes are very sensitive to matrix materials. Red shifts of the absorption and emission spectra are very large when dyes are embedded into solid matrix materials compared to those in liquid materials. Also, the red shift is more obvious for isotropic materials. For both the Coumarin 6 dye and Lumogen Red F 305 dye, brief cross-linking in short time only slightly blue shifted the absorption and emission spectra of dyes. The specific alignment coatings on the inner surfaces of the glass cell affect the absorption properties of contained dyes very weakly.

The phase transition properties studied by DSC show that there is no phase

transition from 0°C to 100°C after cross-linking the sample, therefore we assume that the fixed order in these samples does not change. This is favorable for outdoor applications of the luminescent solar concentrators.

This theoretical and experimental work is very valuable for us to characterize other organic luminescent materials for further aligning them into suitable liquid crystal polymers. It is also helpful for us to understand properties of luminescent materials and matrix materials for the LSC for long term applications and in improving system power conversion efficiency with lower cost and longer life time.

With the development of this research on LSCs, we can imagine how wonderful it would be if windows on every skyscraper are replaced by LSC PV systems as “smar” windows.

Bibliography

- [Abb11] S Abbasoglu. Techno-economic and environmental analysis of pv power plants in northern cyprus. *Energy Education Science and Technology Part a-Energy Science and Research*, 28(1):357–368, 2011.
- [AIM11] V. Avrutin, N. Izyumskaya, and H. Morkoc. Semiconductor solar cells: Recent progress in terrestrial applications. *Superlattices and Microstructures*, 49(4):337–364, 2011.
- [ARW10] H Abdul-Rahman and C Wang. Limitations in current day lighting related solar concentration devices: A critical review. *International Journal of the Physical Sciences*, 5(18):2730–2756, 2010.
- [Bat81] J. S. Batchelder. *The luminescent solar concentrator*. Phd, 1981.
- [BCL⁺11] J. L. Blackburn, H. Chappell, J. M. Luther, A. J. Nozik, and J. C. Johnson. Correlation between photooxidation and the appearance of raman scattering bands in lead chalcogenide quantum dots. *Journal of Physical Chemistry Letters*, 2(6):599–603, 2011.
- [BKY⁺07] M. C. Beard, K. P. Knutsen, P. R. Yu, J. M. Luther, Q. Song, W. K. Metzger, R. J. Ellingson, and A. J. Nozik. Multiple exciton generation in colloidal silicon nanocrystals. *Nano Letters*, 7(8):2506–2512, 2007.
- [BLH⁺07] S. T. Bailey, G. E. Lokey, M. S. Hanes, J. D. M. Shearer, J. B. McLafferty, G. T. Beaumont, T. T. Baseler, J. M. Layhue, D. R. Broussrd, Y. Z. Zhang, and B. P. Wittmershaus. Optimized excitation energy transfer in a three-dye luminescent solar concentrator. *Solar Energy Materials and Solar Cells*, 91(1):67–75, 2007.
- [BMH99] NA Bakr, AF Mansour, and M Hammam. Optical and thermal spectroscopic studies of luminescent dye doped poly(methyl methacrylate) as solar concentrator. *Journal of Applied Polymer Science*, 74(14):3316–3323, 1999.

- [BMHO00] K Barnham, JL Marques, J Hassard, and P O'Brien. Quantum-dot concentrator and thermodynamic model for the global redshift. *Applied Physics Letters*, 76(9):1197–1199, 2000.
- [BOR84] JG BORNSTEIN. Luminescent solar concentrator daylighting. *Proceedings of the Society of Photo-Optical Instrumentation Engineers*, 502:138–145, 1984.
- [CBB⁺04] AJ Chatten, KWJ Barnham, BF Buxton, NJ Ekins-Daukes, and MA Malik. Quantum dot solar concentrators. *Semiconductors*, 38(8):909–917, 2004.
- [CH97] Peter J. Collings and Michael Hird. *Introduction to liquid crystals (chemistry and physics)*. The liquid crystals book series. Taylor and Francis Ltd, London and New York, 1997.
- [CMH⁺08] Michael J. Currie, Jonathan K. Mapel, Timothy D. Heidel, Shalom Goffri, and Marc A. Baldo. High-efficiency organic solar concentrators for photovoltaics. *Science*, 321(5886):226–228, 2008.
- [DCM⁺85] M. S. Decardona, M. Carrascosa, F. Meseguer, F. Cusso, and F. Jaque. Outdoor evaluation of luminescent solar concentrator prototypes. *Applied Optics*, 24(13):2028–2032, 1985.
- [DTK⁺09] M. G. Debije, J. P. Teunissen, M. J. Kastelijn, P. P. C. Verbunt, and C. W. M. Bastiaansen. The effect of a scattering layer on the edge output of a luminescent solar concentrator. *Solar Energy Materials and Solar Cells*, 93(8):1345–1350, 2009.
- [DVN⁺11] MG Debije, PPC Verbunt, PJ Nadkarni, S Velate, K Bhaumik, S Nedumbamana, BC Rowan, BS Richards, and TL Hoeks. Promising fluorescent dye for solar energy conversion based on a perylene perinone. *Applied Optics*, 50(2):163–169, 2011.
- [DVR⁺08] MG Debije, PPC Verbunt, BC Rowan, BS Richards, and TL Hoeks. Measured surface loss from luminescent solar concentrator waveguides. *Applied Optics*, 47(36):6763–6768, 2008.
- [DVV⁺10a] M. G. Debije, M. P. Van, P. P. C. Verbunt, M. J. Kastelijn, R. H. L. van der Blom, D. J. Broer, and C. W. M. Bastiaansen. Effect on the output of a luminescent solar concentrator on application of organic wavelength-selective mirrors. *Applied Optics*, 49(4):745–751, 2010.
- [DVV⁺10b] MG Debije, MP Van, PPC Verbunt, MJ Kastelijn, RHL van der Blom, DJ Broer, and CWM Bastiaansen. Effect on the output of a luminescent solar concentrator on application of organic wavelength-selective mirrors. *Applied Optics*, 49(4):745–751, 2010.

- [EBJ+05] R. J. Ellingson, M. C. Beard, J. C. Johnson, P. R. Yu, O. I. Micic, A. J. Nozik, A. Shabaev, and A. L. Efros. Highly efficient multiple exciton generation in colloidal PbSe and PbS quantum dots. *Nano Letters*, 5(5):865–871, 2005.
- [ER95] S. A. Evenson and A. H. Rawicz. Thin-film luminescent concentrators for integrated devices. *Applied Optics*, 34(31):7231–7238, 1995.
- [ERFS10] A. A. Earp, T. Rawling, J. B. Franklin, and G. B. Smith. Perylene dye photodegradation due to ketones and singlet oxygen. *Dyes and Pigments*, 84(1):59–61, 2010.
- [ESMEB+03] M. G. El-Shaarawy, A. F. Mansour, S. M. El-Bashir, M. K. El-Mansy, and M. Hammam. Electrical conduction and dielectric properties of poly(methyl methacrylate)/perylene solar concentrators. *Journal of Applied Polymer Science*, 88(3):793–805, 2003.
- [FY11] Daniel J. Farrell and Megumi Yoshida. Operating regimes for second generation luminescent solar concentrators. *Progress in Photovoltaics: Research and Applications*, pages n/a–n/a, 2011.
- [GH05] A Goetzberger and V.U. Hoffmann. *Photovoltaic Solar Energy Generation*. Optical Sciences. Springer, Germany, 2005.
- [GKK00] D. Yogi Goswami, Frank Kreith, and Jan F. Kreider. *Principles of Solar Engineering*. CRC Press, 2000.
- [GLS+11] J. B. Gao, J. M. Luther, O. E. Semonin, R. J. Ellingson, A. J. Nozik, and M. C. Beard. Quantum dot size dependent J-V characteristics in heterojunction ZnO/PbS quantum dot solar cells. *Nano Letters*, 11(3):1002–1008, 2011.
- [GPHG09] J. C. Goldschmidt, M. Peters, M. Hermle, and S. W. Glunz. Characterizing the light guiding of fluorescent concentrators. *Journal of Applied Physics*, 105(11):–, 2009.
- [HBte] Christiana Honsberg and Stuart Bowden. Pvcdrom, 2011Cite.
- [Hir12] Linda S Hirst. *Fundamentals of Soft Matter Science*. CRC Pr I Llc, 1 edition, 2012.
- [JB09] HA Jones-Bey. Photovoltaics optical modeling determines luminescent solar-concentrator efficiency. *Laser Focus World*, 45(2):20–+, 2009.

- [JK11] Zhong-Jie Jiang and David F. Kelley. Hot and relaxed electron transfer from the CdSe core and core/shell nanorods. *The Journal of Physical Chemistry C*, 115(11):4594–4602, 2011. doi: 10.1021/jp112424z.
- [JLK09] Zhong-Jie Jiang, Valerie Leppert, and David F. Kelley. Static and dynamic emission quenching in core/shell nanorod quantum dots with hole acceptors. *The Journal of Physical Chemistry C*, 113(44):19161–19171, 2009. doi: 10.1021/jp907728h.
- [KBD09] M. J. Kastelijjn, C. W. M. Bastiaansen, and M. G. Debije. Influence of waveguide material on light emission in luminescent solar concentrators. *Optical Materials*, 31(11):1720–1722, 2009.
- [Keb02] Kebes. Schematic of mesogen alignment in a liquid crystal nematic phase, 2002.
- [KMDN09] M. Kennedy, S. J. McCormack, J. Doran, and B. Norton. Improving the optical efficiency and concentration of a single-plate quantum dot solar concentrator using near infra-red emitting quantum dots. *Solar Energy*, 83(7):978–981, 2009.
- [KSB⁺07] R. Kinderman, L. H. Slooff, A. R. Burgers, N. J. Bakker, A. Buchtemann, R. Danz, and J. A. M. van Roosmalen. I-v performance and stability study of dyes for luminescent plate concentrators. *Journal of Solar Energy Engineering-Transactions of the Asme*, 129(3):277–282, 2007.
- [LA07] Antonio L. Luque and Viacheslav M. Andreev. Concentrator photovoltaics, 2007.
- [LBV11] J Llorente, J Ballestrin, and AJ Vazquez. A new solar concentrating system: Description, characterization and applications. *Solar Energy*, 85(5):1000–1006, 2011.
- [LMB⁺05] A. Luque, A. Marti, A. Bett, V. M. Andreev, C. Jaussaud, J. A. M. van Roosmalen, J. Alonso, A. Rauber, G. Strobl, W. Stolz, C. Algora, B. Bitnar, A. Gombert, C. Stanley, P. Wahnon, J. C. Conesa, W. G. J. H. M. van Sark, A. Meijerink, G. P. M. van Klink, K. Barnham, R. Danz, T. Meyer, I. Luque-Heredia, R. Kenny, C. Christofides, G. Sala, and P. Benitez. Fullspectrum: a new pv wave making more efficient use of the solar spectrum. *Solar Energy Materials and Solar Cells*, 87(1-4):467–479, 2005.
- [MCCS10] RW MacQueen, YY Cheng, RGCR Clady, and TW Schmidt. Towards an aligned luminophore solar concentrator. *Optics Express*, 18(13):A161–A166, 2010.

- [MLU⁺00] K Machida, H Li, D Ueda, S Inoue, and G Adachi. Preparation and application of lanthanide complex incorporated ormosil composite phosphor films. *Journal of Luminescence*, 87-9:1257–1259, 2000.
- [MR97] IS Melnik and AH Rawicz. Thin-film luminescent concentrators for position-sensitive devices. *Applied Optics*, 36(34):9025–9033, 1997.
- [MRV⁺10] C. L. Mulder, P. D. Reusswig, A. M. Velzquez, H. Kim, C. Rotschild, and M. A. Baldo. Dye alignment in luminescent solar concentrators: I. vertical alignment for improved waveguide coupling. *Opt. Express*, 18(S1):A79–A90, 2010.
- [MYR07] K. R. McIntosh, N. Yamada, and B. S. Richards. Theoretical comparison of cylindrical and square-planar luminescent solar concentrators. *Applied Physics B-Lasers and Optics*, 88(2):285–290, 2007.
- [Noz05] A. J. Nozik. Exciton multiplication and relaxation dynamics in quantum dots: Applications to ultrahigh-efficiency solar photon conversion. *Inorganic Chemistry*, 44(20):6893–6899, 2005.
- [Noz10] A. J. Nozik. Nanoscience and nanostructures for photovoltaics and solar fuels. *Nano Letters*, 10(8):2735–2741, 2010.
- [O’N64] M. J. O’Neill. The analysis of a temperature-controlled scanning calorimeter. *Analytical Chemistry*, 36(7):1238–1245, 1964. doi: 10.1021/ac60213a020.
- [PKHG09] Vesselinka Petrova-Koch, Rudolf Hezel, and A Goetzberger. *High-efficient low-cost photovoltaics*. Springer, 2009.
- [PP91] KK PANDEY and TC PANT. Solar-energy concentrator based on uranyl-doped PMMA. *Solar Energy Materials*, 21(4):327–334, 1991.
- [RB78] C. F. Rapp and N. L. Boling. Luminescent solar concentrators. *Thirteenth IEEE Photovoltaic Specialists Conference-1978—Thirteenth IEEE Photovoltaic Specialists Conference-1978*, pages 690–3—1346, 1978. Times Cited: 0 Thirteenth IEEE Photovoltaic Specialists Conference-1978 Washington, DC Usa.
- [RD11] Philip C. Robinson and Michael W. Davidson. Introduction to polarized light microscopy, 2011.
- [Red08] S. M. Reda. Synthesis and optical properties of CdS quantum dots embedded in silica matrix thin films and their applications as luminescent solar concentrators. *Acta Materialia*, 56(2):259–264, 2008.

- [Rei10] R Reisfeld. New developments in luminescence for solar energy utilization. *Optical Materials*, 32(9):850–856, 2010.
- [Ric06] B. S. Richards. Enhancing the performance of silicon solar cells via the application of passive luminescence conversion layers. *Solar Energy Materials and Solar Cells*, 90(15):2329–2337, 2006.
- [Row07] Brenda Rowan. *The development of a quantum dot solar concentrator*. PhD thesis, 2007.
- [RSJ94] R REISFELD, D SHAMRAKOV, and C JORGENSEN. Photo-stable solar concentrators based on fluorescent glass-films. *Solar Energy Materials and Solar Cells*, 33(4):417–427, 1994.
- [RWR08] B. C. Rowan, L. R. Wilson, and B. S. Richards. Advanced material concepts for luminescent solar concentrators. *Ieee Journal of Selected Topics in Quantum Electronics*, 14(5):1312–1322, 2008.
- [SBB⁺08] L. H. Slooff, E. E. Bende, A. R. Burgers, T. Budel, M. Pravettoni, R. P. Kenny, E. D. Dunlop, and A. Buchtemann. A luminescent solar concentrator with 7.1efficiency. *Physica Status Solidi-Rapid Research Letters*, 2(6):257–259, 2008.
- [SJL⁺10] O. E. Semonin, J. C. Johnson, J. M. Luther, A. G. Midgett, A. J. Nozik, and M. C. Beard. Absolute photoluminescence quantum yields of IR-26 dye, PbS, and PbSe quantum dots. *Journal of Physical Chemistry Letters*, 1(16):2445–2450, 2010.
- [SLS⁺11] D. K. Smith, J. M. Luther, O. E. Semonin, A. J. Nozik, and M. C. Beard. Tuning the synthesis of ternary lead chalcogenide quantum dots by balancing precursor reactivity. *Acs Nano*, 5(1):183–190, 2011.
- [SOC07] V. Sholin, J. D. Olson, and S. A. Carter. Semiconducting polymers and quantum dots in luminescent solar concentrators for solar energy harvesting. *Journal of Applied Physics*, 101(12):–, 2007.
- [SRWY90] G. Smestad, H. Ries, R. Winston, and E. Yablonovitch. The thermodynamic limits of light concentrators. *Solar Energy Materials*, 21(2-3):99–111, 1990.
- [TBBD10] S Tsoi, DJ Broer, CWM Bastiaansen, and MG Debije. Patterned dye structures limit reabsorption in luminescent solar concentrators. *Optics Express*, 18(23):A536–A543, 2010.

- [TCS05] AM Taleb, BT Chiad, and ZS Sadik. Spectroscopic study of dcm as an active medium for luminescent solar concentrators. *Renewable Energy*, 30(3):393–398, 2005.
- [THA87] M THACKRAY. The promise of the luminescent solar concentrator. *Endeavour*, 11(1):43–46, 1987.
- [TPS⁺11] M. T. Trinh, L. Polak, J. M. Schins, A. J. Houtepen, R. Vaxenburg, G. I. Maikov, G. Grinbom, A. G. Midgett, J. M. Luther, M. C. Beard, A. J. Nozik, M. Bonn, E. Lifshitz, and L. D. A. Siebbeles. Anomalous independence of multiple exciton generation on different group IV-VI quantum dot architectures. *Nano Letters*, 11(4):1623–1629, 2011.
- [VKH⁺09] P. P. C. Verbunt, A. Kaiser, K. Hermans, C. W. M. Bastiaansen, D. J. Broer, and M. G. Debije. Controlling light emission in luminescent solar concentrators through use of dye molecules aligned in a planar manner by liquid crystals. *Advanced Functional Materials*, 19(17):2714–2719, 2009.
- [vS08] WGJHM van Sark. Simulating performance of solar cells with spectral downshifting layers. *Thin Solid Films*, 516(20):6808–6812, 2008.
- [vSBS⁺08] WGJHM van Sark, KWJ Barnham, LH Slooff, AJ Chatten, A Buchtemann, A Meyer, SJ McCormack, R Koole, DJ Farrell, R Bose, EE Bende, AR Burgers, T Budel, J Quilitz, M Kennedy, T Meyer, CDM Donega, A Meijerink, and D Vanmaekelbergh. Luminescent solar concentrators - a review of recent results. *Optics Express*, 16(26):21773–21792, 2008.
- [vSFB⁺02] WGJHM van Sark, PLTM Frederix, AA Bol, HC Gerritsen, and A Meijerink. Blueing, bleaching, and blinking of single CdSe/ZnS quantum dots. *Chemphyschem*, 3(10):871–879, 2002. Cited References Count:61—WILEY-V C H VERLAG GMBH—PO BOX 10 11 61, D-69451 WEINHEIM, GERMANY.
- [vSFVdH⁺01] WGJHM van Sark, PLTM Frederix, DJ Van den Heuvel, HC Gerritsen, AA Bol, JNJ van Lingen, CD Donega, and A Meijerink. Photooxidation and photobleaching of single CdSe/ZnS quantum dots probed by room-temperature time-resolved spectroscopy. *Journal of Physical Chemistry B*, 105(35):8281–8284, 2001. Cited References Count:30—AMER CHEMICAL SOC—1155 16TH ST, NW, WASHINGTON, DC 20036 USA.
- [vSMS⁺05] WGJHM van Sark, A Meijerink, REI Schropp, JAM van Roosmalen, and EH Lysen. Enhancing solar cell efficiency by using

- spectral converters. *Solar Energy Materials and Solar Cells*, 87(1-4):395–409, 2005. Cited References Count:39—ELSEVIER SCIENCE BV—PO BOX 211, 1000 AE AMSTERDAM, NETHERLANDS.
- [VVSL⁺11] J Vandenberg, I Van Severen, L Lutsen, P Adriaensens, HJ Bolink, TJ Cleij, and D Vanderzande. Tetra-alkoxy substituted ppv derivatives: a new class of highly soluble liquid crystalline conjugated polymers. *Polymer Chemistry*, 2(6):1279–1286, 2011. Cited References Count:38—ROYAL SOC CHEMISTRY—THOMAS GRAHAM HOUSE, SCIENCE PARK, MILTON RD, CAMBRIDGE CB4 0WF, CAMBS, ENGLAND.
- [WARR10a] C Wang, H Abdul-Rahman, and SP Rao. Daylighting can be fluorescent: Development of a fiber solar concentrator and test for its indoor illumination. *Energy and Buildings*, 42(5):717–727, 2010.
- [WARR10b] C Wang, H Abdul-Rahman, and SP Rao. A new design of luminescent solar concentrator and its trial run. *International Journal of Energy Research*, 34(15):1372–1385, 2010.
- [Wea03] R. Weaver. Rediscovering polarized light microscopy. *AMERICAN LABORATORY*, 35:55–61, 2003.
- [WL76] W. H. Weber and J. Lambe. Luminescent greenhouse collector for solar-radiation. *Applied Optics*, 15(10):2299–2300, 1976.
- [WMB⁺05] Roland Winston, Juan C. Minano, Pablo G. Benitez, Narkis Shatz, and John C. Bortz. Nonimaging optics, 2005.
- [WRR⁺10] L. R. Wilson, B. C. Rowan, N. Robertson, O. Moudam, A. C. Jones, and B. S. Richards. Characterization and reduction of reabsorption losses in luminescent solar concentrators. *Applied Optics*, 49(9):1651–1661, 2010.
- [WWW⁺10] WX Wu, TX Wang, X Wang, S Wu, YH Luo, XJ Tian, and QJ Zhang. Hybrid solar concentrator with zero self-absorption loss. *Solar Energy*, 84(12):2140–2145, 2010.
- [Yab80] E. Yablonovitch. Thermodynamics of the fluorescent planar concentrator. *Journal of the Optical Society of America*, 70(11):1362–1363, 1980.
- [YST09] Y. Yang, I. D. W. Samuel, and G. A. Turnbull. The development of luminescent concentrators for pumping organic semiconductor lasers. *Advanced Materials*, 21(31):3205–+, 2009.

- [ZMGN98] A. Zaban, O. I. Micic, B. A. Gregg, and A. J. Nozik. Photosensitization of nanoporous TiO_2 electrodes with InP quantum dots. *Langmuir*, 14(12):3153–3156, 1998.